

Control-oriented modelling and Model Predictive Control for air-based Building-Integrated Photovoltaic/Thermal systems

Anna-Maria Sigounis

A Thesis

in the Department

of

Building, Civil and Environmental Engineering

Presented in Partial Fulfillment of the Requirements

for the Degree of Master of Applied Science (Building Engineering) at

Concordia University

Montréal, Québec, Canada

May 2022

© Anna-Maria Sigounis, 2022

CONCORDIA UNIVERSITY

School of Graduate Studies

This is to certify that the thesis prepared

By: Anna-Maria Sigounis

Entitled: Control-oriented modelling and Model Predictive Control for air-based Building-Integrated Photovoltaic/Thermal systems

and submitted in partial fulfillment of the requirements for the degree of

Master of Applied Science (Building Engineering)

complies with the regulations of the University and meets the accepted standards with respect to originality and quality.

Signed by the final Examining Committee:

_____ Dr. Hua Ge _____ Chair

_____ Dr. Mohamed Ouf _____ Examiner

_____ Dr. Hua Ge _____ Examiner

_____ Dr. Andreas Athienitis _____ Supervisor

Approved by _____ Mazdak Nik-Bakht _____

Chair of Department or Graduate Program Director

_____ Mourad Debbabi _____

Dean of Faculty

Date _____

Abstract

Control-oriented modelling and Model Predictive Control for air-based Building-Integrated Photovoltaic/Thermal systems

Anna-Maria Sigounis

This thesis presents a methodology for the development of a grey-box control-oriented model for air-based open-loop Building Integrated Photovoltaic/Thermal (BIPV/T) systems with the scope to apply Model Predictive Control (MPC) to the air flow within the BIPV/T channel to achieve optimal BIPV/T – HVAC integration. The Varennes library, the first institutional net-zero energy building (NZEB) in Canada and one of a handful of buildings worldwide hosting a full-scale fully operational BIPV/T system, is used as an archetype for this work. The methodology presented can optimize the design of air-based BIPV/T systems or be applied to commissioned systems facilitating the broader realization of net-zero energy buildings.

BIPV/T systems combine the concept of BIPV and thermal collectors producing simultaneously electricity and heat by passing a fluid underneath their surface. The waste heat can be used for various thermal applications, however a key factor for broader BIPV/T realization is optimal control of these systems to maximize the amount of useful heat. As the available heat recovered from the BIPV/T is closely related to the respective weather conditions and the applied flow rate, optimally controlling the fan speed within the BIPV/T channel can significantly improve their performance.

Both a transient and steady-state model are developed and compared. The developed BIPV/T models are calibrated and validated using experimental and real weather data. The development of the MPC strategy for the commissioned BIPV/T system covering 1/6 of the south-facing roof at the Varennes library is presented. In one studied design variation of the existing archetype, the BIPV/T system is considered to simultaneously send heat to an Energy Recovery Ventilator (ERV) and an air-to-water heat pump (HP) while the opportunity to provide excess heat to adjacent buildings is explored, facilitating in the development of net-zero energy neighborhoods. Finally, the benefits of covering additional area of the Library's south-facing roof with BIPV/T are examined to facilitate production of useful heat for other buildings in the community.

Through this work the essential parameters an engineer should have measurements for when applying MPC to a commissioned BIPV/T system are identified. This can prove extremely useful during the design stages as to where sensors should be placed and the relative importance of each measurement.

Through MPC, the fan speed is effectively adjusted simultaneously providing heat to the HP and ERV while adequately cooling the PV panels. The COP of the solar heated air-to-water heat pump showed a maximum increase of 32% for a mild sunny day. The BIPV/T that would cover the whole roof was able to produce up to 1.17 kWh/m² (of roof area) of heat for a mild sunny day and provide 85.5% of this amount to adjacent buildings. Specifically, for a day-care center located near the library the consumed energy related to ventilation could be decreased by up to 36.8% with the heat provided from Library BIPV/T system.

Acknowledgements

I would like to first thank my loving husband Giorgos, who left Greece and moved across the world for me to pursue my dream. I would never have been able to accomplish what I have without you.

I would like to express my sincere gratitude to my supervisor Dr. Andreas Athienitis for giving me the opportunity to work with him and for his guidance and support throughout this journey.

Completing my degree in the middle of the pandemic posed many difficulties, with isolation being one of the hardest to overcome. I want to specially thank Stratos Rounis for introducing me to the world of BIPV/T and Harry Vallianos for being the MPC and Python wizard that he is. Besides their much-appreciated professional guidance, they became very good friends to me and supported me throughout the hard times. I could never thank you enough.

In the duration of my studies, I met and worked with many amazing people. Thank you to Jose Candanedo, Jiwu Rao and to all my colleagues in EV16.117 who made my 1-hour commute to the office worthwhile with interesting conversations and by always creating a positive atmosphere and enjoyable work environment.

Finally, I would like to thank my mom for always believing in me and motivating me to pursue my goals. I would also like to thank my father, my sister and my two little brothers for their unconditional love and encouragement.

Financial support for this work was provided by the NSERC/Hydro Quebec Research Chair, the Faculty of Engineering and Computer Science of Concordia University and a Master's - Alexander Graham Bell Canada Graduate Scholarship.

Table of Contents

List of Figures	viii
List of Tables	xii
Nomenclature	xiv
Chapter 1 Introduction	1
1.1 Overview	1
1.2 Motivation	2
1.3 Main Objective	3
1.4 Thesis Outline	4
Chapter 2 Literature Review	5
2.1 Active Building Envelopes	5
2.2 Building Integrated Photovoltaic (BIPV) systems	6
2.3 Building Integrated Photovoltaic/Thermal (BIPV/T) systems	7
2.4 BIPV/T Categories	8
2.5 BIPV/T Modelling	10
2.6 BIPV/T Efficiency Enhancement	14
2.7 Thermal Applications	20
2.8 BIPV/T Control	25
2.9 Research Needs & Opportunities	29
Chapter 3 Grey-box BIPV/T Modelling	30
3.1 Experimental BIPV/T System	30
3.1.1 Model Development	30
3.1.2 Experimental Procedure	37
3.1.3 Experiment Description	39

3.1.4 Time Constant Evaluation.....	41
3.1.5 Model Calibration	43
3.1.6 Results & Observations.....	44
3.2 Full scale BIPV/T system - Varennes library	47
3.2.1 Archetype system analysis.....	47
3.2.2 Model Calibration	55
Chapter 4 MPC Development.....	62
4.1 Thermal applications.....	63
4.2 Methodology	70
4.3 Scenarios explored	73
4.4 Results & Discussion	76
4.4.1 Transient vs Steady-State.....	76
4.4.2 MPC vs Base Case	79
4.4.3 MPC vs Steady flow	83
4.4.4 Heat Pump COP improvement.....	85
4.4.5 Larger BIPV/T area.....	89
4.4.6 Energy savings for adjacent buildings	95
Chapter 5 Summary & Conclusions	97
5.1 Contributions.....	98
5.2 Future Work	99
Bibliography	101
APPENDIX A.....	107
APPENDIX B	112

List of Figures

Figure 1-1 Generation capacity of various power sources in the Electrification Scenario, 2019-2050, [2].....	1
Figure 1-2 Heat generation and achieved ΔT for different air channel velocities in an air-based BIPV/T system.....	3
Figure 2-1 Placement possibilities for BIPV systems, [54].....	7
Figure 2-2 BIPV/T Categorization, [14].....	8
Figure 2-3 Open and closed loop configurations (the heat exchanger is optional in open loop), [15].....	9
Figure 2-4 Opaque and semi-transparent PV panels with same packing factor used in [16].....	10
Figure 2-5 Typical roof-integrated BIPV/T system.....	11
Figure 2-6 Thermal network for transient and steady state BIPV/T models	12
Figure 2-7 Thermal efficiency of a hybrid UTC and PV/T system, as a function of the mass flow rate, [19].....	15
Figure 2-8 Single and double pass PV/T air collectors investigated by [20].....	16
Figure 2-9 BIPV/T functioning as a curtain wall investigated by [13].....	16
Figure 2-10 Examined systems by [22]. From top to bottom: Reference system, Thin Metal Sheet system, Fin System. Left column: Unglazed Systems, Right column: Glazed Systems	17
Figure 2-11 Schematic diagram of double pass solar air collector with fins and PCM [23].....	18
Figure 2-12 Useful heat production and fan power of proposed collector [23].....	19
Figure 2-13 Effect of mass flow rate on efficiency (left) and outlet temperature (right), [20]	20
Figure 2-14 Schematic of an Energy Recovery Ventilator, [55]	21
Figure 2-15 Air-based BIPV/T system connected to an air-source heat pump that charges a water-based TES, [31]	23
Figure 2-16 Air-based BIPV/T system coupled with a ventilated slab, [59].....	24
Figure 2-17 Survey results of respondents' priorities regarding adaptive facades, [5].....	25
Figure 2-18 Most frequently used control techniques for Active Building Envelope, [6]	27
Figure 3-1 BIPV/T control volume energy balance for (a) steady-state model, (b) transient model	31
Figure 3-2 Scatterplot of predicted and monitored values of the air temperature rise (ΔT) for all tests	36

Figure 3-3 (a) Concordia University Solar Simulator, (b) Experimental set-up of an air-based BIPV/T prototype.....	38
Figure 3-4 Experimental BIPV/T modules with adjustable channel height and interchangeable PV modules (dimensions in mm), [45].....	39
Figure 3-5 Thermocouple placement on the air channel, and the custom manifold used	40
Figure 3-6 Channel configurations and operating conditions used in the measurements [45].....	41
Figure 3-7 System response to different types of step response (a) Exponential decay, (b) Exponential growth.....	42
Figure 3-8 TR and SS model outputs compared to the measured data used for the calibration...	45
Figure 3-9 TR and SS model outputs compared to the measured data the model did not “see” during the calibration process	45
Figure 3-10 Comparison of the two BIPV/T models (TR and SS) for highly variable wind conditions.....	46
Figure 3-11 Left: Photograph of Varennes library source: [57], Right: Schematic of library and integrated energy systems [47]	47
Figure 3-12 Schematic of the south-facing roof of the Varennes library.	48
Figure 3-13 Naturally ventilated configuration with 150 mm air gap	49
Figure 3-14 Mechanically ventilated configuration of BIPV or BIPV/T with 70 mm air gap.....	49
Figure 3-15 RTD placement for PV temperature monitoring.....	50
Figure 3-16 BIPV/T and AHU graphical user interface with sensor placement indication throughout the AHU.	51
Figure 3-17 Recorded ambient and outlet temperatures along with the BIPV/T fan modulation on a cold sunny day (January 9, 2020).	52
Figure 3-18 Recorded ambient and outlet temperatures along with the BIPV/T fan modulation on a mild sunny day (February 24, 2020).....	53
Figure 3-19 Total ventilation flow rate, BIPV/T flow rate and BIPV/T channel air velocity for a cold sunny day (January 9, 2020)	54
Figure 3-20 Total ventilation flow rate, BIPV/T flow rate and BIPV/T channel air velocity for a mild sunny day (February 24, 2020).....	54
Figure 3-21 NRMSE for the outlet temperature, PV temperature using different cost functions for the model calibration.....	57

Figure 3-22 SS model outlet temperature prediction for different a-values.	58
Figure 3-23 TR model outlet temperature prediction for different a-values.	58
Figure 3-24 Weather conditions for the different datasets used for the cross-validation of the models.	59
Figure 3-25 Actual and predicted outlet and PV temperatures using dataset 3 to calibrate the model (training dataset) and dataset 4 to validate the results (test dataset).	61
Figure 4-1 Airstream numbering in an ERV [26].....	63
Figure 4-2 Supply and exhaust airstream temperatures passing through the ERV for two consecutive days.	64
Figure 4-4 Calculated sensible efficiency of ERV for two consecutive days.....	65
Figure 4-5 Electricity heating load for the Varennes library on a cold sunny day	67
Figure 4-6 Heat Pump COP for different air and water temperatures.	67
Figure 4-7 Display of Varennes library and adjacent daycare center (Ateliers De La Maison Bleu) on google maps with estimated distance between them.	68
Figure 4-8 Adjacent daycare center, area estimation on Google maps [58].....	69
Figure 4-9 Flow chart of MPC algorithm	72
Figure 4-10 Discretization of PV systems covering the south-facing roof at the Varennes library. (actual system)	74
Figure 4-11 Different theoretical scenarios of BIPV/T area examined	74
Figure 4-12 Rule-based strategy to avoid overheating the ventilation air under the steady flow control strategy.....	75
Figure 4-13 Description of all the different scenarios examined.....	75
Figure 4-14 PV and Outlet temperature predictions on a windy day (March 13, 2020)	76
Figure 4-15 Mass flow rate profiles on a windy day (March 13, 2020)	77
Figure 4-16 PV and Outlet temperature predictions on a still day (February 02, 2020)	77
Figure 4-17 Mass flow rate profiles on a still day (February 02, 2020)	78
Figure 4-18 Net energy for the four investigated days (base and i-mpc case).	79
Figure 4-19 Mass flow rate profiles for January 20, 2020, a very cold sunny day (base and i-mpc case).	79
Figure 4-20 Power profiles for January 20, 2020, a very cold sunny day (base and i-mpc case). 80	
Figure 4-21 Power profiles for February 28, 2020, a mild sunny day (base and i-mpc case).	81

Figure 4-22 Mass flow rate profiles for February 28, 2020, a mild sunny day (base and i-mpc case).	81
Figure 4-23 Net energy for the four investigated days (i-s and i-mpc case).....	83
Figure 4-24 Mass flow rate profiles for March 13, 2020, a mild semi-cloudy day (i-s and i-mpc case).	84
Figure 4-25 Power profiles for March 13, 2020, a mild semi-cloudy day (i-s and i-mpc case)...	84
Figure 4-26 Mass flow rate sent to the ASHP for January 20, 2020, a very cold sunny day (regular, i-mpc, ii-mpc and iii-mpc cases).	86
Figure 4-27 PV and outlet temperature predictions for January 20, 2020, a very cold sunny day (i-mpc, ii-mpc and iii-mpc cases).	86
Figure 4-28 COP profile for January 20, 2020, a very cold sunny day (regular, i-mpc, ii-mpc and iii-mpc cases).	87
Figure 4-29 PV and outlet temperature predictions for February 28, 2020, a mild sunny day (i-mpc, ii-mpc and iii-mpc cases).	87
Figure 4-30 Mass flow rate sent to the ASHP for February 28, 2020, a mild sunny day (regular, i-mpc, ii-mpc and iii-mpc cases).	88
Figure 4-31 COP profile for February 28, 2020, a mild sunny day (regular, i-mpc, ii-mpc and iii-mpc cases).	88
Figure 4-32 Produced heat for different BIPV/T areas for the four investigated days (i-mpc, ii-mpc and iii-mpc cases).....	89
Figure 4-33 HP and ERV consumed energy for the four investigated days (i-mpc, ii-mpc and iii-mpc cases).	91
Figure 4-34 BIPV/T flow rate profiles for January 20, a very cold sunny day (i-mpc, ii-mpc and iii-mpc cases).	91
Figure 4-35 HP and ERV flow rate profiles for January 20, 2020, a very cold sunny day (i-mpc, ii-mpc and iii-mpc cases).	92
Figure 4-36 Power consumption profiles for January 20, 2020, a very cold sunny day (i-mpc, ii-mpc and iii-mpc cases).....	92
Figure 4-37 BIPV/T flow rate profiles for February 28, 2020, a mild sunny day (i-mpc, ii-mpc and iii-mpc cases).	93

Figure 4-38 HP and ERV flow rate profiles for February 28, 2020, a mild sunny day (i-mpc, ii-mpc and iii-mpc cases).....	93
Figure 4-39 Power consumption profiles for March 13, 2020, a mild semi-cloudy day (i-mpc, ii-mpc and iii-mpc cases).....	94
Figure 4-40 Percentage of produced heat sent to adjacent buildings (i-mpc, ii-mpc and iii-mpc cases).....	95
Figure 4-41 Energy savings for adjacent building (i-mpc, ii-mpc and iii-mpc cases).....	96
Figure 0-1 Scatter plot of predicted and measured ΔT for the Varennes BIPV/T data	107
Figure 0-2 BIPV/T flow rate profiles for February 02, a mild semi-cloudy day (i-mpc, ii-mpc and iii-mpc cases).	109
Figure 0-3 BIPV/T flow rate profiles for March 13, a mild semi-cloudy day (i-mpc, ii-mpc and iii-mpc cases).	110
Figure 0-4 HP and ERV flow rate profiles for February 02, a mild semi-cloudy day (i-mpc, ii-mpc and iii-mpc cases).....	110
Figure 0-5 HP and ERV flow rate profiles for March 13, a mild semi-cloudy day (i-mpc, ii-mpc and iii-mpc cases).	111
Figure 0-6 Net energy for the four investigated days (ii-s and ii-mpc case).	111
Figure 0-7 Net energy for the four investigated days (iii-s and iii-mpc case).	112

List of Tables

Table 3-1 Nusselt number expressions used RMSE for each examined case.....	35
Table 3-2 Time constant for different types of step inputs recorded during the experimental process.....	42
Table 3-3 Identified parameter values and NRMSE for BIPV/T models.....	44
Table 3-4 Initial guesses and bounds for calibrated parameters	55
Table 3-5 NRMSE for calibration cost function (TR model).....	60
Table 3-6 NRMSE for calibration cost function (SS model).....	60
Table 4-1 ERV Manufacturer specifications	63
Table 4-2 Model Predictive Control simulation settings	73

Table 4-3 Net energy consumption for SS model and TR model case.	78
Table 4-4 Energy consumption for base and i-mpc cases.....	81
Table 4-5 Energy consumption for i-s and i-mpc cases.....	84
Table 4-6 Average COP for the four investigated days (regular, i-mpc, ii-mpc and iii-mpc cases).	88
Table 4-7 Total and excess heat produced by the BIPV/T for the four investigated days (i-mpc, ii-mpc and iii-mpc cases).....	90
Table 4-8 HP and ERV consumed energy for the four investigated days (i-mpc, ii-mpc and iii- mpc cases).....	94
Table 4-9 Energy consumption for ventilation air in adjacent building (no assistance, i-mpc, ii- mpc and iii-mpc cases).....	96
Table 0-1 Energy consumption for all scenarios and all four examined days (TR model)	107
Table 0-2 Energy consumption for all scenarios and all four examined days (SS model).....	108

Nomenclature

Symbols

$A_{BIPV/T}$	Area of BIPV/T (m^2)
A_Z	Net occupiable floor area of the zone (m^2)
C_{ins}	Thermal capacitance of insulation ($J/(K \cdot m^2)$)
cp_{air}	Specific heat of air ($J/kg \cdot ^\circ C$)
C_{PV}	Thermal capacitance of PV ($J/(K \cdot m^2)$)
D_h	Hydraulic diameter (m)
f	Darcy friction factor
G	Incident radiation (W/m^2)
h_{c_ins} ($W/m^2 \cdot ^\circ C$)	Convective heat transfer coefficient from insulation to flowing air
h_{c_pv}	Convective heat transfer coefficient from PV to flowing air ($W/m^2 \cdot ^\circ C$)
h_{c_wind}	Convective heat transfer coefficient – wind losses ($W/m^2 \cdot ^\circ C$)
h_i	Film coefficient ($W/m^2 \cdot ^\circ C$)
h_{r_ch}	Radiative heat transfer between the PV and insulation surface ($W/m^2 \cdot ^\circ C$)
h_{r_sky}	Convective heat transfer radiative coefficient – sky losses ($W/m^2 \cdot ^\circ C$)
L	Channel length (m)
\dot{m}	Mass flow rate (kg/s)
m_{ashp}	Mass flow rate sent to ASHP from BIPV/T (kg/s)
m_{erv}	Mass flow rate sent to ERV from BIPV/T (kg/s)
Nu	Nusselt number
P_{elec}	Produced electricity (W/m^2)
PF	Packing Factor
Pr	Prandtl Number
$P_{thermal}$	Produced heat (W/m^2)
P_Z usage	The largest number of people expected to occupy the zone during typical usage
q_{air}	Recovered thermal energy from air (W/m^2)

$Q_{\text{electrical}}$	Electrical energy produced by the BIPV/T system (W)
Q_{ERV}	Additional power required by the EF to reach the ventilation setpoint (kW)
Q_{fan}	Power consumption of the BIPV/T fan (kW)
Q_{HP}	Power consumption of the ASHP (kW)
Q_{PV}	Electricity generation of the BIPV/T system (kW)
Q_{thermal}	Thermal energy produced by the BIPV/T system (W)
R_a	Outdoor airflow rate required per unit area
Re	Reynolds number
R_{ins}	Thermal resistance of insulation ($^{\circ}\text{C}/\text{W}$)
R_P	Outdoor airflow rate required per person
R_{PV}	Thermal resistance of PV ($^{\circ}\text{C}/\text{W}$)
T_{amb}	Ambient temperature ($^{\circ}\text{C}$)
T_{inlet}	Inlet temperature ($^{\circ}\text{C}$)
T_{ins}	Insulation temperature ($^{\circ}\text{C}$)
T_{ma}	Average air temperature inside the air channel ($^{\circ}\text{C}$)
T_{outlet}	Outlet temperature ($^{\circ}\text{C}$)
T_{PV}	PV temperature ($^{\circ}\text{C}$)
T_{room}	Temperature of the adjacent room ($^{\circ}\text{C}$)
T_{sky}	Sky temperature ($^{\circ}\text{C}$)
T_{STC}	PV module cell temperature at standard test conditions (25°C)
u_{ins}	Thermal conductance of insulation ($\text{W}/\text{m}^2\cdot^{\circ}\text{C}$)
u_{PV}	Thermal conductance of PV ($\text{W}/\text{m}^2\cdot^{\circ}\text{C}$)
V	Average air velocity inside the air channel (m/s)
W_{channel}	BIPV/T channel width (m)

Greek Letters

ΔP_f	Pressure drop along the BIPV/T channel due to the frictional losses (Pa)
α	PV absorptance
β_{PV}	PV module temperature coefficient ($\%/^{\circ}\text{C}$)
ΔT	Temperature difference

ε	Emissivity of surfaces
η_{PV}	PV electrical efficiency (%)
η_{STC}	PV module electrical coefficient under standard testing conditions (%)
ρ	Air density (kg/m ³)
σ	Stefan-Boltzmann constant (w/m ² ·K ⁴)
τ	PV transparency

Abbreviations

ABE	Active Building Envelope
AHU	Air Handling Unit
ASHP	Air Source Heat Pump
BIPV	Building Integrated Photovoltaic system
BIPV/T	Building Integrated Photovoltaic / Thermal system
COP	Coefficient of Performance
CPU	Central Processing Unit
DHW	Domestic Hot Water
DSF	Double Skin Facade
EC	Electrochromic
ERV	Energy Recovery Ventilator
EV	Electric Vehicle
GSHP	Ground Source Heat Pump
HDAB	Heat Delivery to Adjacent Buildings
HP	Heat Pump
HRV	Heat Recovery Ventilator
HVAC	Heating Ventilation and Air Conditioning
IAQ	Indoor Air Quality
MPC	Model Predictive Control
NRMSE	Normalized Root Mean Square Error
NZEB	Net-Zero Energy Building
PCM	Phase Change Material

PV	Photovoltaic
PV/T	Photovoltaic/Thermal system
RES	Renewable Energy Sources
RMSE	Root Mean Square Error
SS	Steady State
SSEC	Solar Simulator and Environmental Chamber
STPV	Semi-transparent PV
TES	Thermal Energy Storage
TR	Transient
TW	Thermal Wheel
VCS	Ventilated Concrete Slab

Chapter 1 Introduction

1.1 Overview

In recent years the energy sector has been undergoing a major transformation towards a low-carbon, efficient and environmentally sustainable system. Electrification plays a big part in this transition, by replacing the energy source of processes that traditionally used fossil fuels with electricity generated by zero or low-carbon fuels such as Renewable Energy Sources (RES). Apart from electrical heating and cooling, electrification of transport will create new high loads posing a great demand on the electrical grid. The government of Canada has set a target to reach 100% sales of electric passenger vehicles (EV) by 2035 [1] and the objective is to address these loads with RES.

According to the International Renewable Energy Agency Photovoltaic (PV) energy is one of the fastest-growing power sources. Exploring the scenario of a more extensive penetration of electrical end-use technologies and low-cost renewable energy shows a projected installed capacity of 1.66 TW for PV by 2050 (Figure 1-1). [2]

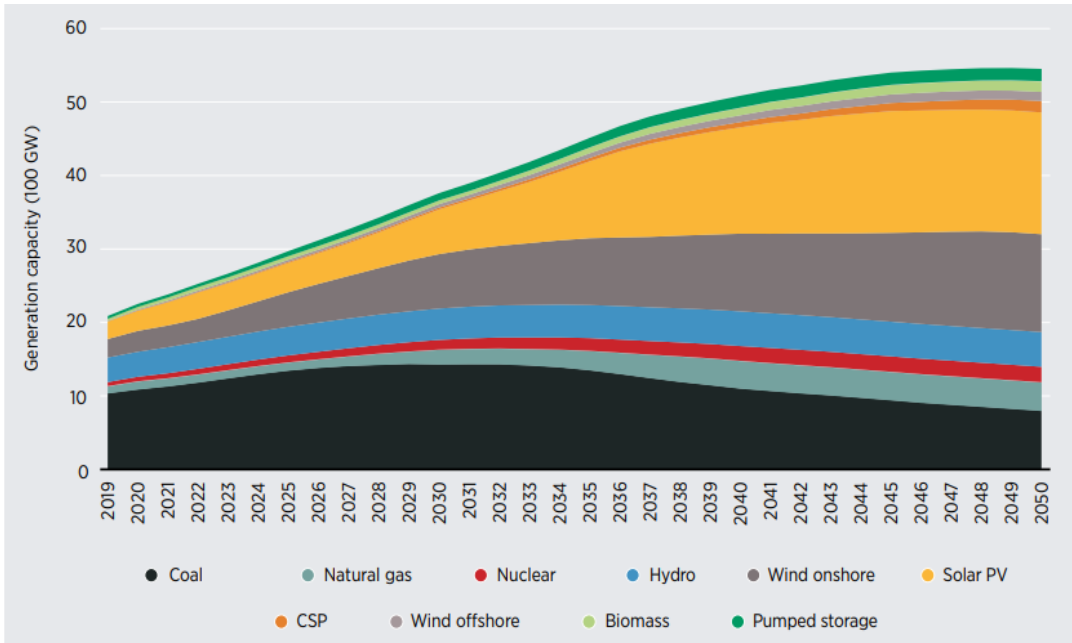


Figure 1-1 Generation capacity of various power sources in the Electrification Scenario, 2019-2050, [2]

However, the penetration of rapidly growing volumes of intermittent non-dispatchable RES into the traditional power system has led to an increasing need for energy flexibility and has highlighted the need for dynamic control of building-grid electricity flows.

Active building envelope design can provide a cost-efficient way to integrate RES creating local electricity generation centers which can minimize distribution losses and present an opportunity to create charging stations for EVs. As the cost of technologies like PV has decreased significantly over the years building integrated PV (BIPV) systems have become more common in new construction as well as renovations of old buildings. BIPV systems integrate solar technology into the building envelope and assist in the transition towards net-zero and net-positive energy buildings. At the same time higher architectural quality can be achieved compared to racked systems. Building Integrated Photovoltaic/ Thermal (BIPV/T) systems, a BIPV subcategory, combine the BIPV and solar thermal collector concepts generating both electricity and heat.

If designed and controlled properly, BIPV and BIPV/T can contribute to the reduction of the energy consumption of buildings and to higher energy flexibility. Although many studies have focus on the design of these systems the control has often been overlooked.

1.2 Motivation

A key factor in broader BIPV/T realization is optimal connection with the building HVAC. However, for successful BIPV/T-HVAC integration a control system must intervene in flows of energy between the building and the external environment. Higher mass flow rate within the BIPV/T channel leads to more heat recovery but lower outlet temperatures and vice versa (Figure 1-2).

A control algorithm regulating the airflow can achieve a balance between the two while considering the end use of the recovered heat and the respective environmental conditions. Attention though needs to be given to the model used for the advanced control strategies such as Model Predictive Control (MPC). Since MPC can add a high load to the CPU of the computer, using a complex high order model can compromise the fast response and negatively affect the performance of the control algorithm. [3]

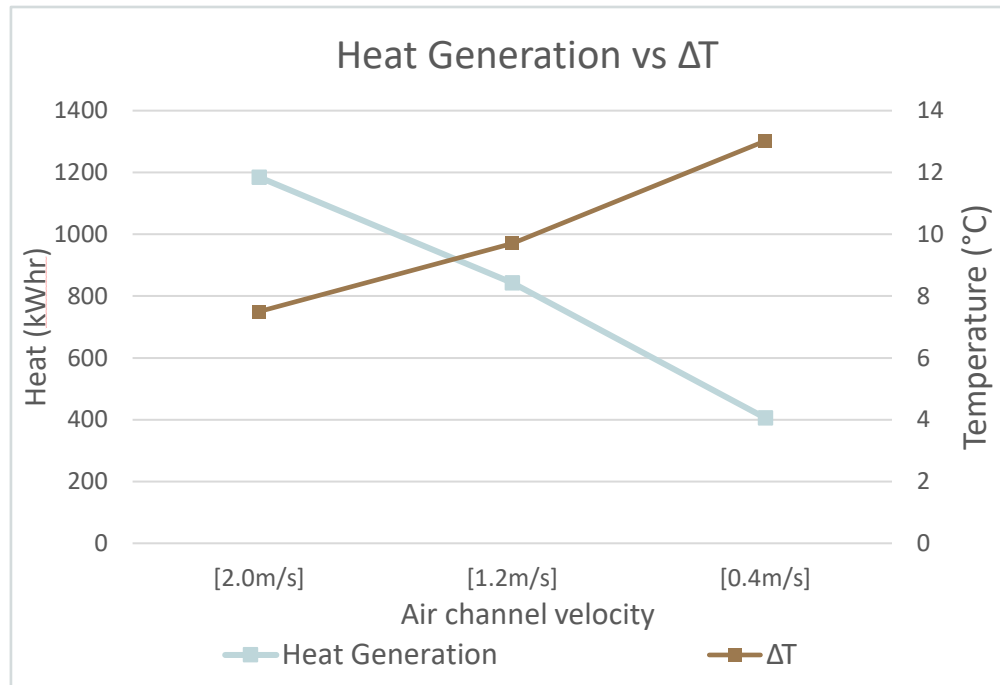


Figure 1-2 Heat generation and achieved ΔT for different air channel velocities in an air-based BIPV/T system

Despite the high quantity of studies focused on BIPV/T systems, optimal control rarely has been investigated. This work aims to provide some guidelines on developing simplified BIPV/T models designed for model-based control and present the benefits of optimal control on BIPV/T systems using a full-scale BIPV/T system as a case study.

1.3 Main Objective

The purpose of this investigation is twofold. Firstly, the development of a control-oriented grey-box BIPV/T model that enables MPC of the BIPV/T flowrate with the objective of optimal integration with the building HVAC. With the grey box modelling approach, the complexity of the model is reduced, compared to a white box, but can still maintain the basic physiological structure of the system. The significance of adding the thermal capacitance of the materials comprising the BIPV/T system for a control-oriented model is evaluated.

Secondly, an MPC strategy for the BIPV/T flow rate is developed. The full-scale BIPV/T system located at the Varennes library is used as a reference to explore different possibilities and improvements that can be made through optimal control. The Varennes library is the first

institutional net-zero energy building in Canada and uses the BIPV/T technology to produce heat along with electricity to pre-heat the ventilation fresh air during the winter months. The commissioned system is controlled through a simple rule-based strategy based solely on the outlet temperature. By applying MPC the control algorithm makes prediction of future conditions and applies a sequence of orders to the model. Different scenarios are explored including half or full roof coverage with BIPV/T (the actual BIPV/T system covers only 16% of the south-facing roof), simultaneous heat delivery to multiple thermal applications and providing excess heat to nearby buildings.

This work can provide useful guidelines and be used by engineers, building operators and scientists in order to apply advanced control strategies in BIPV/T systems either during the design process or for already commissioned systems. This can facilitate in evaluating the energy performance of a BIPV/T system integrated with the building HVAC and help in the selection the most suitable thermal applications for the respective system.

1.4 Thesis Outline

This thesis contains five chapters, the first being the introduction. The rest of the chapters are summarized as follows:

Chapter 2: Literature review of BIPV/T technology and modelling, thermal enhancement methods and possible thermal applications of the collected heat. Different control approaches from various studies are presented.

Chapter 3: The development of the BIPV/T models is described. Initially the model was developed using data from an experimental procedure carried out in the solar simulator. It was concluded that in order to better assess the performance of the models, real weather conditions were necessary. The Varennes library BIPV/T system is introduced followed by a description of the available data for this system. Finally, the calibration and validation of the models using the obtained data is presented.

Chapter 4: The MPC strategy is presented along with the different scenarios explored. The possibility to cover a larger part of the Varennes library roof with BIPV/T is analyzed. Lastly the results and discussion follow.

Chapter 5: In the final chapter, the main findings and contributions of this research are presented.

Chapter 2 Literature Review

This chapter reviews the main literature on BIPV/T technology, common approaches in thermal modelling of BIPV/T systems as well as thermal enhancement methods. Finally, the importance of optimal control in BIPV/Ts is discussed and the most common control approaches are presented. Through this literature review, the most important research needs, and opportunities were identified, which comprise the motivation behind this research.

2.1 Active Building Envelopes

In the approach to achieve net-zero energy buildings a great number of researchers and engineers are actively promoting innovative building envelopes. Although passive building envelope systems dominate building design, active or adaptive building envelope (ABE) systems are rapidly gaining interest as they present great opportunities to address building energy efficiency and occupant comfort. [4]

ABE have the ability to alter their heat and mass transfer characteristics and adapt to or take advantage of changing boundary conditions, such as short-term weather fluctuations, number of occupants and occupant's requirements and preferences. [5], [6]

These systems can actively utilize energy input for space heating and cooling, daylighting, ventilation and water heating directly reducing the demand on the HVAC system and often boosting its performance. ABEs can also capture and convert solar and wind energy in to electrical and/or thermal energy. The energy can then be directly used, sold to the grid, or stored with the objective of achieving higher building energy efficiency and flexibility [6], [4]

Luo et al. [4] categorize ABE in to four main categories:

- i) Air-based active building envelopes. These systems use air as a mean to transfer, remove or collect thermal energy. An air layer-based envelope can achieve higher thermal resistance. Air can have a significant advantage compared to liquid systems

- as it can eliminate the risk of freezing or leakage and requires less frequent maintenance. The thermal energy can be collected either by natural forces (buoyancy induced) or mechanically (fan assisted systems). A common application of air-based ABEs are Double Skin Facades (DSF). [7]
- ii) Water-based active building envelopes. As water has higher thermal capacity and heat transfer capability it is often preferred over air as it can achieve higher system efficiency. Luo et al. point out that there are significantly more studies on water-based systems rather than air-based which reflects this preference. However, great attention must be given to the installation of this type of system as it must be reliable and leak resistant. Pipe-embedded envelope systems are an example of water-based ABEs. [8]
 - iii) Solid-based active building envelopes. Three subcategories are included in solid-based ABEs. PV, electrochromic (EC) and PV-EC. By incorporating PV modules in the building envelope, the building can transition from an energy consumer to an energy producer. EC facades can modify their transmittance and control daylight and heat gains in adjacent zones.
 - iv) Kinetic active building envelopes. The last group of ABEs does not need a working medium. The envelopes have the ability to change and adjust their shape controlling and optimizing light penetration, heat gains, natural ventilation and even generate power.

2.2 Building Integrated Photovoltaic (BIPV) systems

PV has been characterized as one of the pillars of sustainable energy systems with continuing increase in installed capacity and is predicted to reach 43 per cent of the global installed energy capacity by 2050. The globalization of the solar PV market was enabled by the dramatic cost reductions of more than 80% in the last decade. [9]

The transfer of PV into buildings has the potential to bring a building closer to the status of “net-zero energy” or even “net-positive”. The integration into the building skin can be done on the façade, roof or even windows with the use of semi-transparent PV (STPV). Figure 2-1 shows different types of BIPV systems installed on the building envelope.

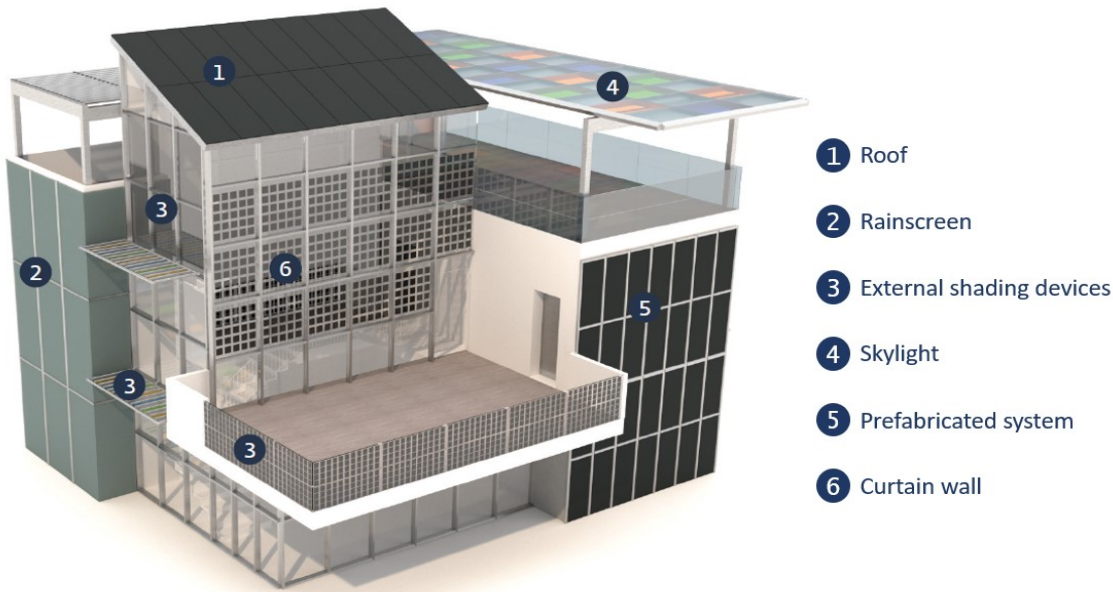


Figure 2-1 Placement possibilities for BIPV systems, [54]

2.3 Building Integrated Photovoltaic/Thermal (BIPV/T) systems

Building Integrated Photovoltaic/ Thermal (BIPV/T) systems are hybrid systems that combine the BIPV and solar thermal collector concepts. By passing a fluid, usually air or water, behind the PV modules heat is extracted cooling down the PV surface which can lead to higher electrical performance and longer PV life expectancy. At the same time the heat can be collected and directly used or stored.

The main advantages of BIPV/T compared to an add-on side-by-side PV and thermal collector can be summarized as:

- a) Higher architectural and aesthetic integration,
- b) Higher energy production from the same surface area
- c) Increased PV performance
- d) Lower material cost by replacing conventional building elements [10]

BIPV/T collectors can be classified based on the fluid type to water/liquid based or air based. [11] Although water-based PV/T systems have significantly higher thermal efficiency air-based systems can be better suited for building integration as they eliminate the risk of leakage and freezing and need less frequent maintenance. [12]

The recovered heat from air-based BIPV/T systems can be utilized in different thermal applications and assist or enhance the performance of the building's HVAC. [13] Some of the most common applications include using the solar heated air as a source for an air-source heat pump, enhancing the performance of an energy recovery ventilator and thermal storage charging.

2.4 BIPV/T Categories

As previously mentioned BIPV/T is a smart energy production system that integrates PV panels in different parts of the building envelope (roof, façade, windows etc.) and at the same time recovers wasted heat which can be utilized for the building needs (preheating ventilation air, assisting air-source heat pumps etc.).

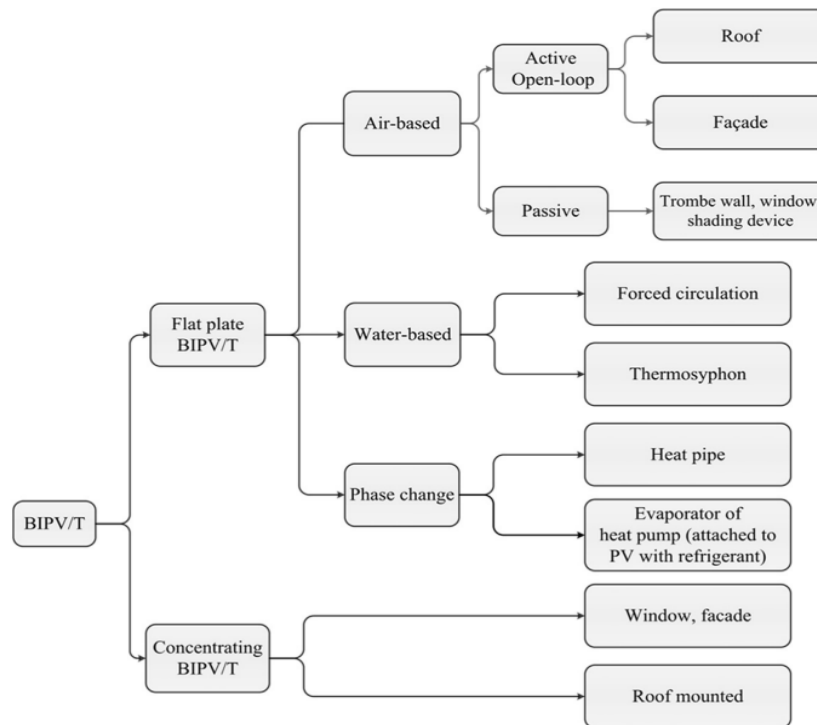


Figure 2-2 BIPV/T Categorization, [14]

BIPV/T systems can be categorized based on the absorber morphology to flat-plate and concentrating collectors. When considering the cooling medium BIPV/Ts can be discretized to air-based and liquid-based (usually water or glycol), while there have also been some examples of systems using a phase change working medium such as BIPV/T with either heat pipe or heat pump evaporator. [14]

Air-based systems can be either open-loop or closed-loop (Figure 2-3). Compared to closed-loop liquid systems, air-based open-loop systems have generally lower initial and maintenance costs, reduced risk of leakage or freezing and are more light-weight and easily attached to the building envelope.

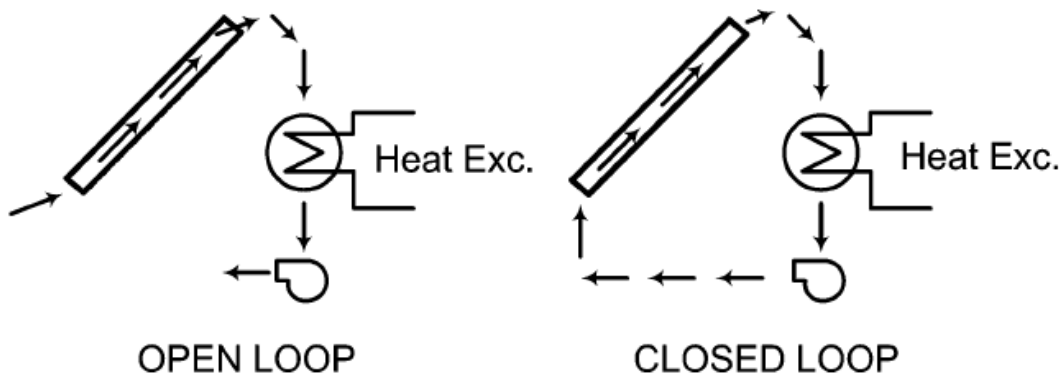


Figure 2-3 Open and closed loop configurations (the heat exchanger is optional in open loop), [15]

By opting for an open-loop system, since the systems runs at lower temperatures, higher thermal efficiency and better PV performance and durability can be achieved. [14]

When the air circulation is driven by a fan the BIPV/T is considered an active system. When the air is buoyancy-driven the system is considered passive. Examples of passive systems include Trombe-walls and buoyancy driven DSFs.

Depending on the transparency, BIPV/T systems can be further categorized as opaque and semi-transparent. Opaque systems are suitable for installation on roofs, facades, as shading devices, and any other part of the building that isn't used for daylighting or view to the outside. On the other hand, semi-transparent systems can present higher flexibility on the installation placement. STPVs can be incorporated in windows and skylights and besides producing electricity and heat, assist in daylighting optimization and control. Apart from the transparent parts of the building

where STPVs would traditionally be placed, locations such as opaque facades or roofs can also benefit by using STPVs. Yang and Athienitis [16] performed an experimental study where two

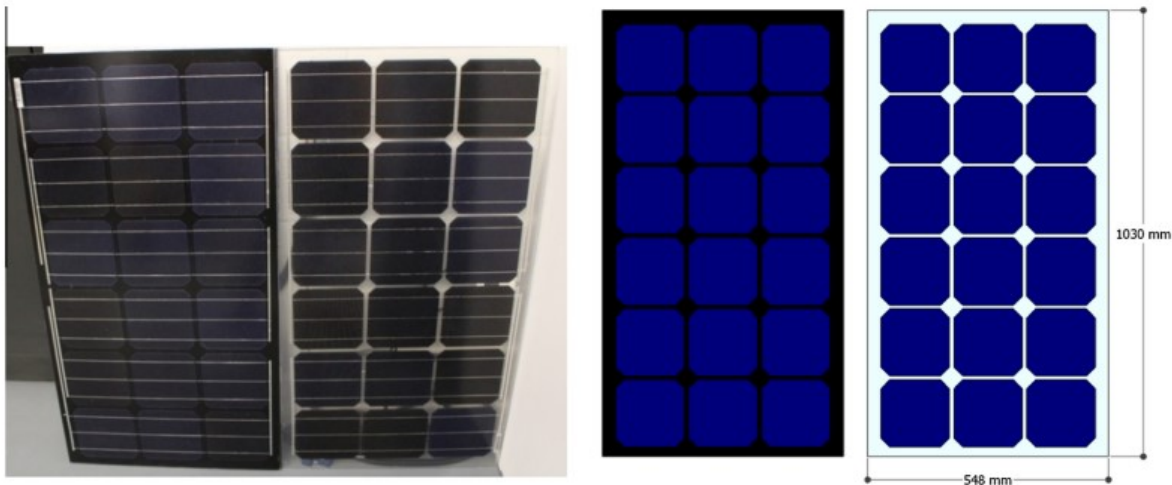


Figure 2-4 Opaque and semi-transparent PV panels with same packing factor used in [16]

BIPV/T systems are investigated, one using opaque and one with semi-transparent PV panels. For both systems with the same packing factor (PF), both electrical and thermal performances increased when using STPV. With the use of STPV the radiation absorbed by the PV layer is reduced and therefore the PV temperature decreases leading to better PV performance. Further, the transmitted radiation to the rear surface facilitates for higher air temperatures.

2.5 BIPV/T Modelling

Typically, air-based BIPV/T systems consist of the PV layer, an air-channel where the air circulates and extracts heat from the PV modules and the back layer which is part of the building envelope (exterior wall or roof with insulation). A typical BIPV/T system functioning as a roof is shown in Figure 2-5.

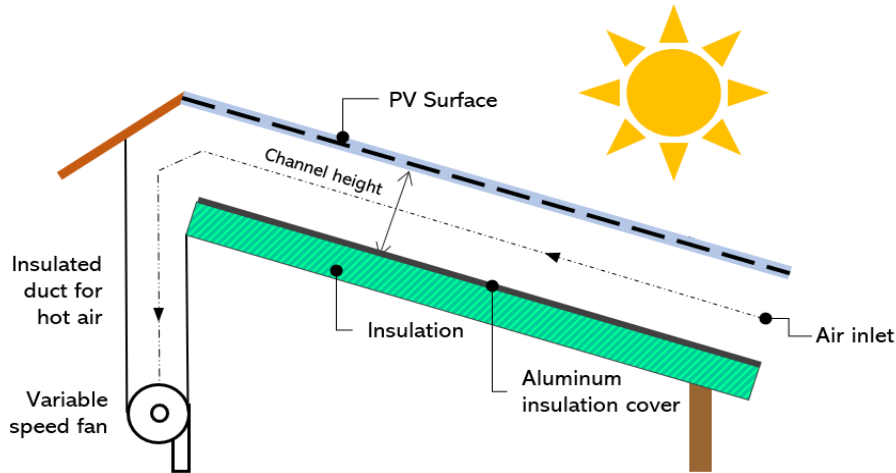


Figure 2-5 Typical roof-integrated BIPV/T system

The energy balance of BIPV/T systems is commonly modelled using thermal network method with finite control volumes. The BIPV/T models can be steady-state (SS) where the model does not consider the thermal capacitance of the materials or transient (TR) where the thermal inertia (capacitance) is included in the energy balance.

Candanedo et al. [15] argue that by incorporating the thermal inertia of the materials, the BIPV/T model predicts a more stable outlet air temperature. This is attributed to the damping effect of the heat capacitance of the materials and can prove extremely useful for control purposes. However, transient models require more inputs and more processing time which can negatively affect the controller's performance.

In a study by Bilbao and Sproul [17] a detailed transient model for a PV/T water collector is developed using RC networks. The authors indicate that as more detailed weather data becomes available, and computers become stronger it is more feasible to develop transient models which can allow a better comparison of experimental data and model performance. Furthermore, transient models can offer more information about the system performance and help optimize new PV/T systems. In this study the developed model is calibrated using experimental data and then compared to a steady-state model. The developed transient model resulted in a lower RMSE and higher R^2 which can be important when transient responses are examined

The solution of the equations of the SS model is independent of previous conditions whereas, at every time step, the TR model requires the solution of the previous time step with a fully explicit finite difference scheme.

Figure 2-6 illustrates a schematic of the energy balance for both types of BIPV/T models.

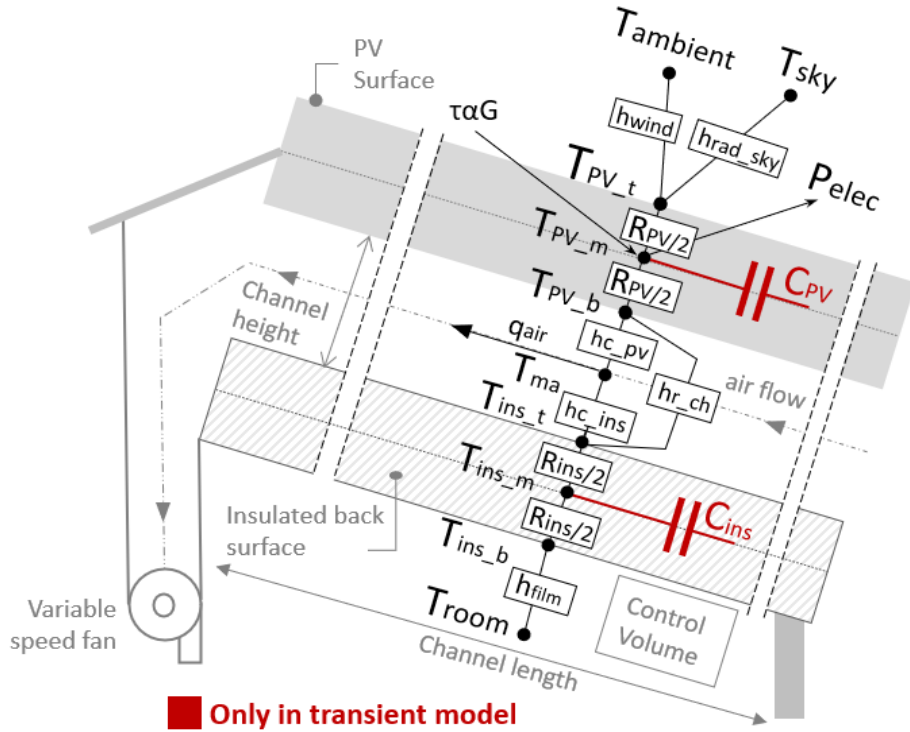


Figure 2-6 Thermal network for transient and steady state BIPV/T models

Where:

- T_{ambient} : the ambient temperature ($^{\circ}\text{C}$).
- T_{sky} : the sky temperature ($^{\circ}\text{C}$)
- T_{PV} : the PV temperature at 3 layers (top, middle, bottom) ($^{\circ}\text{C}$)
- T_{ma} : the average air temperature inside the air channel ($^{\circ}\text{C}$)
- T_{ins} : the insulation temperature at 3 layers (top, middle, bottom) ($^{\circ}\text{C}$)
- T_{room} : the temperature of the adjacent room ($^{\circ}\text{C}$)
- $R_{\text{PV}}, R_{\text{ins}}$: the thermal resistance of PV and insulation ($^{\circ}\text{C}$)
- h_{wind} : the convective heat transfer coefficient – wind losses ($\text{W}/\text{m}^2\cdot^{\circ}\text{C}$)
- $h_{\text{rad_sky}}$: the convective heat transfer radiative coefficient – sky losses ($\text{W}/\text{m}^2\cdot^{\circ}\text{C}$)
- $h_{\text{c_pv}}, h_{\text{c_ins}}$: the convective heat transfer coefficients from the PV and the insulation surface to the flowing air ($\text{W}/\text{m}^2\cdot^{\circ}\text{C}$).
- $h_{\text{r_ch}}$: the radiative heat transfer between the PV and the insulation surfaces ($\text{W}/\text{m}^2\cdot^{\circ}\text{C}$)
- $\tau\alpha G$: absorbed incident radiation by the PV layer (W/m^2)

- P_{elec} : produced electricity (W/m^2)
- C_{PV}, C_{ins} : thermal capacitance of PV and insulation respectively ($J/(K \cdot m^2)$)

At each node the temperature is calculated using the following explicit finite difference equation:

$$T_i^{p+1} = \frac{\Delta t}{C_i} \cdot \left[Q_i^p + \sum_{j=1}^n \frac{T_j^p - T_i^p}{R_{ij}} \right] + T_i^p \quad \text{where} \quad \Delta t \leq \frac{C_i}{\sum_{j=1}^n U_{ij}} \quad (2-1)$$

The electrical efficiency of a PV modules is related to its temperature and can be determined from equation [18]:

$$\eta_{PV} = \eta_{STC} \cdot (1 - \beta_{PV} \cdot (T_{PV} - T_{STC})) \quad (2-2)$$

where:

- η_{STC} : the PV module electrical coefficient under standard testing conditions (%)
- β_{PV} : the PV module temperature coefficient ($\%/^{\circ}C$) (usually between 0.004 – 0.006)
- T_{PV} : the measured PV module cell temperature ($^{\circ}C$)
- T_{STC} : the PV module cell temperature at standard test conditions ($25^{\circ}C$)

As the temperature of the module increases over $25^{\circ}C$ the electrical efficiency decreases. This highlights the importance of efficiently cooling the PVs.

In order to simplify BIPV/T thermal modeling several assumptions are commonly made such as:

- 1) The temperatures of the surfaces (PV, steel sheet, insulation board) are assumed to be uniform inside the control volume.
- 2) The temperatures of the solar cells, the air within the channel and the insulation vary only in the direction of flow of the air. For each control volume of the energy balance, the heat path is assumed perpendicular to the layers comprising the control volume. This results in an average temperature for each layer of the control volume. (1-D simulation inside the control volume)
- 3) The fluid medium is assumed to have a uniform velocity profile and an average fluid velocity throughout the channel.
- 4) The heat loss from the side of the system is negligible

2.6 BIPV/T Efficiency Enhancement

Quantifying the performance of BIPV/T systems, which produce two types of energy, presents the challenge of fairly evaluating both thermal and electrical energy produced. The most common approach to evaluate the BIPV/T performance is to sum the electrical and thermal efficiencies. However, this can be misleading when estimating the actual useable energy delivered. [12] In most applications electrical energy has a higher value than thermal thus a conversion factor should be used to calculate the combined efficiency of the system.

Athienitis et al. [19] present a study of a prototype PV/T system integrated with a transpired collector and introduce an equivalent thermal efficiency calculation. In this approach the electrical energy is converted into equivalent thermal energy by multiplying by the heat pump coefficient of performance (COP).

The equivalent thermal efficiency of the BIPV/T is given by:

$$\eta_{BIPV/T} = \frac{Q_{thermal} + COP \cdot Q_{electrical}}{A_{BIPV/T} \cdot G} \quad (2-3)$$

Where,

- $Q_{thermal}$: Useful thermal energy produced by the BIPV/T system (W)
- $Q_{electrical}$: Electrical energy produced by the BIPV/T system (W)
- $A_{BIPV/T}$: Area of BIPV/T (m^2)
- COP: Coefficient of Performance of Heat Pump
- G: Incident Solar Radiation (W/m^2)

This equation is suited to a system that heats ventilation air and is possibly not suited to other applications. Nevertheless, more work is needed on this topic.

The overall thermal performance of the hybrid system was lower than that of an Unglazed Transpired Collector (UTC). However, if the energy produced was expressed in terms of

equivalent thermal energy, the overall efficiency of the hybrid system was calculated 7-17% higher than that of the traditional UTC (Figure 2-7).

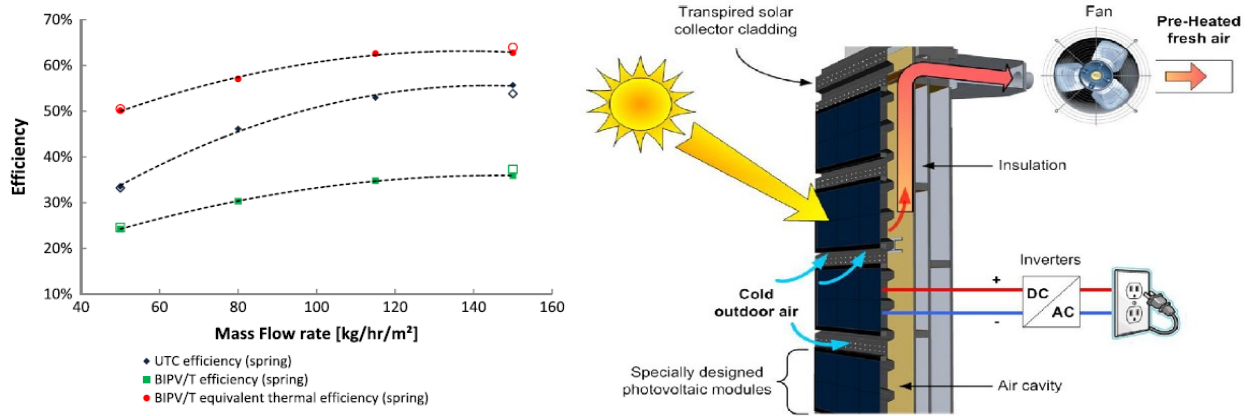


Figure 2-7 Thermal efficiency of a hybrid UTC and PV/T system, as a function of the mass flow rate, [19]

The parameters that affect the thermal and electrical performance of a BIPV/T collector are:

- i) the geometry of the channel (length, height etc.)
- ii) the inclination angle
- iii) the characteristics of the PV modules (electrical efficiency, absorptance, transmittance, packing factor, glazed/unglazed)
- iv) the respective weather conditions (ambient temperature, irradiance, wind speed)
- v) the mass flow rate

Parameters (i)-(iii) are determined during the design stage of the system and are to a certain degree restricted to the geometry and desirable appearance of the building element (façade, roof etc.) the BIPV/T will be incorporated in.

Longer air-channels have been proven to contribute to higher outlet temperatures but may lead to overheating of the PVs at the end part of the channel. Based on this, a common method to increase thermal efficiency is the development of double pass PV/T collectors. Sopian et al. [20] studied the performance of both single and double-pass PV/T air collectors. The double-pass photovoltaic thermal solar collector appeared to have better performance over the single-pass model at a normal operational mass flow rate range. The improved performance can be attributed to the cooling of the PV and reduction in the temperature of the glass cover. [20]

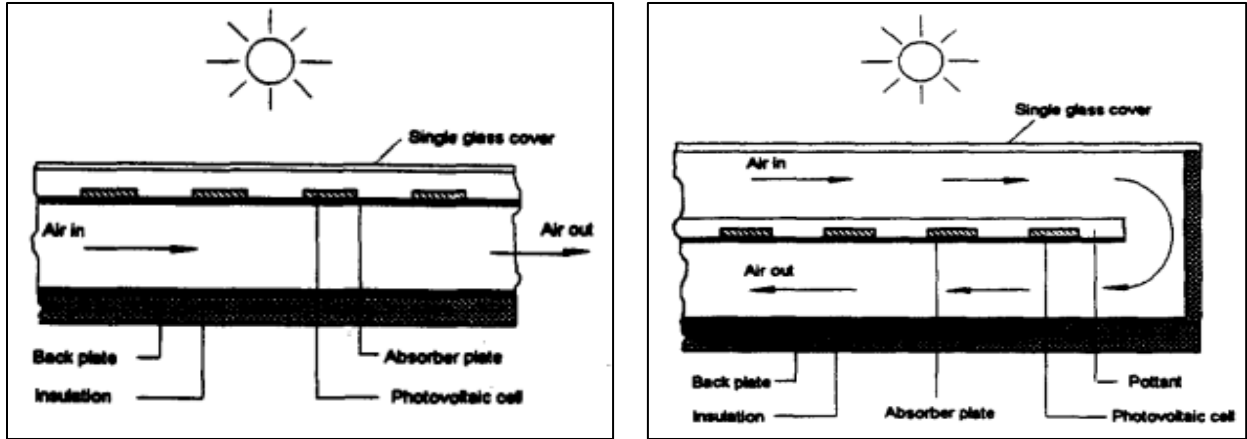


Figure 2-8 Single and double pass PV/T air collectors investigated by [20]

Agrawal and Tiwari [21] developed a BIPV/T model and four different design cases are compared. Amongst the 4 design cases 6 BIPV/T rows are connected either in parallel in series or in a mixed connection and provide heated air into a room. Results showed that for a constant mass flow rate the BIPV/T connected in series, the system with one long channel, provided a higher outlet temperature. The BIPV/T system connected in parallel, shorter multiple channels, collected higher amount of heat with thermal efficiency of 50% (higher than any other case) and maintained lower PV temperatures thus higher electrical efficiency.

Rounis et al. [13] developed a BIPV/T curtain wall prototype and evaluated various thermal enhancement methods including multiple inlets in the air channel using semi-transparent instead of opaque PV and the use of a flow deflector. The prototype design was based on a well-established building practice and was tested under experimental conditions.

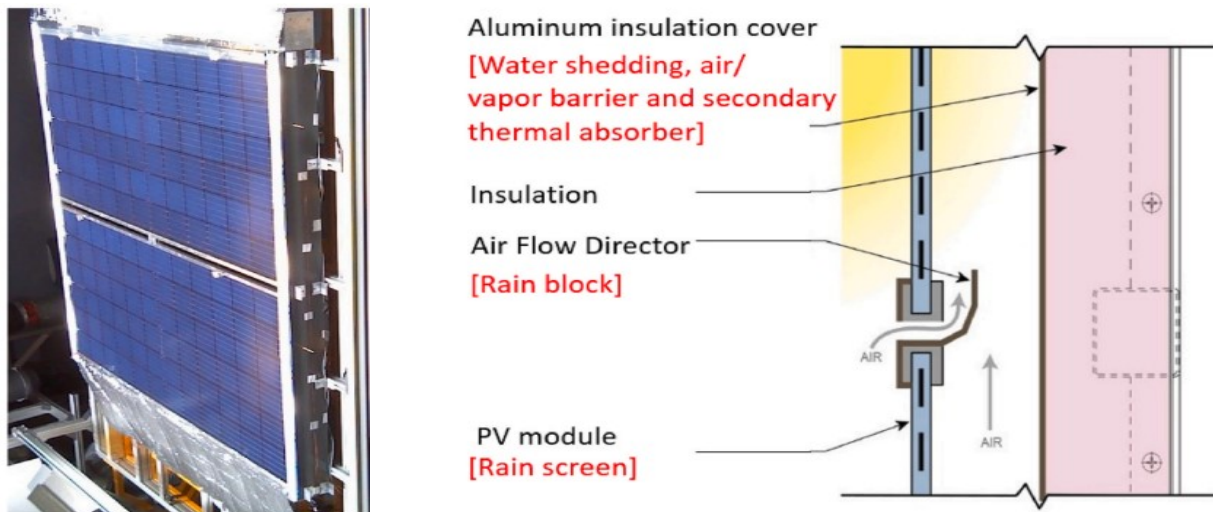


Figure 2-9 BIPV/T functioning as a curtain wall investigated by [13]

Results showed that the use of multiple inlets and a flow deflector unit improved the thermal performance of the BIPV/T by up to 16% and had a small positive effect on the electrical efficiency by decreasing the maximum PV temperatures by up to almost 4°C. The use of STPV lead to more heat recovery from the back side of the air channel.

Another approach to increase the efficiency of PV/T collector is the use of a glass cover over the PV cells. The glass cover can protect the PVs from external damaging conditions and help reduce the heat losses to the surroundings. However, a glazing layer can reduce the solar radiation that can reach PV cells and can lead to PV overheating as the natural cooling by the external wind is diminished. This can have a negative impact on the electrical performance of the collector. Depending on the targeted energy one or more glass covers can be added. For higher electricity production unglazed systems are preferred while glazed systems promote higher heat production.

Various modification within the air channel such as the addition of fins, thin metal sheets and Phase Change Materials (PCM) can contribute to higher thermal efficiency.

Tonui and Tripanagnostopoulos [22] investigate the addition of fins (FIN) attached to the back wall and a thin metal sheet (TMS) suspended at the middle of the air-channel with the goal to enhance heat transfer to air stream within the air channel. The addition of a glazing cover was also examined. A numerical model was developed and validated against the experimental data.

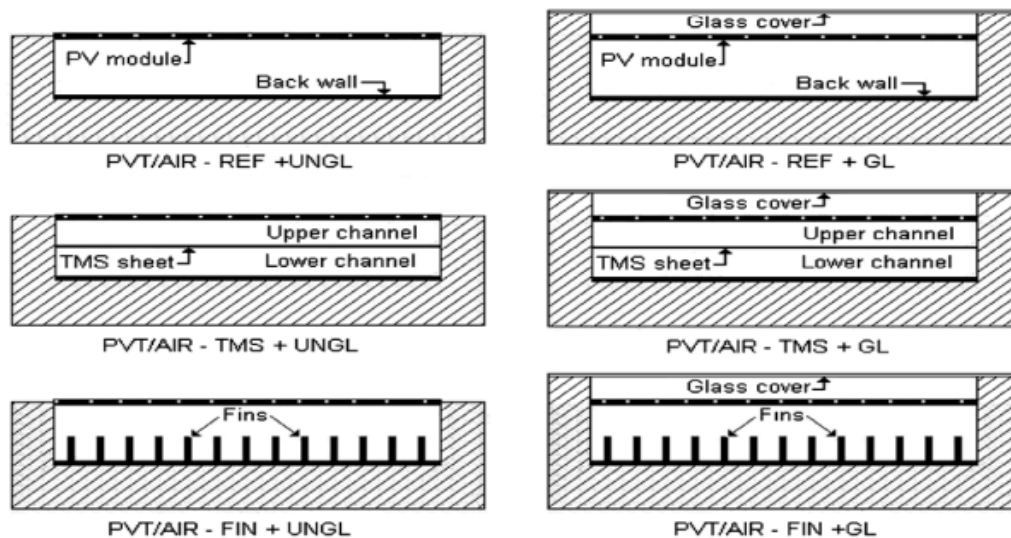


Figure 2-10 Examined systems by [22]. From top to bottom: Reference system, Thin Metal Sheet system, Fin System. Left column: Unglazed Systems, Right column: Glazed Systems

The modified systems performed better contributing positively towards enhancing heat extraction from PV module for better electrical and thermal energy production. The glazed systems exhibited higher thermal performance but appeared to result in higher PV temperatures reducing the produced electricity. The authors conclude that these modifications can be a cost-effective way to achieve higher efficiency and are suitable for building integration.

In Assadeg et al. [23] the energy performance of a double pass solar air collector with fins and phase change material is analyzed Figure 2-11. The addition fins allows more heat to be absorbed by the air in the bottom duct, in addition to the stored heat by the PCM which helps in reduce heat losses inside the system. With the proposed system the energy efficiency improvement potential is +5.8% for a solar radiation of 1000 W/m^2 and mass flow rate 0.09 kg/s .

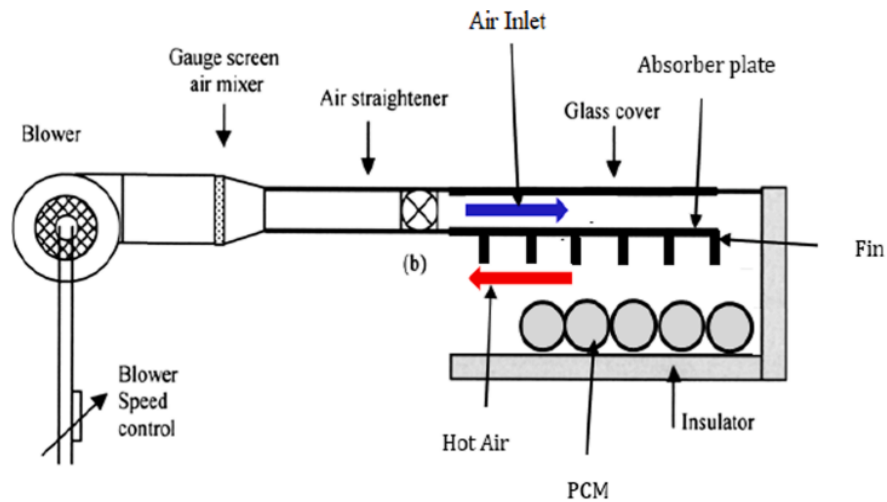


Figure 2-11 Schematic diagram of double pass solar air collector with fins and PCM [23]

Curpek et al. [24] performed an experimental study to evaluate the effect of PCM installed on the rear side of the PV panel of a ventilated PV façade system. An experimental procedure was conducted at an outdoor full-scale setting under real climatic conditions. The air flow within the ventilated façade was buoyancy driven and the tests were conducted during the cooling season, when there is a higher chance of the system overheating. By installing PCM in the PV system this study showed a decrease in the operating temperature of the PVs within a max range of 6-9 °C with a 2-h delay between peaks caused by the high thermal inertia of the PCM. During the night when the PCM freezes the temperature of the PVs increases up to 6°C. A similar pattern was observed for the air temperature within the cavity as well. The authors conclude that the two

main benefits of incorporating PCM into a BIPV/T are the decrease of the PV panels temperature and therefore higher electrical performance and the increase of the overall thermal inertia of the system.

The amount of heat transferred to the moving fluid within a BIPV/T system is calculated by:

$$Q_{thermal} = \dot{m} \cdot c_p \cdot \Delta T \quad (2-4)$$

where:

- $Q_{thermal}$: the thermal energy transferred to the moving fluid (W)
- \dot{m} : the mass flow rate inside the channel (kg/s)
- c_p : the specific heat capacity of the moving fluid (J/kg/°C)
- ΔT : the temperature difference between the collector and the fluid (°C)

By examining the above equation, it is evident that higher mass flow rate within the collector can lead to increased production of thermal energy. However high mass flow rates can reduce the outlet temperature of the BIPV/T decreasing the achieved ΔT .

Assadeg et al. [23] evaluate the performance of their solar air collector under different mass flow rates and observe a raise in energy efficiency by 156.14% by increasing the mass flow rate up

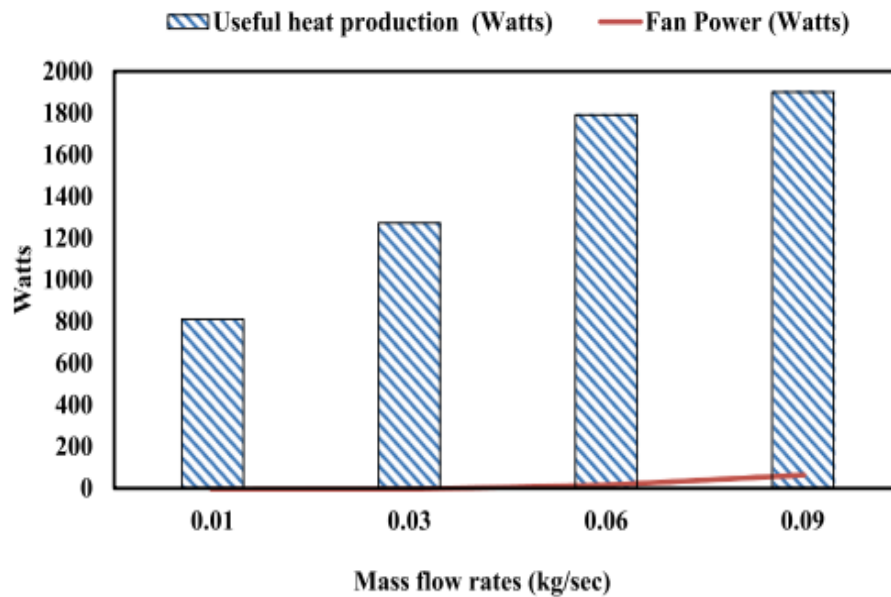


Figure 2-12 Useful heat production and fan power of proposed collector [23]

until 0.06kg/s. After a flow rate of 0.06 kg/sec the increment in efficiency seems to decrease in value while the fan consumption increases (Figure 2-12).

Similarly, Sopian et al. [20] examine the effect of the mass flow rate on the collector efficiency and show that the electrical, thermal and combined efficiencies increase as the mass flow rate increases, since the absorber plate will be cooled by the incoming working fluid. After a certain point the rate of increase in efficiency decreases. On the other hand, increasing the mass flow rate decreased the outlet temperature of the collector.

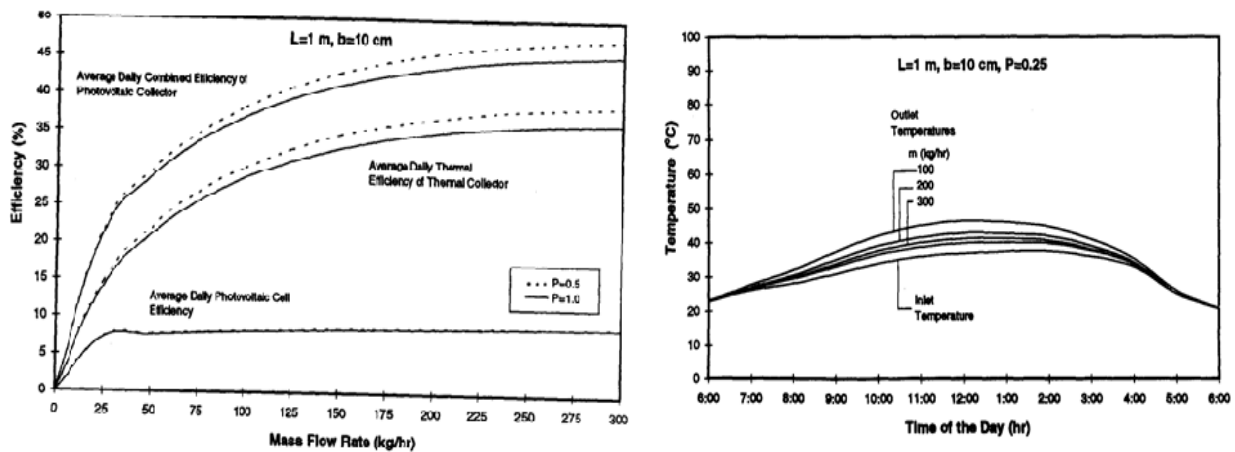


Figure 2-13 Effect of mass flow rate on efficiency (left) and outlet temperature (right), [20]

It is important to note that while methods such as addition of fins, the addition of a glazing cover, incorporating PCM in the channel or the decision of single or double pass channels need to be made during the design process or would require a major modification of an actual system.

Optimal control of the BIPV/T mass flow rate needs little to no physical interventions and can be easily applied to an existing operating system.

2.7 Thermal Applications

The decision of the optimal mass flow rate, and therefore outlet temperature, of a BIPV/T system heavily depends on where the recovered heat is intended to be used. The heated air from air-based BIPV/T systems can be utilized in different thermal applications and enhance the performance of the HVAC system of the building. Some of the most common applications include being a heat source for an air-source heat pump (ASHP), enhancing the performance of

an energy recovery ventilator (ERV), heating water through an air-water heat exchanger and thermal storage charging.

Energy Recovery Ventilator

The importance of improving Indoor Air Quality (IAQ) has become more prominent than ever considering the recent developments on public health and the ongoing pandemic. New measures addressing HVAC operation strategies promoting healthier occupant conditions have taken place including the increase of outdoor air ventilation and minimization of the recirculation air. [25] BIPV/T systems can increase the supply of fresh air by mitigating the additional required consumption.

Air-to-air ERVs recover heat and/or moisture between two airstreams at different temperatures and humidities. By incorporating ERVs into the Air Handling Unit of the building can significantly contribute to maintaining acceptable IAQ while reducing the overall energy consumption and carbon dioxide emission. [26] Higher supply temperature can facilitate in reducing the risk of frost within the ERV during low outside temperatures and overall can help improve the performance of the equipment. Figure 2-14 illustrates a typical schematic of an-air to-air ERV.

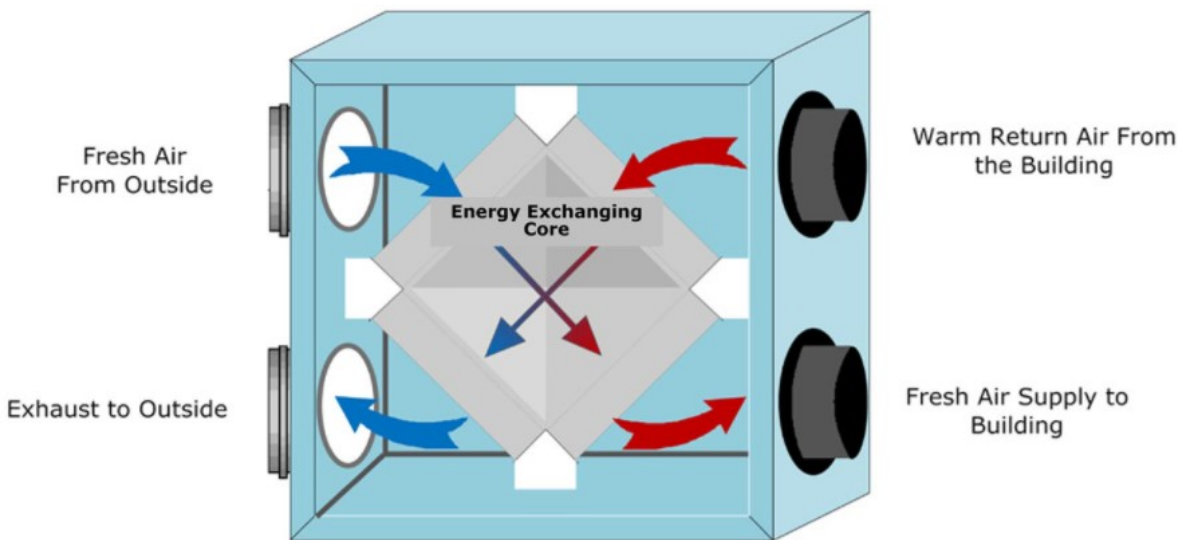


Figure 2-14 Schematic of an Energy Recovery Ventilator, [55]

Ahn et al. [27] study how coupling a PV/T collector with a Heat Recovery Ventilator (HRV) can improve the ventilation efficiency. An experimental procedure was conducted where two cases

were compared. Using the preheated air from the PV/T versus outdoor air as an inlet for the HRV. The flow rate and room temperature were set a constant values. A temperature difference of 7-15 °C between the inlet and outlet of the PV/T was achieved. Thus, problems caused by very low temperatures could be avoided. The heat transfer efficiency of the HRV was also improved by 20% when using PV/T preheated air.

In a study by Shahsavar and Khanmohammadi [28] a hybrid BIPVT and thermal wheel (TW) system are investigated where the energy and exergy are compared for different systems (BIPVT, TW, BIPVT + TW). Through a multi-objective optimization technique, the optimal combination of parameters is obtained in order to achieve the highest annual energy and exergy of the system. The authors conclude that using the BIPVT + TW system is more efficient than using traditional heat recovery wheel or only a photovoltaic thermal system.

Ahmed-Dahmane et al. [29] examine a BIPV/T system connected to an air handling unit (AHU). The simulated system is integrated in a high-rise office building and the air flow rate of the PV/T is calculated based on the ventilation requirements of the building. During cold weather by preheating the ventilation air the average rate of saved useful thermal energy was 24.20%.

Air-Source Heat Pump

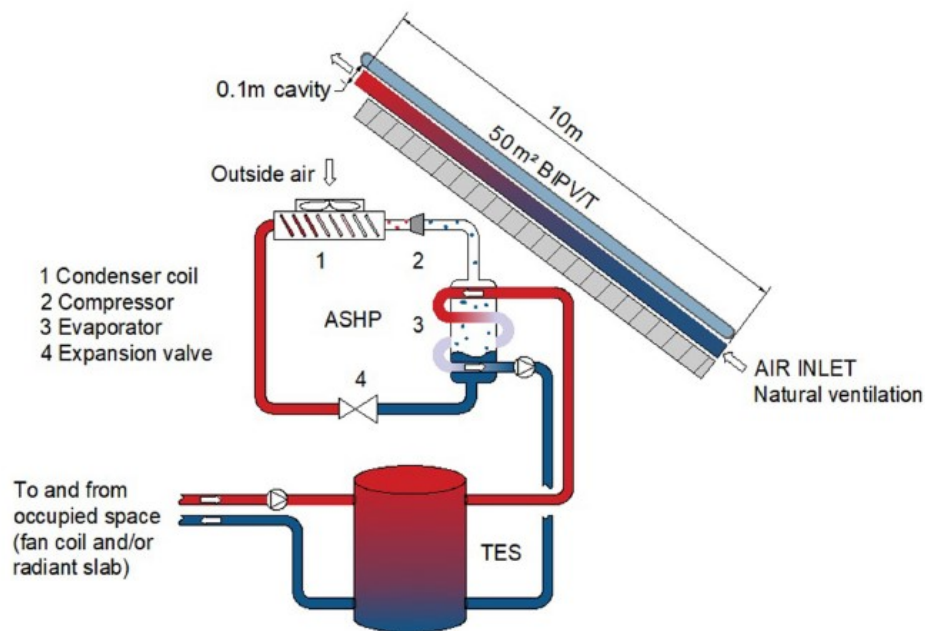
A key technology to eliminate the use of fossil fuels is the ASHP but their usage is restricted in cold climates due to reduced heating performance. During the winter months the outside temperature can often drop below 0°C leading to a decrease in the heat pump capacity and coefficient of performance. Solar assisted heat pumps have become popular as they can minimize the risk of freezing and reach a higher COP by achieving warmer source side temperatures. [11], [30] Heat pumps can be used for space heating, domestic hot water (DHW) or for thermal storage changing which can contribute to higher building energy flexibility.

Kamel and [11] develop a model of a BIPV/T and use the preheated air as a source for an ASHP. By integrating the two technologies a highly efficient heating system can be achieved with higher heat pump COP. During the analysis it was observed that by increasing the mass flow rate the temperature rise within the BIPV/T system (ΔT) decreased towards zero, reducing the improvement of the COP of the heat pump. Two constant mass flowrates were tested (0.4 kg/s and 0.1 kg/s) and it was concluded that low air flow rate, thus higher ΔT , is preferred to boost the

heat pump COP. At the same time though, the combined system needs enough air flow to match the heat pump minimum airflow over the heat pump outdoor coil, according to the manufacturer manual. This means adequate thermal energy to be absorbed by the evaporator in the heating season. The use of the combined BIPV/T +HP system resulted in average monthly savings of 24\$.

Dumoulin et al. [31] investigate the energy flexibility potential of a residential building in Montreal with an air-based BIPV/T system coupled to an air-source heat pump (Figure 2-15).

The mass flow rate of the BIPV/T was set to match the flow rate for the external unit of the heat



Solar-assisted air-source heat pump coupled with the BIPV/T system and water-source TES.

Figure 2-15 Air-based BIPV/T system connected to an air-source heat pump that charges a water-based TES, [31]

pump and the BIPV/T outlet air was sent to the evaporator coil. The heat pump then was used to charge water-based sensible thermal energy storage (Figure 2-15). The average COP of the solar assisted heat pump increased by 22% and over 50% during peak sunlight hours.

Thermal Energy Storage

There have not been many studies examining thermal energy storage (TES) coupled with PV/T systems. TES can significantly improve the flexibility potential of a building as it can present an opportunity for load shifting and shedding at peak demand hours. The TES system can be

charged during peak sunlight exposure (usually between 11am-2pm) when the BIPV/T system will produce the highest amount of energy. The stored heat can then be released during the evening peak (5-8pm.) significantly reducing the demand on the grid and the overall energy consumption of the building.

Additionally, in times where there is no need for direct space heating or ventilation air preheating the heated BIPV/T air can be directed to an air-water heat exchanger so that the excess solar radiation supplements the DHW heating system. This application can be suitable especially for the summer months as it will require higher outlet temperatures and space heating is not needed.

In [30] the authors examine an air-based BIPV/T system coupled to an ice-latent storage tank in an energy-efficient home located in Montreal, Canada. Results showed that using the preheated air for charging the ice-latent storage tank provided up to 22% energy savings in space and DHW heating and 50% in the total mechanical energy consumed by the house.

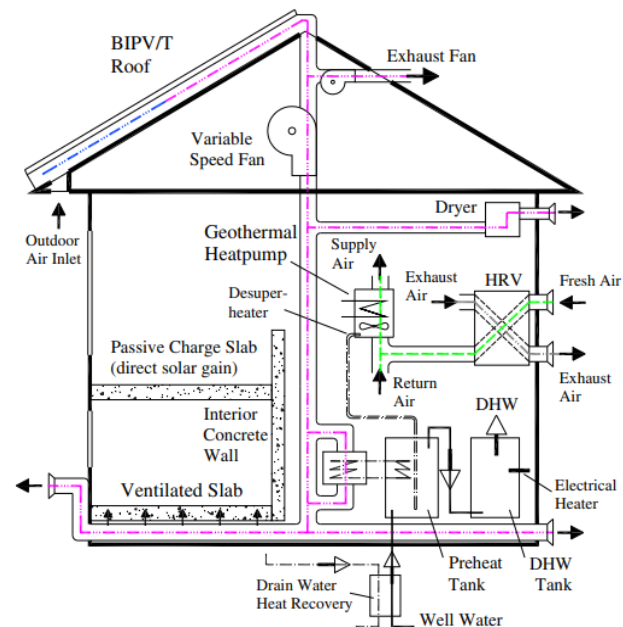


Figure 2-16 Air-based BIPV/T system coupled with a ventilated slab, [59]

Chen et al. [32] examined the performance BIPV/T system where the heated air is used for charging a ventilated concrete slab (VCS), DHW heating (through air-water heat exchanger) and cloth drying in a near net zero energy solar house located near Montreal, Quebec (Figure 2-16). Monitored data showed that the VCS was able to store 9–12 kWh from the BIPV/T during a

clear sunny day with average ambient temperature 0 °C. It was also found that the VCS could gather thermal energy during consecutive clear sunny days without overheating its surface.

2.8 BIPV/T Control

Uncertainties or changes in the weather conditions can have a significant impact on the performance of a BIPV/T system and can result in a deviation from its desired performance. By implementing an optimal control strategy on the mass flow rate, the size of possible errors can be minimized.

The importance of optimal BIPV/T control which will enable efficient HVAC integration is highlighted by [5] who performed a survey on the priorities regarding adaptive façade development. The two most highly ranked answers by the participants were integrating multi-disciplinary approaches for smart façade operation and development of integrated systems with the building HVAC (Figure 2-17).

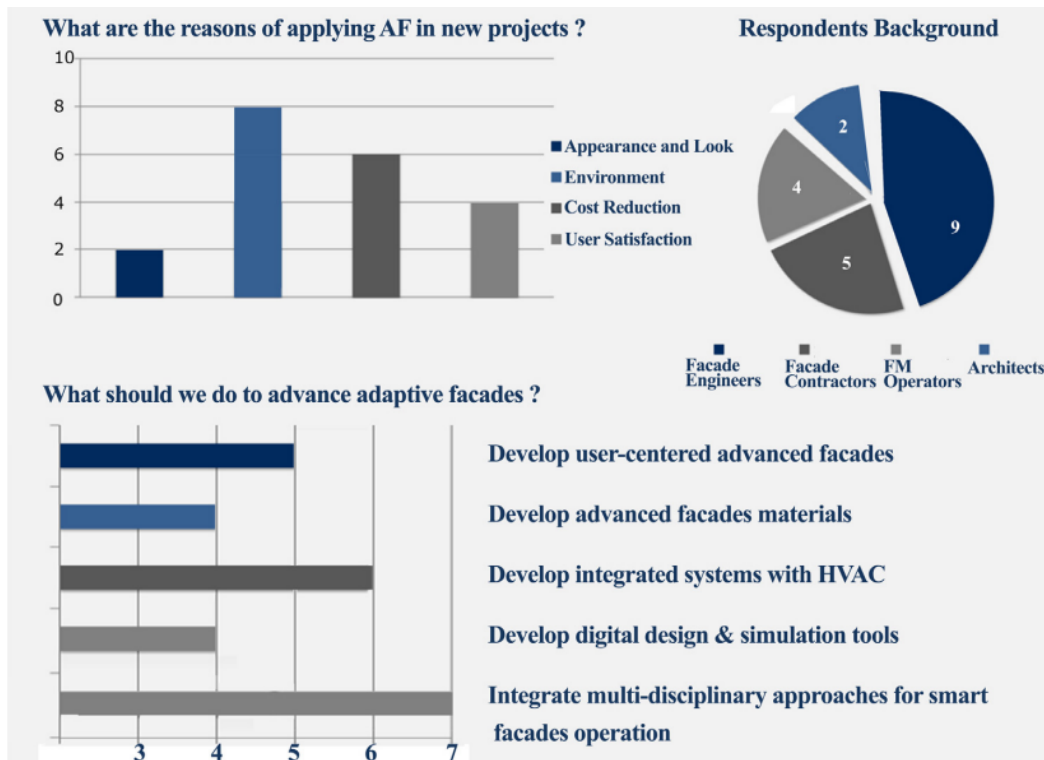


Figure 2-17 Survey results of respondents' priorities regarding adaptive facades, [5]

The applied control technique can be classical control techniques. Classical control techniques can be derived in two main categories:

- i) Rule-based: Are commonly referred to as on/off strategies as well and use predefined instructions (if...then... etc.) and control the given processes with the objective to keep a parameter within given boundaries. Rule-based control is the most common technique used for temperature control. [6]
- ii) Proportional Integral Derivative (PID): PID controllers use feedback from sensors in order to adjust. There are three controllers that are included in a PID controller, a) the proportional controller that produces an output proportional to the error by comparing the feedback signal with the set point, b) the integral controller that removes the error by integrating the error over time until the value of the error comes to zero and (c) the derivative controller which minimizes overshooting by slowing down the correction factor. [6]

Both of these methods are fairly simple and easy to implement but often lead to higher energy consumption compared to other controlling techniques as they are not able to adapt to continuously changing conditions. [6]

Advanced controls determine future action of a system based on a building model and has the ability to adapt under rapidly changing conditions or disturbances. Advanced control techniques can be categorized in to i) model-predictive control, ii) optimal control iii) adaptive control iv) feedforward/feedback v) robust control. [6]

Model Predictive Control (MPC) is an advanced closed-loop control strategy that has mostly been used to control the behavior of complex dynamic systems. MPC uses a dynamic model of a system and information about future conditions and environmental disturbances to perform a sequence of control actions for optimal planning. [33], [34], [35]

The main parameters defined in MPC are: i) the prediction horizon, ii) the control horizon, iii) the objective function, iv) the manipulated variables, v) the optimization algorithm, vi) the feedback signal. [6]

In a review of the most frequently adapted control techniques for ABE Alkhatib et al. [6] found Model Predictive Control (MPC) as the most used (Figure 2-18).

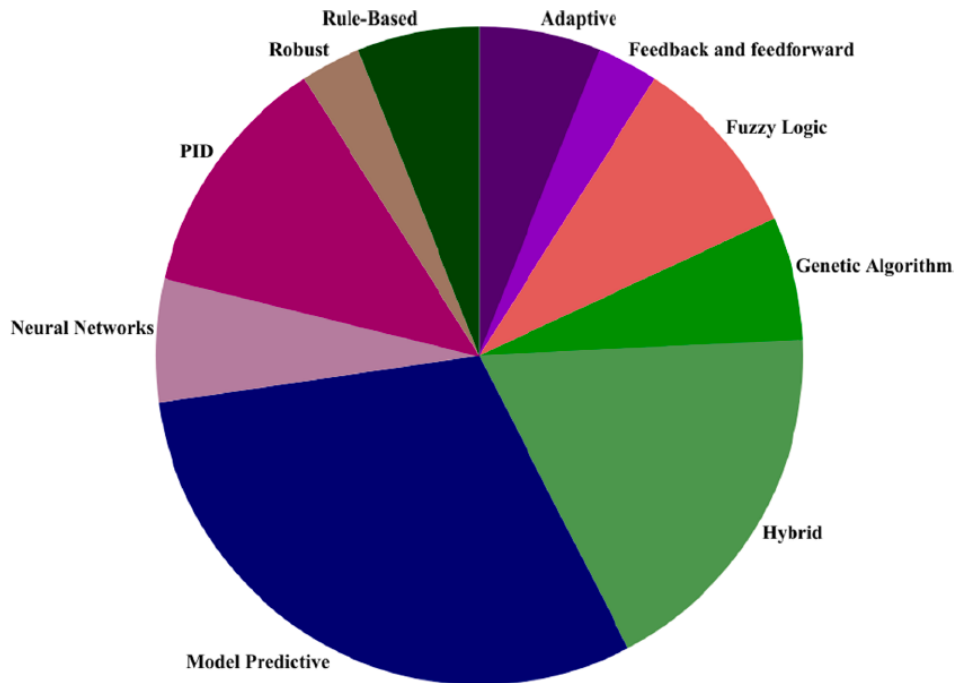


Figure 2-18 Most frequently used control techniques for Active Building Envelope, [6]

For each time step, MPC adjusts the specified control parameters through an optimization algorithm and sets a sequence of control inputs over a specified time horizon. The first control action in this sequence is applied to the plant and then the process is repeated. This way the system can effectively respond to any current or future change in the internal or outdoor conditions. [6], [33]. The main difference between MPC and traditional control methods is that in MPC the optimization problem is refined and solved online at every sampling moment while traditional control outputs a control signal offline and applies it to the system once. [36]

To apply MPC an important decision is the appropriate complexity of the system model. The models that can be used can vary from black box models, data driven models, to white box models, detailed physical models. [3] Black box models are developed using purely data measurements to determine the behavior of a system. Although these models can be fairly simple with small computational cost, they often are unable to capture the systems response to external disturbances and are often challenging to develop. [6] White box models are based on the physical properties of the system and use detailed heat and mass balance equations to precisely

capture the system dynamics. Although highly accurate these models are hardly used for control purposes due to the nonlinear dynamics of the complex physical phenomena which significantly increase their computational requirements. [35], [6]

Since MPC can add a high load to the CPU of the computer, using a complex high order model can compromise the fast response and negatively affect the performance of on-line MPC. [36]

Control-oriented grey-box models can give optimal balance between accuracy and simplicity. Grey box models are hybrid models which are based on energy balance equations but also use measured data to adjust some of their parameters to match the system performance. [35], [6]

In a study by Ma et al. [37] a comparison between three different control strategies for liquid-based PV/T assisted heat pumps was conducted in order to identify the key parameters of each system. The control strategies tested were:

- 1) on-off control strategy, where the heat pump flow rate is controlled by an on-off controller and is determined by the temperature difference (dt) between the outlet temperature of the PV/T and the fluid temperature in the storage tank
- 2) continuous control strategy, where a continuous feedback controller sets the flow rate so the dt is equal or higher than a specified value
- 3) outlet temperature control strategy, where the strategy ensures that the PV/T outlet temperature reaches a specified desired value by regulating the flow rate with a continuous controller

Results showed that the PV/T system control strategy plays an important role in the overall system performance. The authors found that there was an optimum outlet temperature that maximized the system performance for the outlet temperature control strategy and concluded that the outlet temperature of the PV/T has a significant effect on the electricity generation, average heat pump COP and overall system performance.

Pintaldi et al [33] present a solar thermal cooling system connected with thermal energy storage controlled through a model predictive control (MPC) approach. The main objective of controlling the system was to minimize the amount of auxiliary energy used by controlling the system flowrates without compromising the cooling energy delivered. The results demonstrate that the MPC reduced the auxiliary energy usage 10% compared to a rule-based control strategy.

The authors of [38] develop a liquid-based PVT collector model and compare its performance for different locations under two control strategies. The PVT system was operated under a constant optimized flow rate as well a variable flow which is optimized at each time step. Both control strategies were optimized with the objective to achieve a higher electrical yield. When comparing the optimal constant flow for the three locations examined, the authors concluded that a higher flow rate was needed for locations with higher solar radiation and ambient temperature. Results showed that by using the variable flow strategy the electrical production increased in the range of 7-27% in all locations compared to the reference case. However, since the thermal energy produced is considerably higher than the electrical the authors recommended more focus towards efficient integration of thermal energy with the building HVAC.

Li et al. [35] study different integration approaches of air-based BIPV/T systems and the building HVAC to maximize energy production and utilization. The study focuses on an office space in which the BIPV/T system preheats the ventilation air, and the remaining preheated air is directed to an air-to-water heat pump which is used to charge a thermal energy storage tank. The objective function of the MPC strategy is to minimize electricity consumption with the manipulated variable being heating power provided by the heat pump. The authors conclude that MPC can have a significant potential for energy savings (up to 34.5%) for systems with large thermal capacitance. A reduction up to 10.8% of electricity for heat pump operation was achieved.

2.9 Research Needs & Opportunities

Air-based BIPV/T systems are a promising technology that can have low cost and low maintenance. However, a limited number of studies have emphasized the integration of BIPV/T systems with the building HVAC using optimal control strategies for the mass flow rate. Most studies investigate only one thermal application at a time and usually supply the HVAC equipment with a constant flow rate coming from the BIPV/T. The available heat recovered from BIPV/Ts is closely related to the respective weather conditions and the optimal flow rate/outlet temperature combination can highly vary during different times of the day. In this study an MPC strategy on the air flow rate of a BIPV/T system is developed which determines the optimal mass flow rate according to the current and future environmental conditions and thermal needs of the

building. To successfully apply MPC a suitable BIPV/T model is needed. A lack of investigation in the literature on control-oriented model development for BIPV/T systems is noted with most researchers using physics-based models. This can cause long computation times and negatively affect the control algorithm. A few studies have mentioned the use of the thermal capacitance in BIPV/T models to be useful for control purposes, but no deeper investigation has been done. There is therefore a great research opportunity for the development of control oriented BIPV/T models which enable advanced model-based control strategies.

Chapter 3 Grey-box BIPV/T

Modelling

This chapter introduces the grey-box modelling approach, to develop a control-oriented BIPV/T model. The first part of this chapter presents the development of the BIPV/T model based on data obtained from the experimental procedure carried out at the Solar Simulator and Environmental Chamber (SSEC) laboratory in Concordia University. The second part introduces the full-scale BIPV/T system located at the Varennes library and the calibration of the model using monitored data from the commissioned BIPV/T.

3.1 Experimental BIPV/T System

3.1.1 Model Development

Two different versions of the BIPV/T model are developed. A steady-state (SS), where no thermal capacitances are considered, and a transient (TR) model, where the capacitances of the PV modules and the rear side of the channel are included. The two models considered here are shown schematically in Figure 3-1.

In the case of the steady state model the solution of the equations is independent of previous conditions. For the transient model however, at every time step, the solution of the previous time step is required with a fully-explicit finite difference scheme. The BIPV/T channel can be divided

into an arbitrary number of control volumes. The inlet conditions of a control volume are equivalent to the outlet conditions of the previous control volume.

3.1.1.1 Steady-State Model

The equations corresponding to a representative control volume in the SS model are shown below. Equations (3-1) through ((3-6) respectively correspond to energy balances at the top, middle and bottom surface of the PV module, air node and the top and bottom surface of the insulation. Equations (3-7) and (3-8) show the recovered thermal energy and outlet temperature of the PV. Finally, equation (3-9) expresses the PV efficiency as a function of the PV temperature while equation (3-10) the thermal energy absorbed by the PV surface.

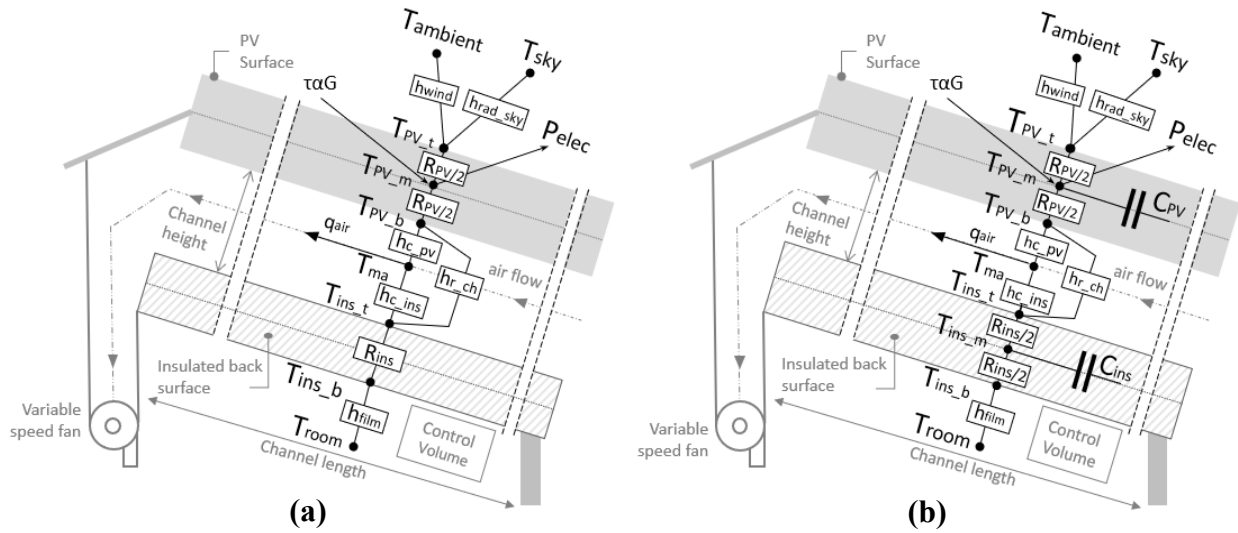


Figure 3-1 BIPV/T control volume energy balance for (a) steady-state model, (b) transient model

$$T_{PV_t} = \frac{T_{amb} \cdot h_{c_{wind}} + T_{sky} \cdot h_{r_{sky}} + T_{PV_m} \cdot 2u_{PV}}{h_{c_{wind}} + h_{r_{sky}} + 2u_{PV}} \quad (3-1)$$

$$T_{PV_m} = \frac{T_{PV_t} \cdot 2u_{PV} + T_{PV_b} \cdot 2u_{PV} + P_{thermal}}{4u_{PV}} \quad (3-2)$$

$$T_{PV_b} = \frac{T_{PV_m} \cdot 2u_{PV} + T_{ma} \cdot h_{c_{PV}} + T_{ins_t} \cdot h_{r_{ch}}}{2u_{PV} + h_{c_{PV}} + h_{r_{ch}}} \quad (3-3)$$

$$T_{ma} = \frac{1}{\Delta x} \cdot \int_0^{\Delta x} \left[\frac{h_{c_{PV}} \cdot T_{PV_b} + h_{c_{ins}} \cdot T_{ins_t}}{h_{c_{PV}} + h_{c_{ins}}} + \left(T_{inlet} - \frac{h_{c_{PV}} \cdot T_{PV_b} + h_{c_{ins}} \cdot T_{ins_t}}{h_{c_{PV}} + h_{c_{ins}}} \right) \cdot e^{-\frac{W_{channel} \cdot (h_{c_{PV}} + h_{c_{ins}})}{\dot{m} \cdot c_{p_{air}}}} \right] \quad (3-4)$$

$$T_{ins_t} = \frac{T_{ma} \cdot h_{c_{ins}} + T_{ins_b} \cdot u_{ins} + T_{PV_b} \cdot h_{rch}}{h_{c_{ins}} + u_{ins} + h_{rch}} \quad (3-5)$$

$$T_{ins_b} = \frac{T_{ins_t} \cdot u_{ins} + T_{room} \cdot h_{film}}{u_{ins} + h_{film}} \quad (3-6)$$

$$q_{air} = h_{c_{PV}} \cdot (T_{PV_b} - T_{ma}) + h_{c_{ins}} \cdot (T_{ins_t} - T_{ma}) \quad (3-7)$$

$$T_{outlet} = T_{inlet} + \frac{q_{air}}{\dot{m} \cdot c_{p_{air}}} \quad (3-8)$$

$$\eta_{PV} = \eta_{STC} \cdot [1 - \beta \cdot (T_{PV} - 25^\circ C)] \quad (3-9)$$

$$P_{thermal} = G_{incident} \cdot \alpha_{PV} - \eta_{PV} \cdot PF \cdot G_{incident} \quad (3-10)$$

3.1.1.2 Transient Model

The transient model includes the thermal capacitance of the *PV* modules and the materials composing the rear side of the system. The small capacitance of the glass-on-glass PV modules results to very small critical time steps (Δt) required for numerical stability¹. This can be considered as one of the major downsides of control-oriented transient BIPV/T modules as it can lead to high computational times which negatively affects the performance of the controller.

¹ For more details on the critical Δt calculation refer to equation (2-1)

In the equation system listed below equations (3-11) through (3-17) respectively correspond to energy balances at the top, middle and bottom surface of the PV module, air node and top, middle and bottom surface of the insulation. Equation (3-18) shows the recovered thermal energy (3-19) based on the outlet temperature of the PV. Similarly, with the SS model, equations (3-20) and (3-21) indicate the PV efficiency as a function of the PV temperature and the thermal energy absorbed by the PV surface.

$$T_{PV_t}[i+1] = \frac{T_{amb}[i] \cdot h_{cwind}[i] + T_{sky}[i] \cdot h_{rsky}[i] + T_{PV_m}[i] \cdot 2u_{PV}}{h_{cwind}[i] + h_{rsky}[i] + 2u_{PV}} \quad (3-11)$$

$$T_{PV_m}[i+1] = T_{PV_m}[i] + \frac{\Delta t}{C_{PV}} \cdot \{(T_{PV_t}[i] - T_{PV_m}[i]) \cdot 2u_{PV} + (T_{PV_b}[i] - T_{PV_m}[i]) \cdot 2u_{PV} + P_{thermal}[i]\} \quad (3-12)$$

$$T_{PV_b}[i+1] = \frac{T_{PV_m}[i] \cdot 2u_{PV} + T_{ma}[i] \cdot h_{cPV}[i] + T_{inst}[i] \cdot h_{rch}[i]}{2u_{PV} + h_{cPV}[i] + h_{rch}[i]} \quad (3-13)$$

$$T_{ma}[i] = \frac{1}{\Delta x} \cdot \int_0^{\Delta x} \left[\frac{h_{cPV}[i] \cdot T_{PV_b}[i] + h_{cins}[i] \cdot T_{inst}[i]}{h_{cPV}[i] + h_{cins}[i]} + \left(T_{inlet}[i] - \frac{h_{cPV}[i] \cdot T_{PV_b}[i] + h_{cins}[i] \cdot T_{inst}[i]}{h_{cPV}[i] + h_{cins}[i]} \right) \cdot e^{-\frac{W_{channel} \cdot (h_{cPV}[i] + h_{cins}[i])}{\dot{m} \cdot c_{p,air}}} \right] \quad (3-14)$$

$$T_{ins_t}[i+1] = \frac{T_{ma}[i] \cdot h_{cins}[i] + T_{ins_m}[i] \cdot 2u_{ins} + T_{PV_b}[i] \cdot h_{rch}[i]}{h_{cins}[i] + 2u_{ins} + h_{rch}[i]} \quad (3-15)$$

$$T_{ins_m}[i+1] = T_{ins_m}[i] + \frac{\Delta t}{C_{ins}} \cdot [(T_{ins_t}[i] - T_{ins_m}[i]) \cdot 2u_{ins} + (T_{ins_b}[i] - T_{ins_m}[i]) \cdot 2u_{ins}] \quad (3-16)$$

$$T_{ins_b}[i + 1] = \frac{T_{ins_m}[i] \cdot 2u_{ins} + T_{room}[i] \cdot h_i}{2u_{ins} + h_i} \quad (3-17)$$

$$q_{air}[i + 1] = h_{c_{PV}}[i] \cdot (T_{PV_b}[i] - T_{ma}[i]) + h_{c_{ins}}[i] \cdot (T_{ins_t}[i] - T_{ma}[i]) \quad (3-18)$$

$$T_{outlet}[i + 1] = T_{inlet}[i] + \frac{q_{air}[i]}{\dot{m} \cdot c_{p_{air}}} \quad (3-19)$$

$$\eta_{PV}[i + 1] = \eta_{STC} \cdot [1 - \beta \cdot (T_{PV}[i] - 25^\circ\text{C})] \quad (3-20)$$

$$P_{thermal}[i + 1] = G_{incident}[i] \cdot \alpha_{PV} - \eta_{PV}[i] \cdot PF \cdot G_{incident}[i] \quad (3-21)$$

In the equations presented, T_{PV} , T_{ma} , T_{ins} , q_{air} , T_{outlet} , η_{PV}^2 , and $P_{thermal}$ are unknown variables. The rest of the parameters used, $W_{channel}$: channel width (m), C : thermal capacitance ($\text{J}/\text{m}^2\text{K}$), \dot{m} : mass flow rate (kg/s), $c_{p_{air}}$: specific heat of air ($\text{J}/\text{kg}\cdot\text{C}$), h_i : film coefficient, $G_{incident}$: incident solar radiation (W/m^2), α_{PV} : PV absorptance and PF : packing factor are known.

However, several additional equations are used:

Radiative heat transfer

The radiative heat transfer coefficient, h_r ($\text{W}/\text{m}^2\text{K}$) between two parallel surfaces, 1 and 2, is given by:

$$h_r = \sigma \cdot VF \cdot \frac{(T_1 + T_2) \cdot (T_1^2 + T_2^2)}{\left(\frac{1}{\varepsilon_1} + \frac{1}{\varepsilon_2} - 1\right)} \quad (3-22)$$

where,

- σ : $5.67 \cdot 10^{-8} \text{ w}/\text{m}^2 \cdot \text{K}^4$ (Stefan-Boltzmann constant)
- VF : View factor between the two surfaces
- $\varepsilon_{1,2}$: Emissivity of surfaces

² For more details refer to equation (2-2) in Chapter 2.

- $T_{1,2}$: Temperature of surfaces

Convective interior heat transfer correlations

Accurate convective heat transfer calculation in BIPV/T systems presents several challenges mainly due to the asymmetric heating (the major component of heat transfer occurs through the exterior side of the BIPV/T channel) and the more complex geometry. Most researchers have used Nusselt number correlations developed for pipes and ducts with uniform boundary conditions for a given cross section, such as the Dittus-Boelter [39] correlation. In many cases these correlations underestimate the convective heat transfer coefficients, as several heat-transfer enhancing factors are not considered (presence of the framing structure, surface imperfections which act as turbulence promoters). [15]

However, after examining three different convection coefficients against the data from the experiments in the SSEC, it was found that the Dittus-Boelter coefficient gave the smallest Root Mean Square Error (RMSE) for that specific system (Table 3-1). This can be attributed to the fairly smooth surfaces of the air channel, glass-on-glass PV modules on the exterior side and an aluminum sheet insulation cover on the rear surface, which could have resembled the function of a pipe or duct. The steady environmental conditions within the laboratory could have also contributed to this outcome, as well as the shorter length (up to 3 m) with mainly developing flow conditions. The results of the analysis are shown in Figure 3-2.

Table 3-1 Nusselt number expressions used RMSE for each examined case

Nu Correlations		Re	RMSE
Dittus-Boelter [39]	$Nu = 0.023 \cdot Re^{0.8} \cdot Pr^{0.4}$	$Re > 10.000$ $L/D > 10$ $0.7 < Pr < 160$	1.565
Yang & Athienitis [16]	1 st section: $Nu = 0.014Re^{0.9}Pr^{0.4}$	$1453 < Re < 14322$	2.371
	2 nd section: $Nu = 1.451Re^{0.44}Pr^{0.4}$	$3600 < Re < 19034$	
Candanedo et al. [40]	Top: $Nu = 0.052Re^{0.78}Pr^{0.4}$	$250 < Re < 7500$	2.626

	Bottom: $Nu = 1.017Re^{0.471}Pr^{0.4}$		
--	---	--	--

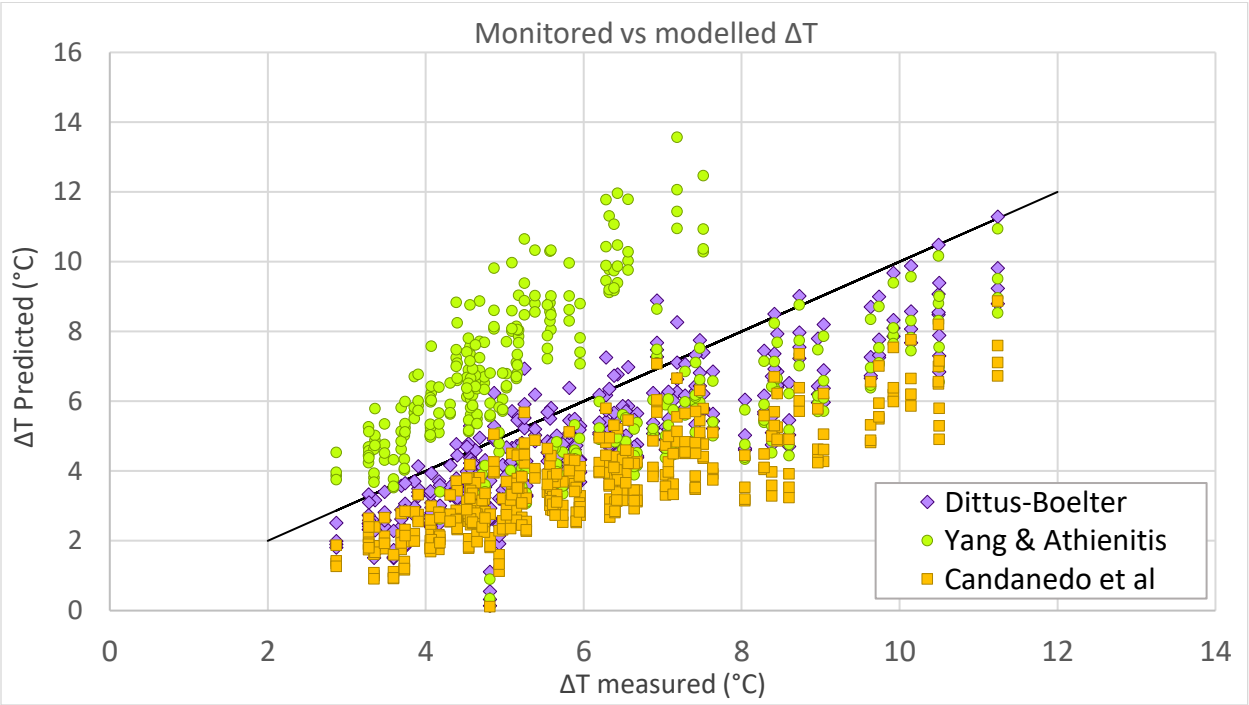


Figure 3-2 Scatterplot of predicted and monitored values of the air temperature rise (ΔT) for all tests

Convective exterior heat transfer correlations

The heat loss to the surroundings due to wind effects were found to have a great impact on the BIPV/T performance as the PV surface for a BIPV/T system is often in direct contact with the ambient environment. [12] The suitability of a wind-driven convection correlation is highly associated with the local conditions, orientation and size of the system. [12]

The wind-driven convective heat transfer coefficient (W/m^2K) was calculated using the correlation developed by [41].

$$\begin{aligned}
 h_{wind} &= 7.4 + 4.0 \cdot V_{wind} \quad (\text{windward}) \\
 h_{wind} &= 4.2 + 3.5 \cdot V_{wind} \quad (\text{leeward})
 \end{aligned}
 \tag{3-23}$$

where,

- V_{wind} : wind speed (m/s)

Sky Temperature

The sky temperature employed to calculate the radiative heat losses to the exterior was obtained using the formula used by [42], [43]:

$$T_{sky} = T_{ambient} - 20 \quad (3-24)$$

3.1.2 Experimental Procedure

A series of experiments in the Solar Simulator - Environmental Chamber (SSEC) laboratory in Concordia University took place with the objective to facilitate in the calibration and validation of the above described model. The laboratory can provide ideal conditions for a model development as the environment is highly controllable while all the data can be meticulously recorded.

3.1.2.1 Solar Simulator & Environmental Chamber

The Solar Simulator - Environmental Chamber laboratory in Concordia University is an internationally unique facility which enables accurate and repeatable testing of solar systems and active building envelopes. Indoor testing can greatly facilitate in the development and assessment of BIPV/T systems by providing controlled repeatable environmental conditions. [16]

The Solar Simulator is designed to reproduce sunlight and test different solar systems such as BIPV, BIPV/T, STPV etc. under various environmental conditions. The Solar Simulator consists of:

- i) A lamp field emulating the sunlight. The lamp field is composed by 8 metal halide lamps which can produce irradiance intensities from 500 to 1200 W/m² with a uniformity of up to 97%. The spectral quality of the lamps meets specifications of standards EN 12975:2006 and ISO 9806-1:1994.

- ii) A testing platform where the test specimens are mounted on. Both the testing platform and the lamp field can be setup to have an angle of 0-90° simulating different building envelope slopes.
- iii) An artificial sky placed between the lamp fiend and test platform. By passing cold air between two low-iron anti-reflection glass panes blocks the infrared radiation emitted by the lamps and simulates the sky temperature.
- iv) A customized solar air collector which can be attached to the test specimen and produce air flow within the air channel. The BIPV/T mass flow rate is measured by an orifice flow meter featuring three different pressure transduces.
- v) A linear variable-speed fan that emulated wind driven convection by blowing air parallel to the specimen with speed up to 14 m/s.
- vi) A pyranometer and anemometer mounted on a transverse system above the testing area and measure irradiation and wind speed respectively, with a minimum measurement spacing of 15 cm. [16], [44]

The temperature of the room where the solar simulator is located is kept between 20-22oC while relative humidity varies between 25-35%. A cooling unit is used to remove the heat generated by the lamps from the room. [44] A picture of the solar simulator can be seen in Figure 3-3.

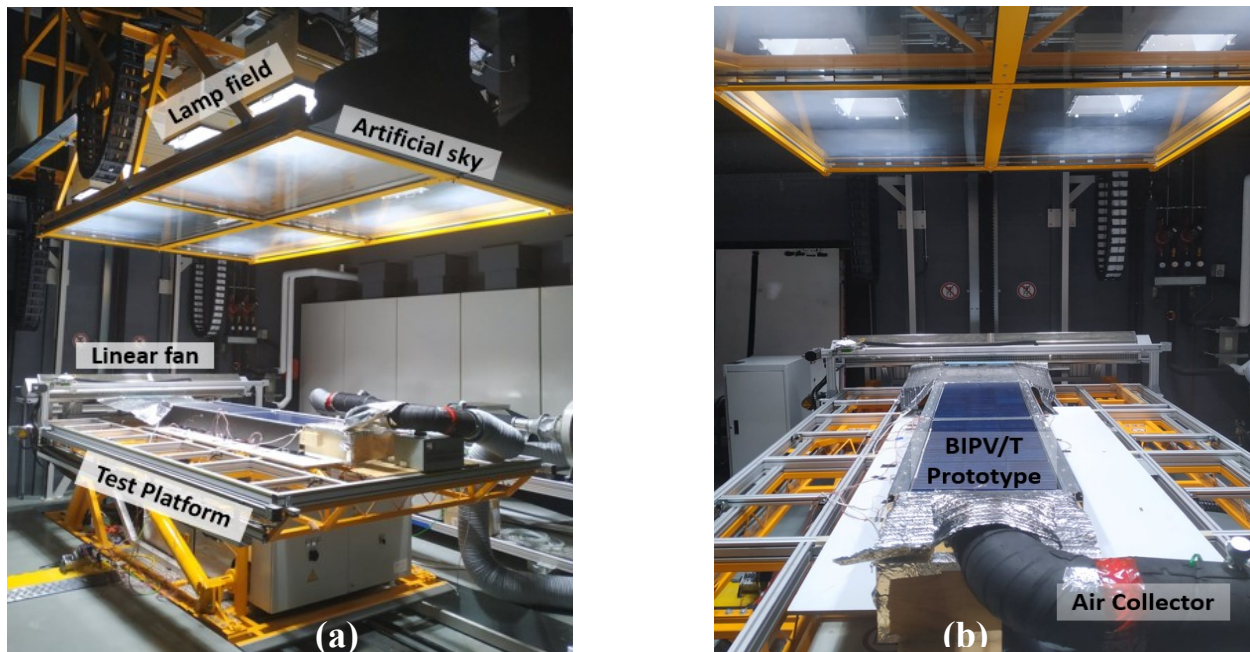


Figure 3-3 (a) Concordia University Solar Simulator, (b) Experimental set-up of an air-based BIPV/T prototype

3.1.3 Experiment Description

A series of experiments were carried out in the Concordia University Solar Simulator, testing a curtain wall BIPV/T prototype under different mass flow rates and various environmental conditions. [45]

The BIPV/T prototype used in the experiments is based on the curtain wall approach as described in Rounis et al. [13] and was designed to facilitate multiple testing configurations with adjustable channel height and interchangeable PV modules of different transparency (Figure 3-4). The framing consists of two 1.05m long side mullions where the rear side of the air channel can be connected at different elevations. The rear side consists of 51 mm of extruded polystyrene (XPS) insulation sandwiched between two aluminum sheets. The front aluminum sheet (interfacing with the air channel) acts as a secondary absorber for the part of solar irradiation that is transmitted in the cases where STPVs were used and was painted black to increase its absorptance. Adhesive insulation was used at the side walls of the air channel, to minimize lateral heat losses. Overall, a near adiabatic boundary was formed for the sides and rear of the air channel. Two of these systems were connected to form a 2.09 m by 0.48 m specimen (net channel dimensions).

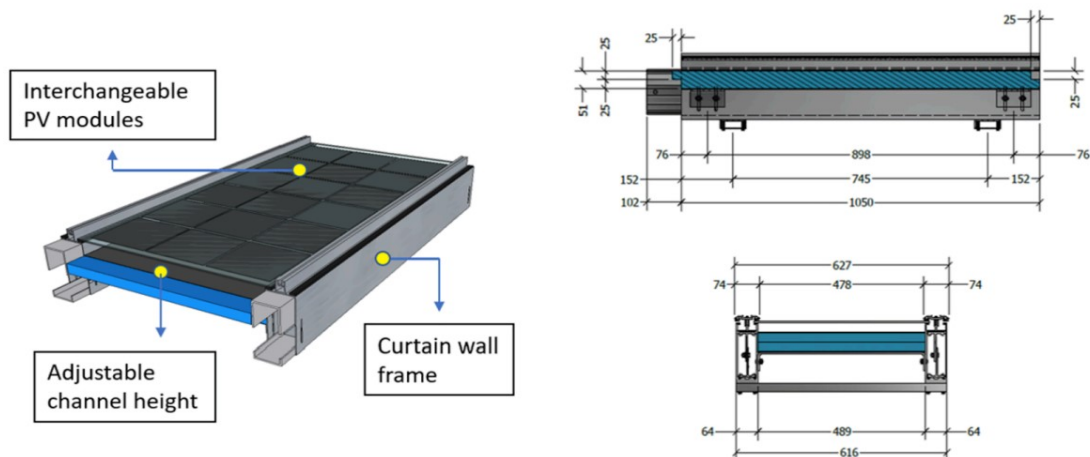


Figure 3-4 Experimental BIPV/T modules with adjustable channel height and interchangeable PV modules (dimensions in mm), [45]

The channel depth was set at two heights (0.03 m and 0.06 m), with respective hydraulic diameters of 0.057 m and 0.107 m, channel cross sectional areas of 0.029 m² and 0.015 m², and two channel aspect ratios (L/Dh) of 19.55 and 36.96 [45]

Two 1.04 m × 0.515 m glass-on-glass PV modules were custom fabricated each featuring 18p-Si PV cells, with a peak power output of 80 W ($\eta_{STC} = 12.7\%$) and a packing factor (PF) of 85.94%. [45] In one of the modules the area between the PV cells was transparent allowing part of the solar radiation to pass through and reach the rear side of the air channel. The other module was left opaque throughout its whole surface. The PV modules were placed at the top side of the mullions and secured in place with pressure plates. Reflective insulation was placed over potential openings to prevent thermal bridging.

A total of 36 T-type thermocouples ($\pm 0.3^\circ\text{C}$ measuring uncertainty) were used to monitor the temperature of the insulation/secondary absorber, the air within the channel and the PV surface. Additional thermocouples were used to monitor the inner and outer surface temperatures of the frame, as well as the air film temperatures over the PV surface to account for the effect of wind.

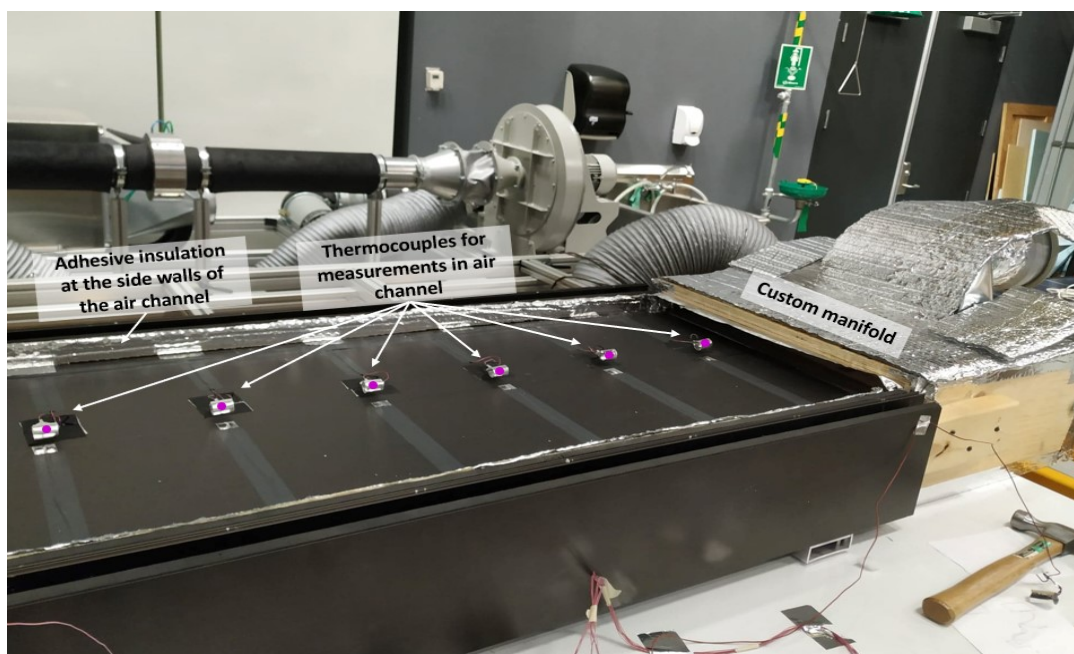


Figure 3-5 Thermocouple placement on the air channel, and the custom manifold used

The outlet of the prototype was attached to a custom manifold connected to the air collector of the solar simulator, which allows manual manipulation of the mass flow rate. Figure 3-5 shows the prototype connected to the manifold before the PV modules are placed. The wind velocity profile over the BIPV/ T module was measured above the PV panel with a TSI hot-wire anemometer and averaged over the collector's length. This was done for three distinct settings of the linear fan [45] Two sets of experiments were conducted, one using the transparent PV modules and one with the

opaque. For each set of experiments, two channel depths were considered, specifically 0.06 m and 0.03 m. Each configuration was tested under three irradiation levels (807 W/m² , 928 W/ m² , 1058 W/m²), three mass flow rates (120 kg/h·m² , 180 kg/h·m² and 240 kg/h·m²) and three wind speeds (1.53 m/s, 2.32 m/s, 3.18 m/s). All tests were carried out under room temperature of 21 °C ± 1 °C. [45] Figure 3-6 illustrates the various cases tested.

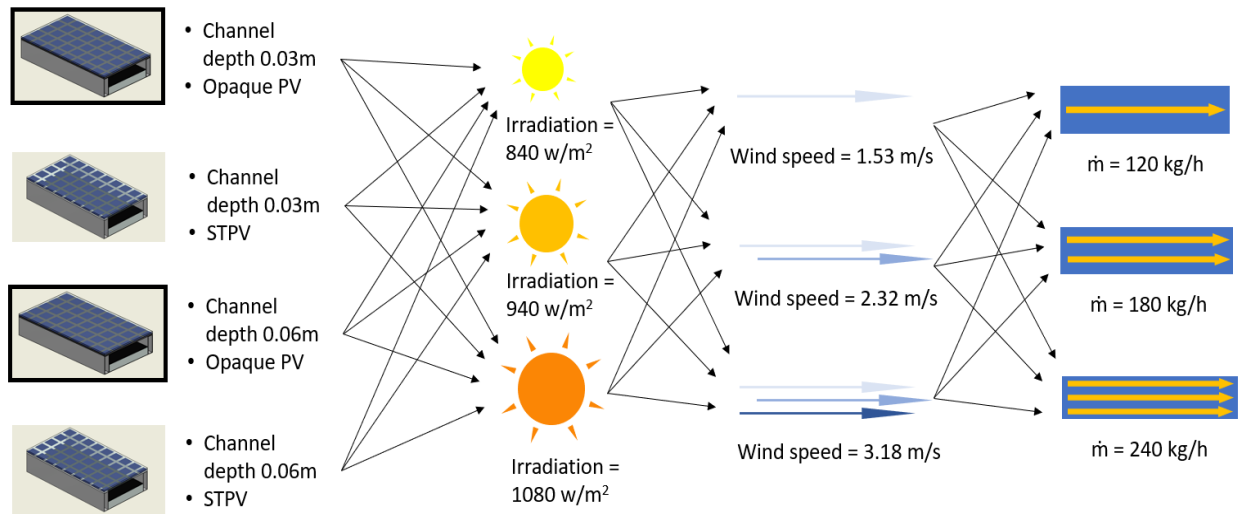


Figure 3-6 Channel configurations and operating conditions used in the measurements [45]

3.1.4 Time Constant Evaluation

The time constant (τ) of a system is defined as the time it takes for the controlled variable to reach 63.2% of its final value after a rapid change in the input. Systems with small time constants alter their output rapidly, while systems with larger time constants take longer to respond to input alterations. [46] The time constant can be found by applying a step input to the system, and then record the time when 63.2% of the final value obtained.

Three types of step inputs were recorded during the series of experiments in the solar simulator lab. Namely, change only in wind speed, change in wind speed and mass flow rate, change in wind speed, mass flow rate and irradiation. An increase in wind speed and mass flow rate result in lower PV and outlet temperatures as convective coefficients will increase. On the contrary, an increase in irradiation will cause the temperatures to rise as higher levels of solar energy reach the BIPV/T. Depending on the type of change, two types of step response curves were recorded

during the experimental process. An exponential decay when the type of step input causes the temperature to decrease and an exponential growth when the temperature increased (Figure 3-7). However, for the purpose of calculating the time constant only the cases where one input was changed were deemed as suitable.

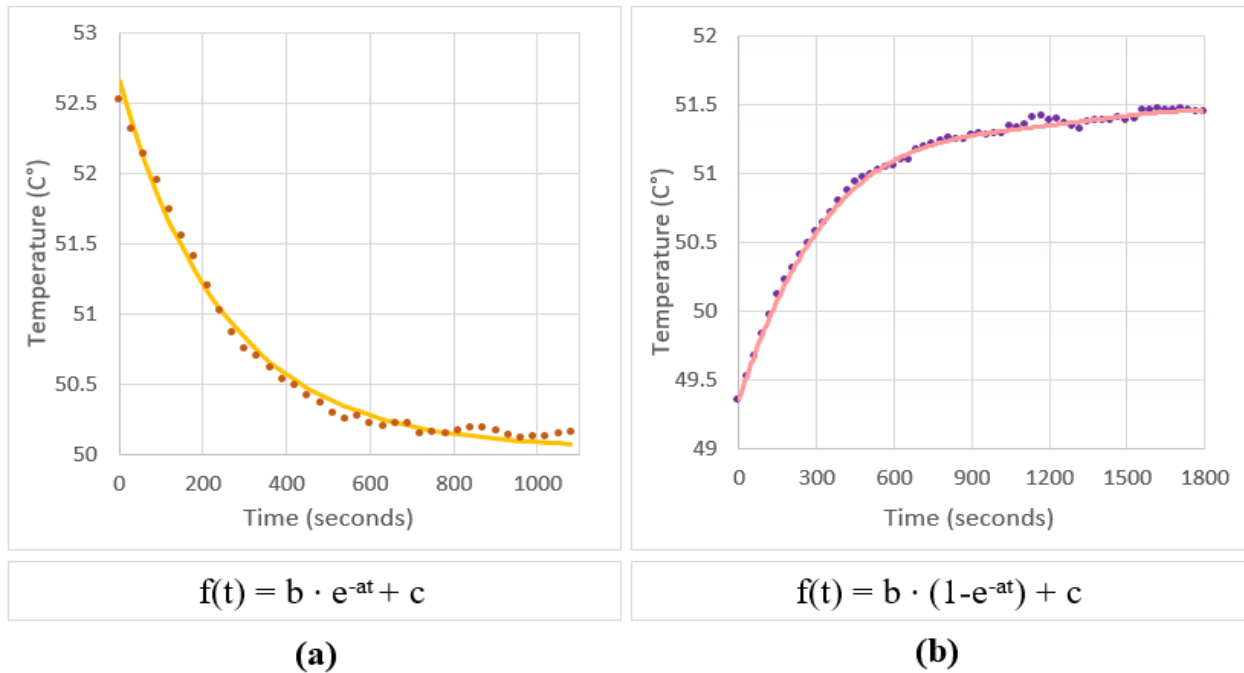


Figure 3-7 System response to different types of step response (a) Exponential decay, (b) Exponential growth

In total, 56 curves were derived from the data and analysed resulting in an average time constant. To calculate the time constant for each curve, the demand *curve_fit* from the *SciPy.Optimize* library in python was used. The time constant (τ) is equal to parameter $1/a$ seen in Figure 3-7.

The results from the previous described analysis are presented in Table 3-2.

Table 3-2 Time constant for different types of step inputs recorded during the experimental process

Step Input	Time Constant τ (minutes)	ΔT (time to reach steady state)
Wind Speed (+10%)	5.14	15.43

The time constant evaluation can give a good understanding of how the studied system behaves under a rapid change of either the controlled input or a disturbance which can prove extremely

useful for the development of control strategies. For BIPV/T control, the mass flow rate would be considered the controlled variable while weather fluctuations (wind, irradiance, ambient temperature) are disturbances.

3.1.5 Model Calibration

3.1.5.1 Grey-Box Method

In the grey-box approach, the developed models keep their general physical connections and are based on energy balance equations, but use measured data to replace some of their parameters. Grey-box models tend to have high accuracy and adaptability to different external conditions but are kept simple making them often the optimal solution for control algorithms.

The parameters chosen to be calibrated in the developed models of this study include the thermal conductance (U value) of the PV module and the rear side of the channel and the thermal capacitance (C value) of the PV module since this element is exposed to rapidly changing weather conditions including wind and irradiation.

The difference between the measured temperatures of the outlet and PV surface from the experiments and the simulate respective outputs of the developed models, is quantified by the Normalized Root Mean Square Error (NRMSE). The cost function for the calibration is formulated as:

$$J = \frac{\sqrt{\sum_{i=1}^n \frac{(\hat{T}_{outlet_i} - T_{outlet_i})^2}{n}}}{T_{outlet_{max}} - T_{outlet_{min}}} + \frac{\sqrt{\sum_{i=1}^n \frac{(\hat{T}_{PV_i} - T_{PV_i})^2}{n}}}{T_{PV_{max}} - T_{PV_{min}}} \quad (3-25)$$

where,

- \hat{T}_{outlet} : predicted outlet temperature (°C)
- T_{outlet} : measured outlet temperature (°C)
- \hat{T}_{PV} : predicted PV temperature (°C)
- T_{PV} : measured outlet temperature (°C)
- n : number of datapoints

The search space for the calibrated parameters was selected to be constrained to be one magnitude higher/lower of their physical properties. The given bounds can be formulated as:

$$\begin{aligned}
757.85 \leq C_{PV} \leq 75,785.37 \\
48.6 \leq u_{PV} \leq 4860 \\
0.056 \leq u_{bot} \leq 5.6
\end{aligned}
\tag{3-26}$$

The calibration process results into a constrained non-linear optimization problem. For the solution, the *minimize* function with method '*SLSQP*' available in the Python library *SciPy.Optimize* was used. The initial guesses for the calibrated parameters were based on the estimated physical properties of the materials. Although the system identification process should provide reasonable values for the calibrated parameters the results are not identical to the actual physical values of the building materials. [35]

Li et al. [35] mention that during nonlinear optimization problems when the true global minimum value is too far away from the initial guess, the algorithm will only be able to find a local minimum, which highlights the importance of a good initial guess.

As the data used for the calibration process comes from indoor experimental testing where no rapid environmental changes (wind gusts, passing clouds) took place during the data recording. This can be associated with a low effect of the thermal capacitance of the PV modules on the BIPV/T model performance. The primary reason to include the capacitance in a BIPV/T model is to use the damping effect during acute weather fluctuations and indoor testing may not be suitable to validate this theory.

3.1.6 Results & Observations

The identified parameter values along with the NRMSE for both models for the training and test dataset (a dataset the model did not “see” during the calibration process) are presented in Table 3-3. The results of the calibration process are shown in Figure 3-8 and Figure 3-9 shows the models against a testing dataset. It can be seen that both models match the data very well.

Table 3-3 Identified parameter values and NRMSE for BIPV/T models

	SS Model	TR Model
C_{PV} (J/m²K):	-	11,583.94
U_{PV} (W/m²K):	342.92	618.9
U_{BOT} (W/m²K):	2.41	1.157

NRMSE (Training dataset):	0.188	0.177
NRMSE (Test dataset):	0.28	0.31

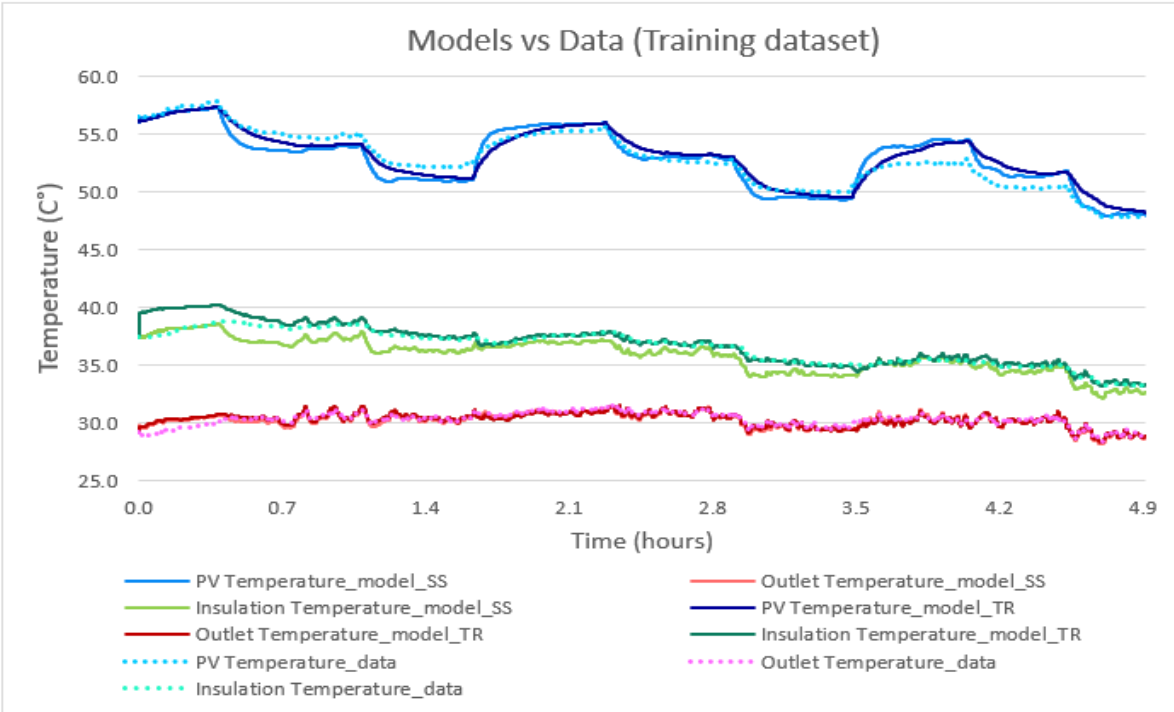


Figure 3-8 TR and SS model outputs compared to the measured data used for the calibration

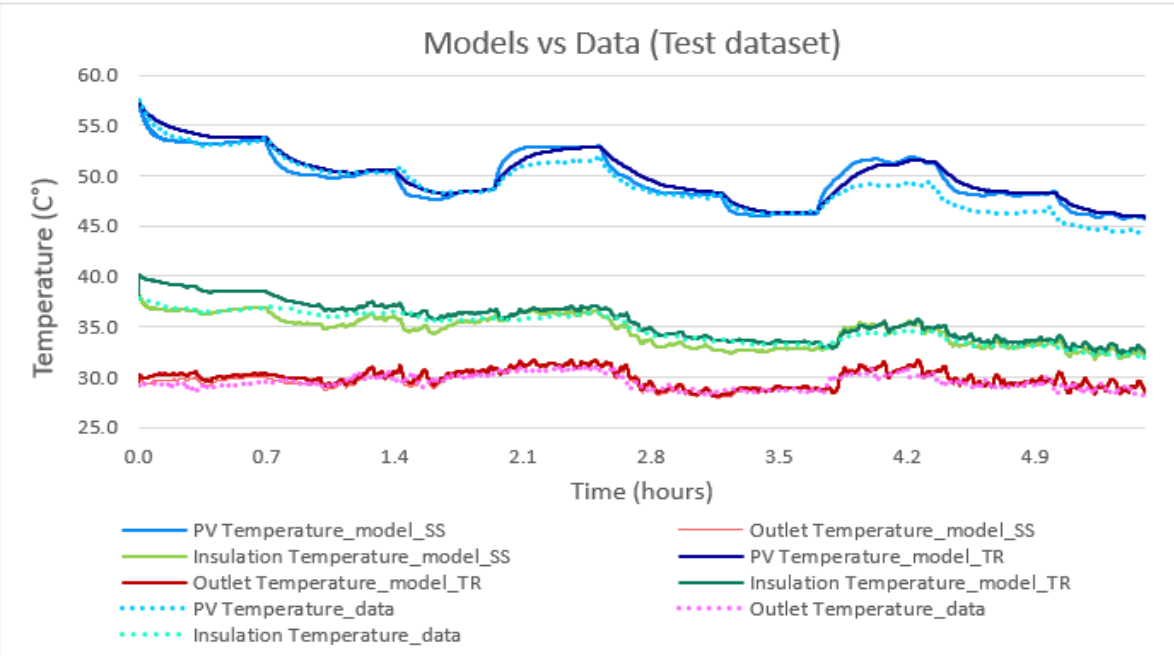


Figure 3-9 TR and SS model outputs compared to the measured data the model did not “see” during the calibration process

The two models give almost identical results for the outlet temperature prediction. This supports the hypothesis that indoor testing under a relatively constant temperature did not facilitate in evaluating the importance of including the thermal capacitance in the BIPV/T model.

A manual manipulation of the wind speed was conducted, and the steady-state and transient BIPV/T models were compared for highly variable wind conditions with rapid changes. Figure 3-10 illustrates the results of this process. Even though the transient model does give a slightly “smoother” profile the difference is very small. This is further investigated in the next chapter where real weather data and a monitored full-scale BIPV/T system are used as a case study.

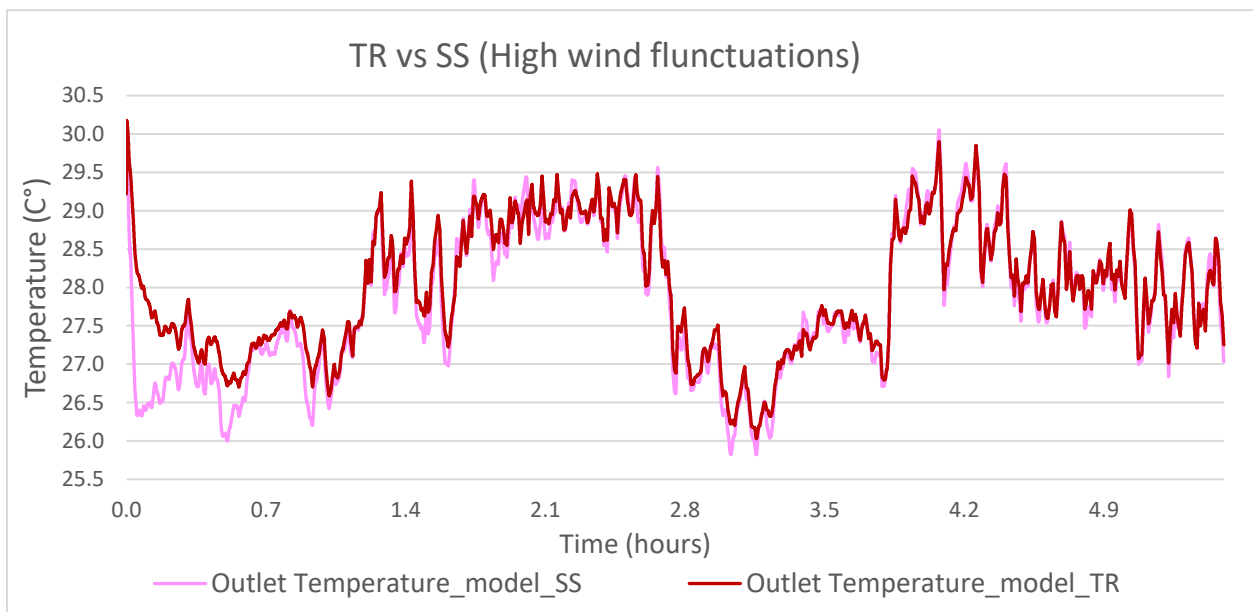


Figure 3-10 Comparison of the two BIPV/T models (TR and SS) for highly variable wind conditions

3.2 Full scale BIPV/T system - Varennes library

3.2.1 Archetype system analysis

The Varennes library is the first institutional Net-Zero Energy building in Canada. The design of the library required the collaboration of many specialists such as architects, engineers, researchers of various disciplines due to the complexity and involvement of different types of systems which substantially reduced the energy demand of the building. To name a few: ground-source heat pumps, hydronic radiant slab, EV charging stations, motorized windows for natural cooling, horizontal exterior louvers on south façade for daylight control and optimized Window to Wall Ratio.

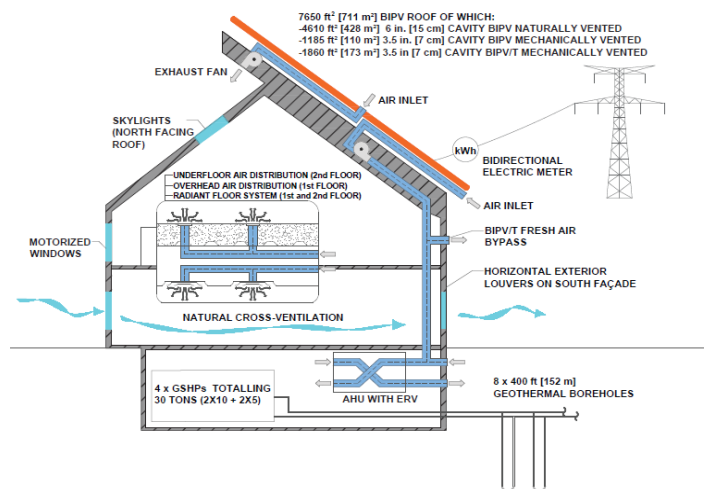


Figure 3-11 Left: Photograph of Varennes library source: [57], Right: Schematic of library and integrated energy systems [47]

One of the key technologies integrated to the building facilitating the net-zero energy goal is the use of BIPV covering the near south-facing part of the roof. During the design phase the annual energy consumption was estimated to be around 147,000 kWh per year. To reach site energy net-zero using solar electricity generated by an optimally titled and south oriented PV system a 110-120 kW system was deemed necessary. [47] The realized BIPV system covers approximately 700m² of roof area and is nearly optimally tilted at 37°. The system is comprised by three different sub-systems (Figure 3-12):

- i) Naturally ventilated BIPV. Covers the larger part of the roof (428m^2). An air cavity of 150mm is placed behind the PVs and a buoyancy driven airstream passes behind their surface reducing their temperature. The air is not collected or used for the building.
- ii) Mechanically ventilated BIPV. Covers approximately 168m^2 of roof area. The air is mechanically driven through a 70mm high air channel and is then discarded. The only purpose the ventilation serves is to prevent PV overheating.
- iii) BIPV/T. 110m^2 of the south-facing roof are covered by a BIPV/T system. Similarly, with the previous category, the air is mechanically driven by variable-speed fans through a 70mm high air channel but in this case is collected and used as pre-heated ventilation air during the heating season and discarded in summer. The BIPV/T channel is 5.55m long and 19.80m wide as illustrated in Figure 3-12.

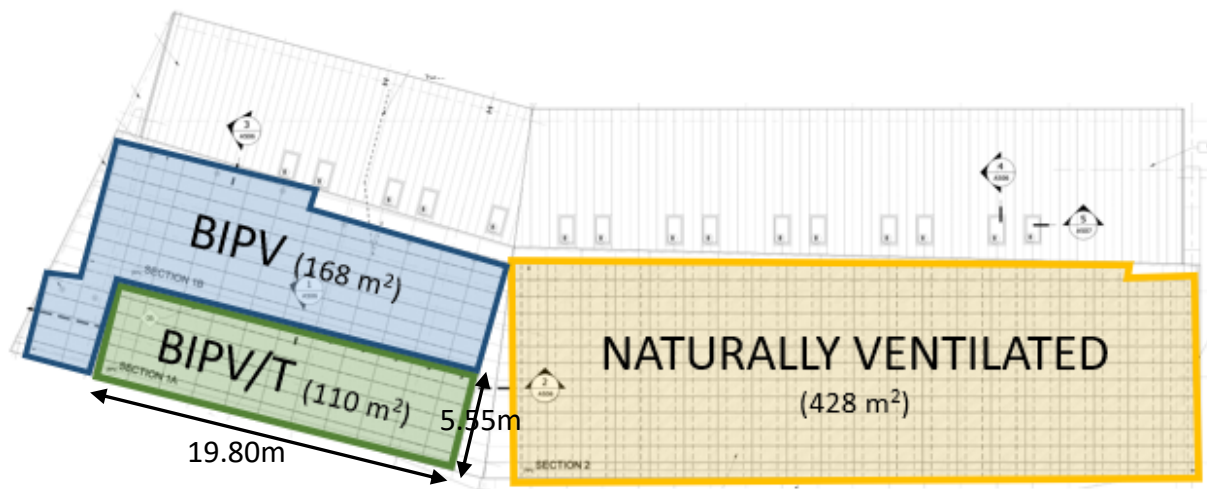


Figure 3-12 Schematic of the south-facing roof of the Varennes library.

The two types of configurations (70mm air gap, 150mm air gap) are illustrated in Figure 3-13 and Figure 3-14.

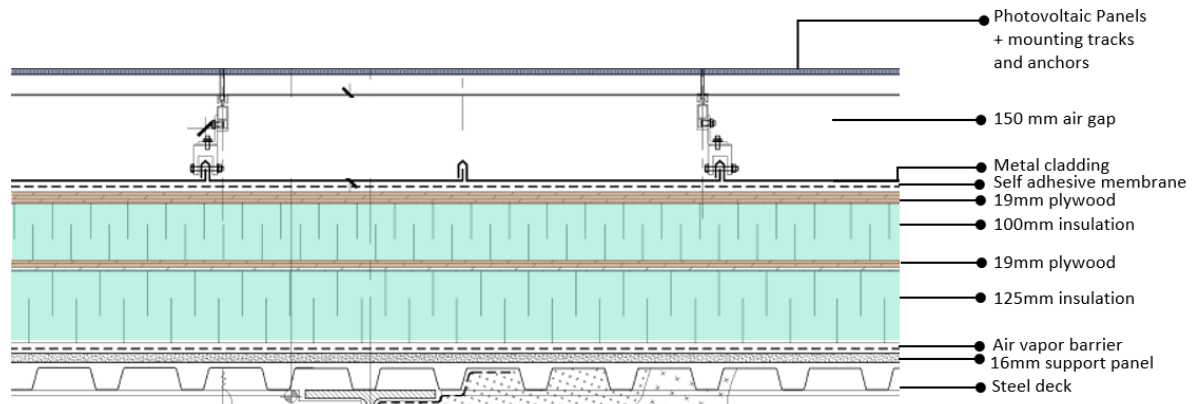


Figure 3-13 Naturally ventilated configuration with 150 mm air gap

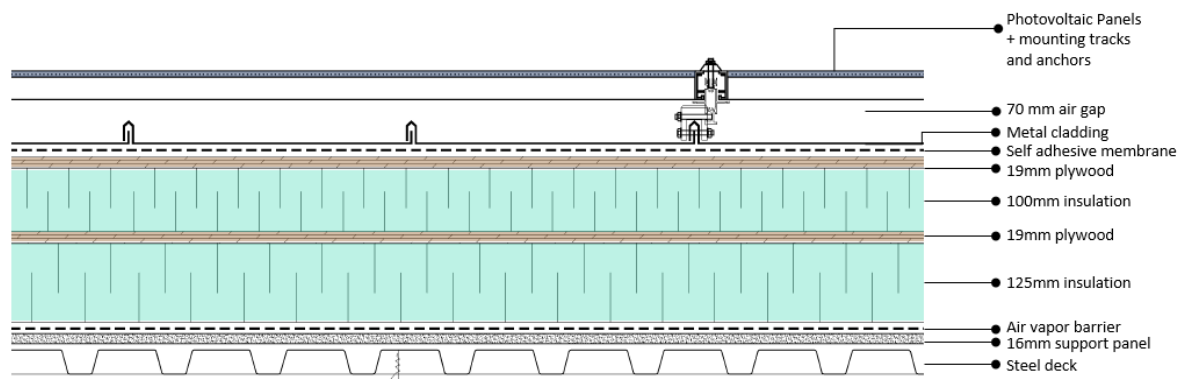


Figure 3-14 Mechanically ventilated configuration of BIPV or BIPV/T with 70 mm air gap

The Varennes library presents a great opportunity to serve as an archetype for development and optimization of design and control strategies for air-based BIPV/T systems as it is one of the few installed and fully operational full-scale systems globally. As it is closely monitored with sensors placed along the whole system and an installed weather station, detailed data is available enabling a broad range of possibilities.

To determine the PV temperature an RTD sensor (model: OMEGA SA1-RTD-4W-SB, type: 100 Ω DIN Class A, Surface RTD, accuracy: $\pm 0.15^\circ\text{C}$ at 0°C) placed on the PV back surface is used. The readings are at 1-minute interval and the placement of the sensor is shown in Figure 3-15. However, since the RTD sensor is placed in the beginning of the BIPV/T channel the reading is expected to be a lower temperature than what the PV temperature will be towards the end of the channel. Besides the RTD sensor, thermal cameras are placed at the Varennes library and take pictures of the roof in 15-minute intervals. In order to have a more accurate dataset for the PV temperatures the ΔT between the PV temperature at the start and end of the BIPV/T channel was

calculated through the data given by the thermal cameras. Then this ΔT was added to the RTD reading.

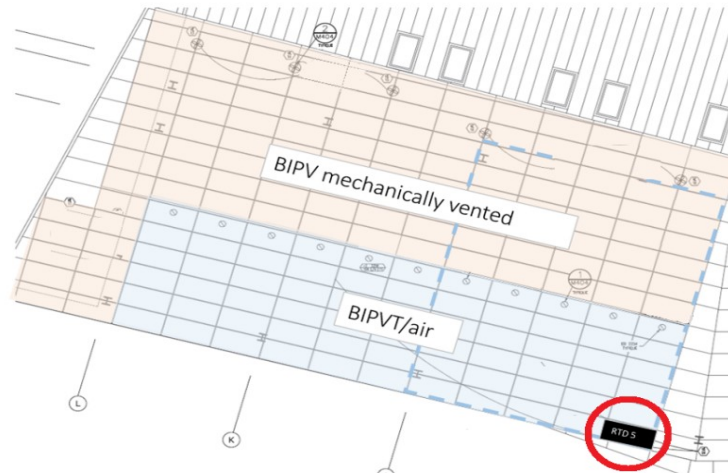


Figure 3-15 RTD placement for PV temperature monitoring

The speed of the BIPV/T recovery fan (VE-04) is set to either 33% or 80% with the objective to maintain the BIPV/T outlet temperature below 25°C. In cases where the BIPV/T outlet temperature is above 25°C for longer than 60 minutes, the fan increases its speed from 33% to 80%. [48]

The ventilation air is comprised either fully by the BIPV/T or by a mix of BIPV/T and fresh air. The air then passes through a thermal wheel and is further heated. During operational hours of the library the supply temperature setpoint is set to 18°C and if the air temperature deviates from the setpoint boundary, the heating/cooling coil located after the thermal wheel is activated. Sensors placed inside the Air Handling Unit record the data in 15-minute intervals, including temperature of the BIPV/T outlet air, the mixed air (BIPV/T + fresh air), the supply air after passing through the thermal wheel and heating/cooling coil and the exhaust air before and after the thermal wheel. The total mass flow rate delivered to and exhausted from the building is also measured. A schematic of the Air Handling Unit and the available sensors is shown in Figure 3-16. Additionally, weather data is available from an installed weather station at the library providing the ambient temperature (1-minute intervals), wind speed (10-second intervals) and irradiation (10-second intervals).

It is important to note that there is no measurement of the mass flow rate going through the BIPV/T channel. Even though the BIPV/T fan (VE-04) modulation is known this alone cannot give an accurate representation of the BIPV/T flow rate as the suction within the AHU can be partly attributed to the central fans (VA-01 to VA-04) located at the main duct from where the total supply ventilation air passes. (Figure 3-16)

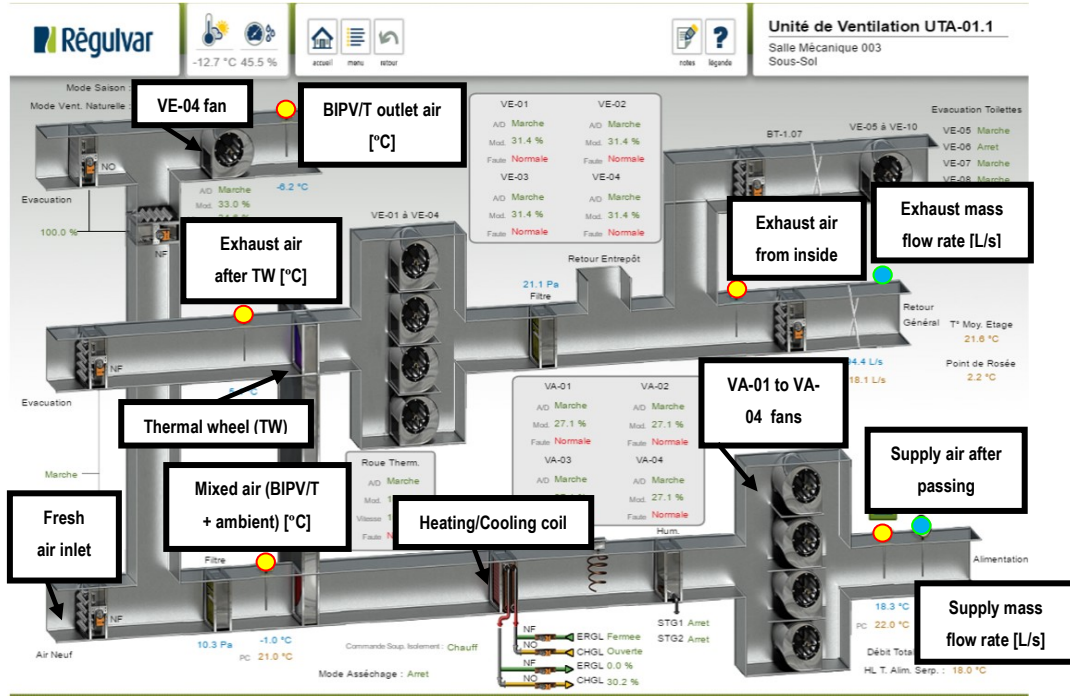


Figure 3-16 BIPV/T and AHU graphical user interface with sensor placement indication throughout the AHU.

3.2.1.1 Mass flow rate calculation

In this section an analysis for a typical cold sunny day is presented and the process of the mass flow rate calculation within the BIPV/T channel is demonstrated. As mentioned previously there is no sensor placement in the BIPV/T channel for measurements of the air flow passing through the BIPV/T. The mass flow rate is an extremely important parameter in order to be able to accurately calibrate the BIPV/T models with the Varennes library dataset. The recovery fan (VE-04), which ventilates the PV cells of BIPV/T, has a flowrate capacity of 1142 L/s and operates only during hours where the BIPV systems generates energy. [48] The speed of the fan is determined by the BIPV/T outlet temperature as shown in (3-27).

$$BIPV/T \text{ FAN CONTROL} = \begin{cases} 33\%, & T_{outlet} < 25^\circ\text{C} \\ 80\%, & T_{outlet} \geq 25^\circ\text{C} \end{cases}, \text{deadband} = 1 \text{ hour} \quad (3-27)$$

where,

- T_{outlet} : outlet Temperature of the BIPV/T

In Figure 3-17 the ambient temperature along with the BIPV/T outlet temperature and fan modulation are illustrated for a cold sunny day. During the first examined day, January 9 2020, as the ambient temperature is low, less than -10°C , the BIPV/T outlet temperature never goes over 25°C . Consequently, the fan remains at the low-speed setting (33%) during the hours the BIPV/T operates, in this case 07:30 – 16:00.

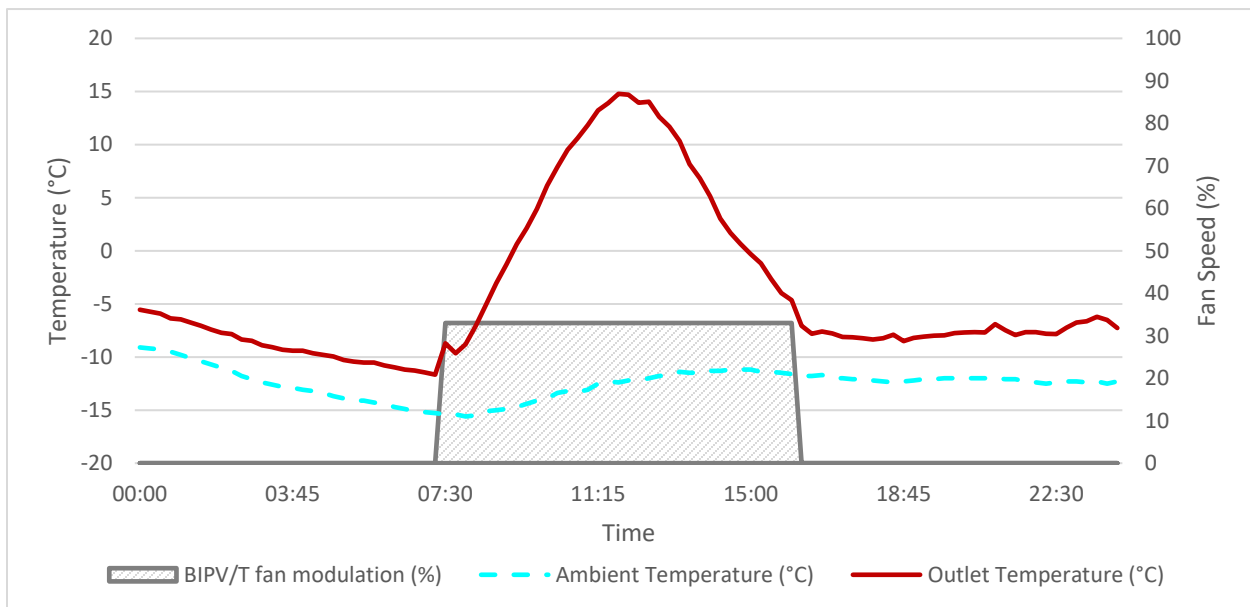


Figure 3-17 Recorded ambient and outlet temperatures along with the BIPV/T fan modulation on a cold sunny day (January 9, 2020).

On a warmer day, February 24 2020, where the ambient temperature fluctuates between $2\text{-}9^\circ\text{C}$, the BIPV/T outlet temperature is able to reach a maximum of 30°C during peak irradiation hours. This causes the fan to increase its speed to 80% between 10:30-15:30, when the outlet temperature is over 25°C . (Figure 3-18).

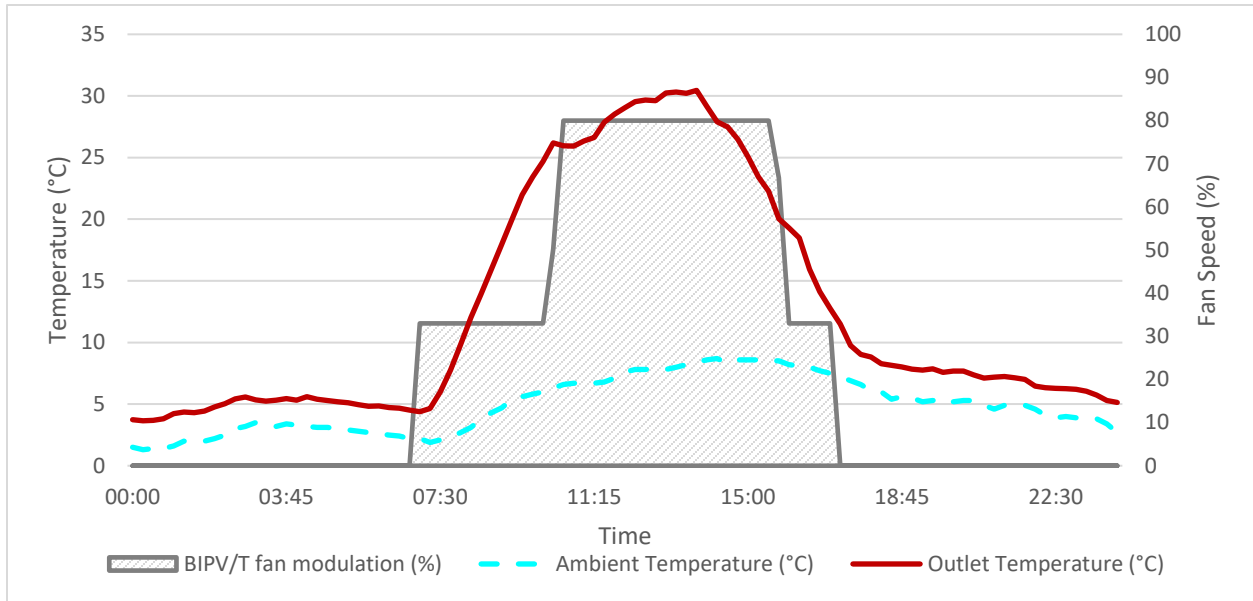


Figure 3-18 Recorded ambient and outlet temperatures along with the BIPV/T fan modulation on a mild sunny day (February 24, 2020).

A significant limitation in modelling this system is the lack of a mass flow rate sensor for the air passing through the BIPV/T channel. To estimate the BIPV/T air flow rate an enthalpy balance was conducted. Since the BIPV/T outlet temperature, outdoor air temperature and mixed (BIPV/T + fresh) temperature along with the total supply flow rate are known, the flow rate coming directly from the BIPV/T can be estimated by using the following equations for the different airstreams:

$$\dot{m}_{BIPV/T} \cdot h_{BIPV/T} + \dot{m}_{outside} \cdot h_{outside} = \dot{m}_{total} \cdot h_{total} \quad (3-28)$$

$$\dot{m}_{total} = \dot{m}_{BIPV/T} + \dot{m}_{outside} \quad (3-29)$$

where,

- $\dot{m}_{BIPV/T}$: mass flow rate coming from the BIPV/T channel (kg/s)
- $\dot{m}_{outside}$: mass flow rate coming from outside (kg/s)
- \dot{m}_{total} : mass flow rate of combined airstream sent to the building (kg/s)
- $h_{BIPV/T}$: enthalpy of airstream coming from the BIPV/T channel (kJ/kg)
- $h_{outside}$: enthalpy of airstream coming from outside (kJ/kg)
- h_{total} : enthalpy of combined airstream sent to the building (kJ/kg)

The results of this analysis are shown in Figure 3-19 and Figure 3-20 for January 9 and February 24 respectively. During the cold day (January 9) it can be observed that the portion of the total ventilation air coming from the BIPV/T is very high throughout the day with the BIPV/T fully supplying the AHU at the beginning and end of the irradiance hours. On the contrary during a mild day with an average outdoor temperature of around 5°C, the portion of outdoor air mixed into the total ventilation air is significantly higher especially during midday when the BIPV/T outlet temperature is high (>20°C).

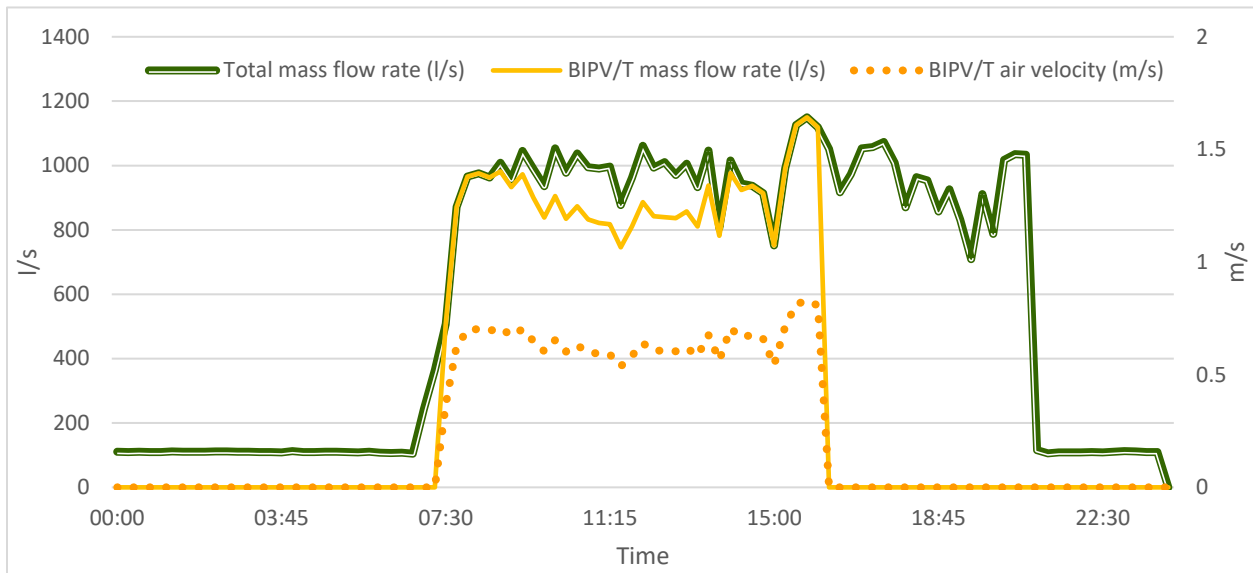


Figure 3-19 Total ventilation flow rate, BIPV/T flow rate and BIPV/T channel air velocity for a cold sunny day (January 9, 2020)

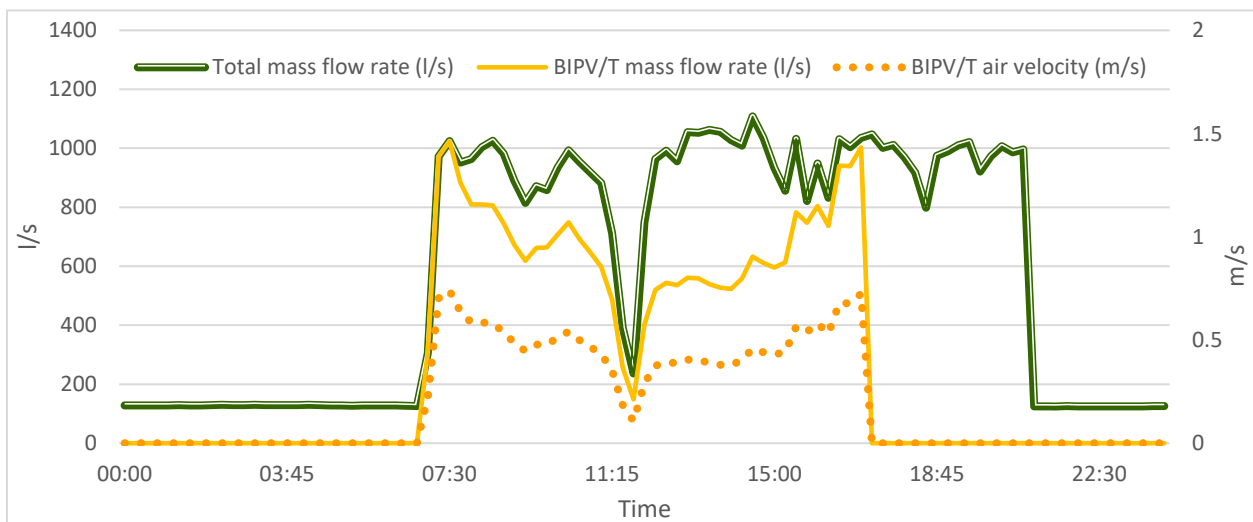


Figure 3-20 Total ventilation flow rate, BIPV/T flow rate and BIPV/T channel air velocity for a mild sunny day (February 24, 2020)

From both Figure 3-20 and Figure 3-19 it can be seen that the portion of the total supply air coming from the BIPV/T is found to be consistently over 70% at times when the fan operated at the low-speed setting. This rises the concern that either the general supply fans, VA-01.1-VA01.4, significantly contribute to the air suction from the BIPV/T channel or that one of the measured temperatures used in the enthalpy balance (mixed air or BIPV/T air) is overestimated leading to higher BIPV/T mass flow rate estimations. As the mixed air sensor is placed right next to the thermal wheel it may be affected by heat from coming it (Figure 3-16) resulting in higher readings. For this work the mass flow rate measurement is considered accurate and is used for the model calibration, however further investigation is needed to ascertain the source of error.

3.2.2 Model Calibration

The methodology described in section 3.1.5.1- Grey-Box Method is followed, using the Varennes dataset this time, in order to “match” the parameters of the BIPV/T model with this specific system. Both SS and TR models are calibrated and the same parameters as in section 3.1.5.1 are chosen to be adjusted; the thermal conductance (U value) of the PV module and the rear side of the channel and the thermal capacitance (C value) of the PV module (only for the TR model). The initial guesses of the parameters are estimated based on the materials used on the system which are presented in Figure 3-14. Table 3-4 lists the initial value of the calibrated parameters and the bounds used for the calibration process.

Table 3-4 Initial guesses and bounds for calibrated parameters

Parameter	Initial guess	Bounds
C_{PV} (J/m ² K)	7578.6	$757.86 < C_{PV} < 75786$
U_{PV} (W/m ² K)	241.43	$24.143 < U_{PV} < 2414.3$
U_{BOT} (W/m ² K)	0.119	$0.0119 < U_{BOT} < 1.19$

During the initial stages of testing the developed BIPV/T models against the Varennes data it became evident the models were underestimating the outlet temperature. A brief analysis comparing the convective heat transfer coefficients with this dataset was conducted. The same 3 Nusselt number expressions tested in section 3.1.1 were used here as well. The results of the

analysis showed that the best performing CHTC for this system was the one by Candanedo et al. which is specifically developed for BIPV/T systems.

3.2.2.1 Cost function optimization

The cost function used in the calibration initially was the summation of the NRMSE created by the outlet temperature and the PV temperature. However, it was observed that the calibration would “favour” a smaller NRMSE for the PV temperature which led to an increase in the respective error for the outlet temperature. As the primary goal of this model is the control of the mass flow rate with the aim to achieve higher thermal utilization efficiency, it was deemed that the accuracy of the outlet temperature prediction was more critical than that of the PV temperature. A brief parametric analysis with a variable multiplication factor as a means to find a good balance between the two NRMSEs was conducted. The variable cost function used for this process is:

$$J = a \cdot \frac{\sqrt{\sum_{i=1}^n \frac{(\hat{T}_{outlet_i} - T_{outlet_i})^2}{n}}}{T_{outlet_{max}} - T_{outlet_{min}}} + (1 - a) \cdot \frac{\sqrt{\sum_{i=1}^n \frac{(\hat{T}_{PV_i} - T_{PV_i})^2}{n}}}{T_{PV_{max}} - T_{PV_{min}}} \quad (3-30)$$

where,

- \hat{T}_{outlet} : predicted outlet temperature (°C)
- T_{outlet} : measured outlet temperature (°C)
- \hat{T}_{PV} : predicted PV temperature (°C)
- T_{PV} : measured outlet temperature (°C)
- n : number of datapoints
- a : multiplication factor

The multiplication factor varied from 0 to 1 and for each value the NRMSE of the outlet temperature, the PV temperature and the total were recorder for a test dataset. Figure 3-21 shows the results of this analysis. When α was set to 0.6 the NRMSE of the outlet temperature was minimized, but the PV error increased compared to when α was set to 0.4 or 0.5. When α was set at higher values (≥ 0.8) the total NRMSE started increased significantly. It can also be noticed

that the models generally perform better when the calibration is aimed to minimize the PV temperature error rather than the outlet temperature. If the calibration is done with the goal to have only an accurate outlet temperature prediction, then the transient model gives better results.

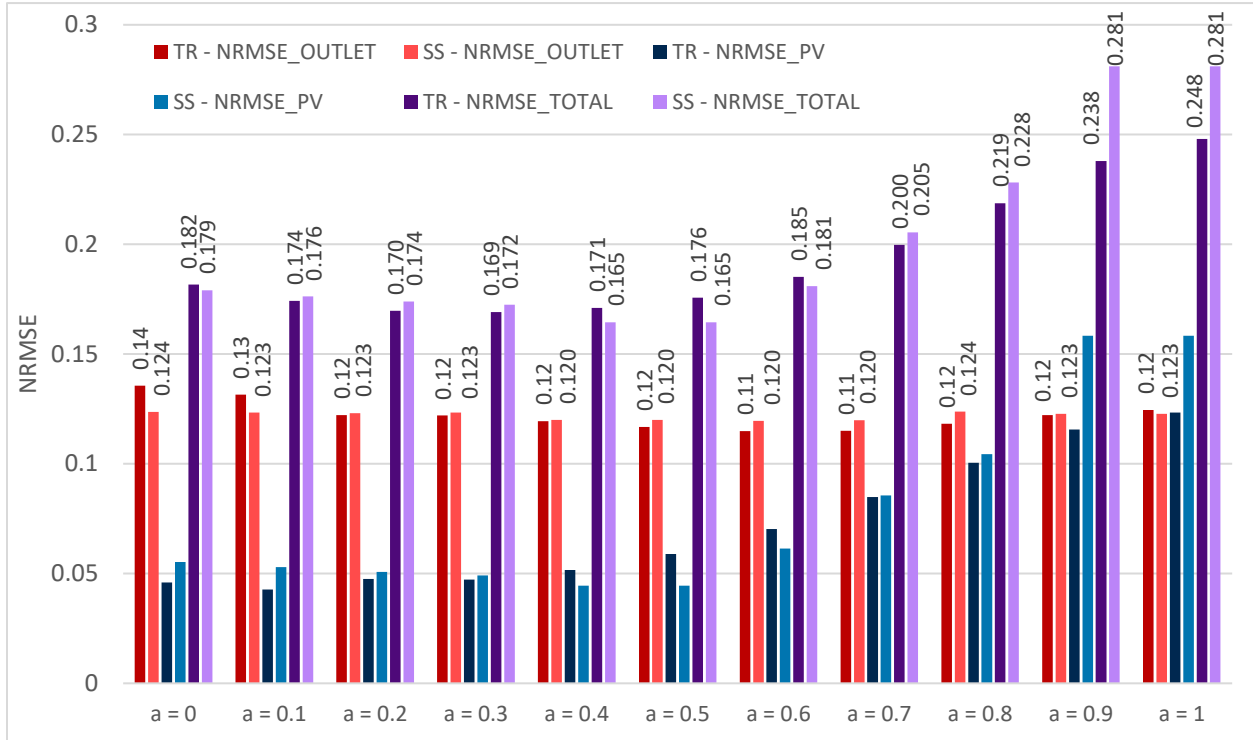


Figure 3-21 NRMSE for the outlet temperature, PV temperature using different cost functions for the model calibration

However, besides overall accuracy another important aspect a control-oriented BIPV/T model should have, is to be able to keep a fairly steady outlet temperature prediction in order to prevent the control algorithm from constantly changing settings due to instantaneous fluctuations. Figure 3-22 illustrates the prediction of the SS model for different α -values. As the α -value increases the fluctuations in the outlet temperature become more acute. When α is set to 0.6 the outlet temperature prediction is fairly stable. When $\alpha=1$ the model predicts very well the outlet temperature during the off-peak irradiance hours (06:30 – 09:00 & 15:00 – 15:30). However, during the high irradiance time (mid-day) the outlet temperature is overpredicted. When looking at the respective graph for the TR model predictions (Figure 3-23) the damping effect of the PV module thermal capacity can be clearly observed which leads to more “stable” predictions regardless of the α -value. From the calibration process it was noticed that as the α increased, the thermal capacity of the PV modules decreased, reducing the overall damping effect. Thus, the

outlet temperature prediction increased bringing it closer to the measured data. Setting α between 0.4 and 0.6 was found to be the best range which can achieve good accuracy and lower fluctuations of the outlet temperature prediction.

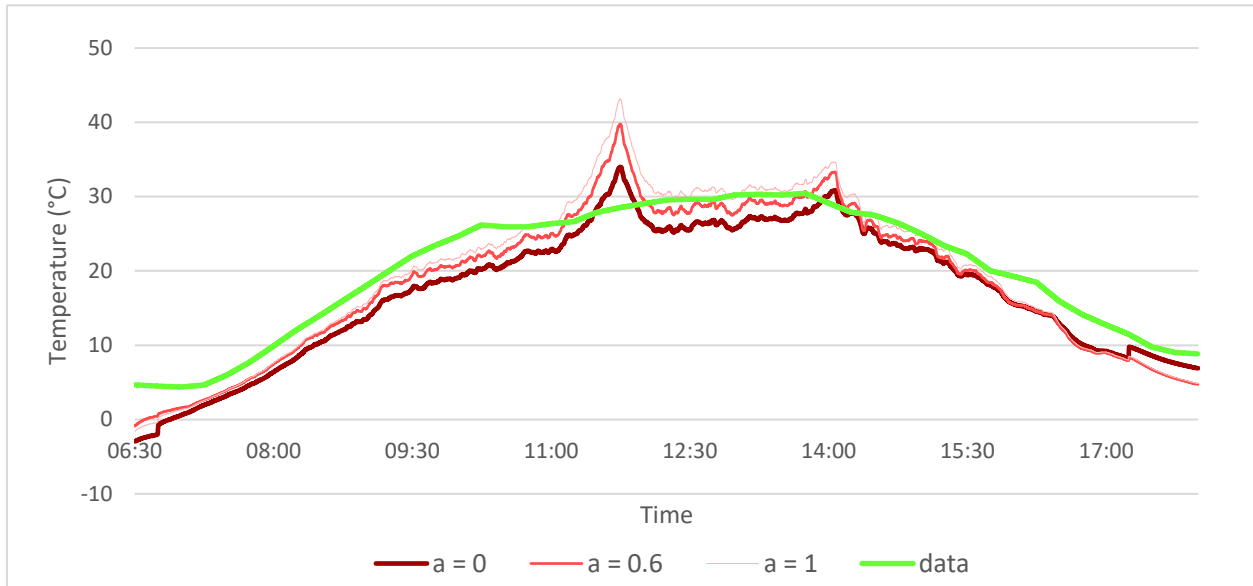


Figure 3-23 TR model outlet temperature prediction for different α -values.

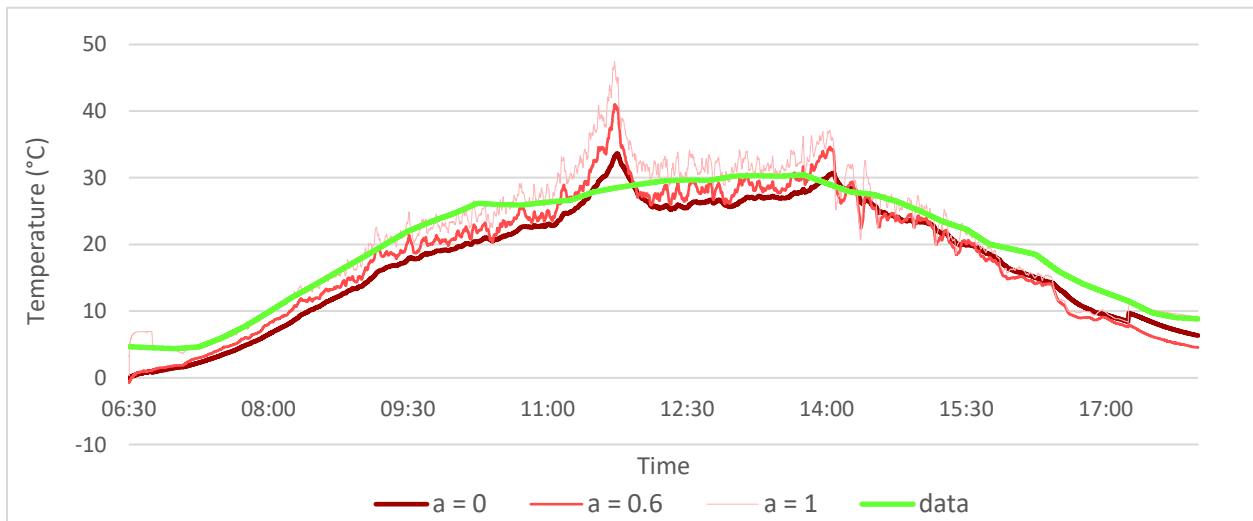


Figure 3-22 SS model outlet temperature prediction for different α -values.

3.2.2.2 Cross-validation

In order to have a more accurate and robust calibration, a cross-validation between four different datasets was implemented. Four days with different wind profiles irradiance levels and outside

temperature were used to test the model performance under different environmental conditions. The weather conditions of the four days are illustrated in Figure 3-24.

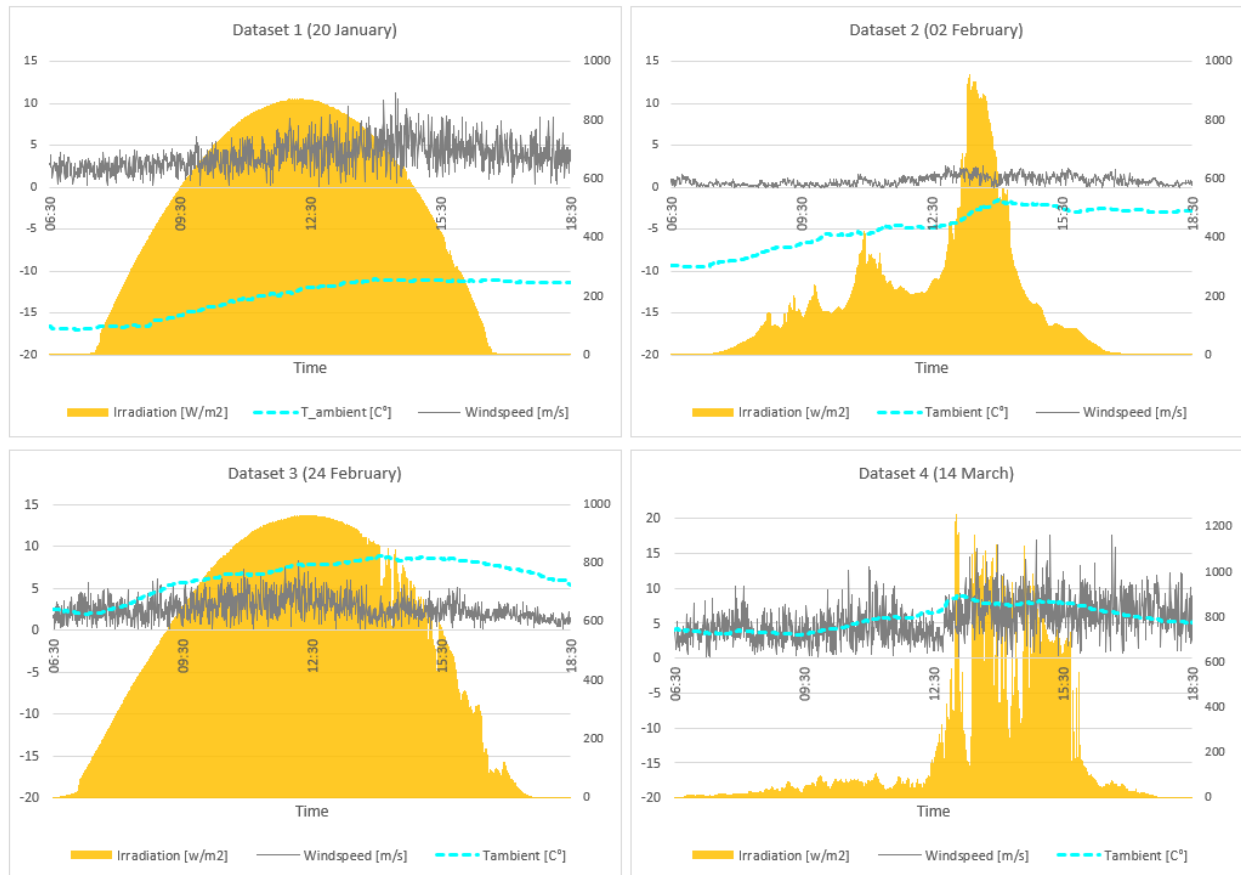


Figure 3-24 Weather conditions for the different datasets used for the cross-validation of the models.

Cross-validation is a technique used to assess how well the results given from a developed model will generalize when using an independent dataset. When performing cross-validation the available data is split to different parts and each time a different portion of the data is used to train and test the model. It is commonly used in cases where the goal of the model is prediction and can give a good estimation of how accurately the model will perform. In this case a 4-fold cross validation is performed; the data is split in to 4 different days. For each time, the model uses one of the given days to perform the calibration process (training dataset) and set values to the calibrated parameters and then is tested under the other three days (test dataset) in order to validate the model performance and be able to identify possible problems such as overfitting.

[49]

Table 3-5 and Table 3-6 list the NRMSE for both BIPV/T models for the 64 different combinations of training and test datasets. The NRMSE of the cost function used for the calibration, described in section 3.2.2.1, varies between 0.05 – 0.29. Thus, the model is able to accurately predict the outlet and PV temperature under different environmental conditions. The diagonal cells of Table 3-5 and Table 3-6 represent the NRMSE of the cases where the model is calibrated and tested using the same dataset. This is the “optimal” case leading to the smallest NRMSE compared to when the same dataset is used as a test dataset but is calibrated using another one. This means that for every row in the tables the smallest value is the respective diagonal cell of that row. If this were not the case that would mean the calibration process did not result in the best combination of values for the calibrated parameters. Finally, it can also be observed that in the majority of cases the TR model performs slightly better (gives smaller NRMSE) than the SS model.

Table 3-5 NRMSE for calibration cost function (TR model)

NRMSE_TR_COST_FUNCTION	Training Dataset				
Test Dataset		Dataset 1	Dataset 2	Dataset 3	Dataset 4
	Dataset 1	0.19 °C	0.29 °C	0.25 °C	0.25 °C
	Dataset 2	0.19 °C	0.14 °C	0.15 °C	0.14 °C
	Dataset 3	0.16 °C	0.10 °C	0.07 °C	0.08 °C
	Dataset 4	0.11 °C	0.07 °C	0.05 °C	0.05 °C

Table 3-6 NRMSE for calibration cost function (SS model)

NRMSE_SS_COST_FUNCTION	Training Dataset				
Test Dataset		Dataset 1	Dataset 2	Dataset 3	Dataset 4
	Dataset 1	0.19 °C	0.19 °C	0.25 °C	0.19 °C
	Dataset 2	0.19 °C	0.15 °C	0.16 °C	0.15 °C
	Dataset 3	0.20 °C	0.12 °C	0.08 °C	0.11 °C
	Dataset 4	0.13 °C	0.09 °C	0.07 °C	0.07 °C

Figure 3-25 is a visual representation of the model performance where dataset 3 is used to train the model which is then tested against dataset 4. As mentioned previously the SS model tends to

have more acute fluctuations in its predictions when compared to the TR model. This can clearly be seen in this graph as well.

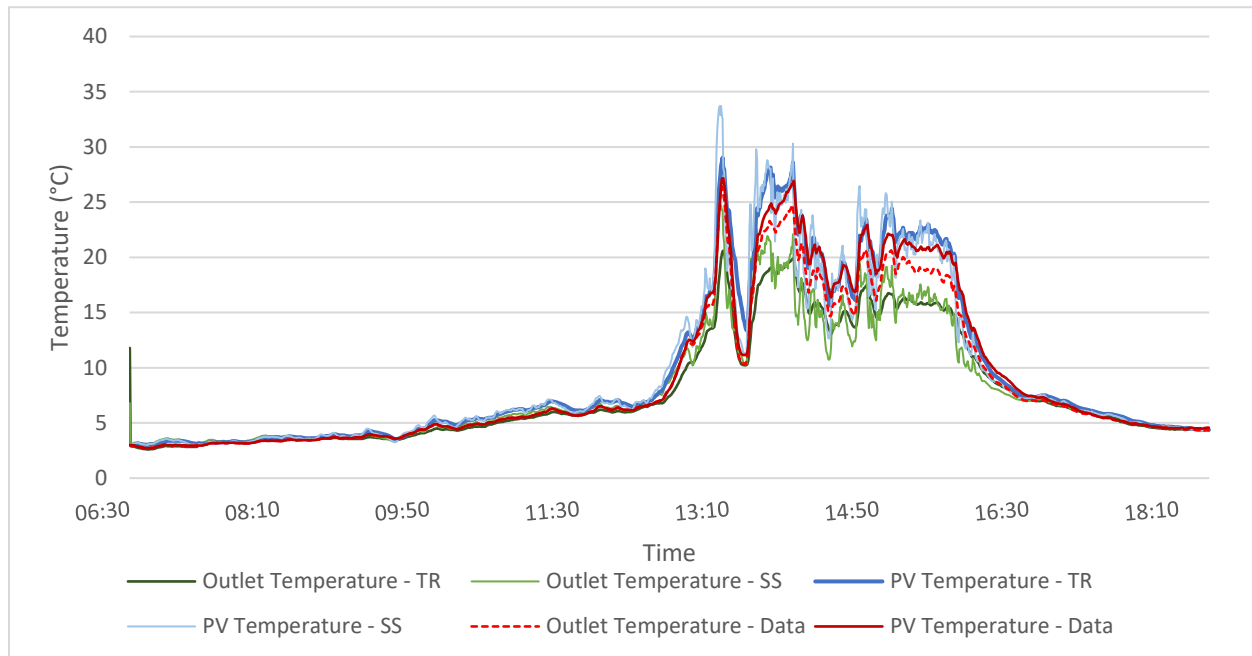


Figure 3-25 Actual and predicted outlet and PV temperatures using dataset 3 to calibrate the model (training dataset) and dataset 4 to validate the results (test dataset).

When using the Varennes dataset, the BIPV/T models do not perform as well as when using the experimental data, which is an indicator of the uncertainties coming with a dataset of an actual commissioned system.

One of the crucial parameters that clearly affected the calibration process and therefore the model's performance is the lack of a mass flow rate measurement at the BIPV/T outlet. In the attempt to overcome this barrier an enthalpy balance was conducted for the different airstreams within the AHU with the aim to estimate the air flow passing through the BIPV/T, however many assumptions and simplifications were deemed necessary. In many instances throughout the data, the mixed air (BIPV/T + outdoor) temperature was higher than that of the outlet BIPV/T air temperature. Since the precise placement of the sensors within the AHU is unknown, this led to the suspicion that the mixed air sensor is placed very close to the ERV resulting in overestimated readings. If this is indeed the case the enthalpy balance will lead to an overestimation of the BIPV/T air flow rate. From Figure 3-25 it is evident that the main source of error comes from the underestimation of the outlet temperature by the models, which may be caused by a higher mass flow rate approximation. Further investigation is needed to fully resolve this matter.

Furthermore, the PV temperatures also have a certain level of uncertainty as the only highly accurate measurement is the RTD placed at the beginning of the channel. The measured ΔT between the beginning and end of the BIPV/T channel from the thermal cameras was used to come closer to the PV temperature at the end of the channel, however the thermal camera readings can be easily affected by glare and generally have lower accuracies ($\pm 2^\circ\text{C}$).

Despite the limitations, this analysis gave a good indication of which parameters would be necessary to apply model-based control on a commissioned BIPV/T system. Priority would be to have reliable measurements of the mass flow rate, outlet temperature, PV temperature at the end of the channel, as this is the most vulnerable to overheat, and BIPV/T channel dimensions. A weather station measuring ambient temperature, irradiation levels and wind speed on site would be useful but not necessary as close by weather stations could give a good indication of the environmental conditions. A measurement of the PV temperature at the beginning of the channel can be valuable so as to have the full PV temperature range of the BIPV/T channel. Finally, the BIPV/T material properties (thermal resistance, thermal capacitance, optical properties etc.) could prove useful but are not essential as they can be estimated by calibrating the model.

Chapter 4 MPC Development

The two main components required for MPC are the dynamic system model and the optimization algorithm. The model is used to predict future behaviour of the controlled system and give specific outputs, such as temperatures, which are derived by the respective environmental conditions and disturbances on the system. Additionally, using the model other metrics can be evaluated such as energy efficiency and cost of the system. The optimization algorithm uses the model predictions and adjusts the control settings according to the respective goal specified by the user. [35] The end goal of the optimization algorithm is commonly referred to as the cost function of the control strategy which is the metric the algorithm aims to minimize. In this study the controlled system is the BIPV/T, the manipulated variable is the mass flow rate or air velocity within the channel and the cost function the net energy consumption of the system. In this chapter the optimization algorithm for MPC strategy followed is presented along with the scenarios considered. Finally, the results and discussion comprise the last part of the chapter.

4.1 Thermal applications

The use of the thermal energy produced by the BIPV/T is considered to be used in one or more of these thermal applications:

Energy Recovery Ventilator (ERV)

The solar heated air is further heated by passing through an enthalpy wheel located in the AHU of the Varennes library. In the actual system this is the only application available for the utilization of the BIPV/T heat. The specifications of the ERV are listed in Table 4-1. The thermal efficiency claimed by the manufacturer is 74.4%. To validate the actual thermal efficiency of the system a brief analysis using the 2 airstreams (supply and exhaust) passing through the ERV was conducted.

Table 4-1 ERV Manufacturer specifications

Brand	Model	Type	Efficiency	
			Sensible	Latent
INNERGY TECH	ERW 3000	Enthalpy / Variable speed	74.4%	65%

The efficiency of the ERV was calculated based on the methodology described by ASHRAE for air-to-air energy recovery equipment [26]. A conceptual ERV is illustrated in Figure 4-1. Heat and moisture are transferred between the two airstreams without mixing them, whenever there is a difference in temperature or vapor pressure between them. [26]

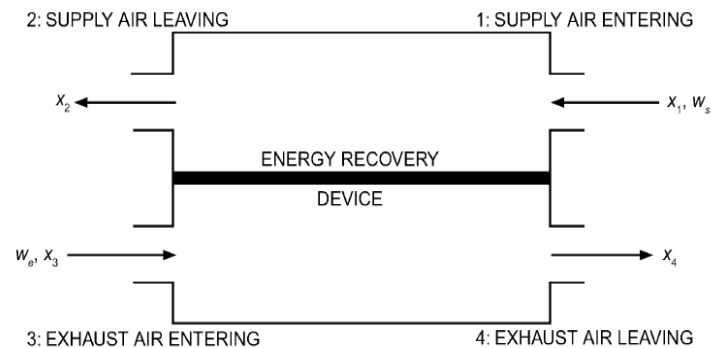


Figure 4-1 Airstream numbering in an ERV [26]

As there weren't enough humidity measurements to evaluate the actual latent efficiency of the equipment, the sensible efficiency was used to verify whether the claimed efficiency from the manufacturer corresponded to the actual value.

The sensible efficiency of an ERV is calculated by [26]:

$$\epsilon_{sensible} = \frac{\dot{m}_2 \cdot (c_{p,1} \cdot T_3 - c_{p,2} \cdot T_4)}{\dot{m}_{min} \cdot (c_{p,1} \cdot T_3 - c_{p,3} \cdot T_1)} \quad (4-1)$$

where,

- \dot{m}_n : mass flow rate at station n, (kg/s)
- \dot{m}_{min} : minimum of \dot{m}_2 and \dot{m}_3 , (kg/s)
- $c_{p,n}$: specific heat of dry air at station n, (kJ/kg·K)
- T_n : dry-bulb temperature at station n, (°C)

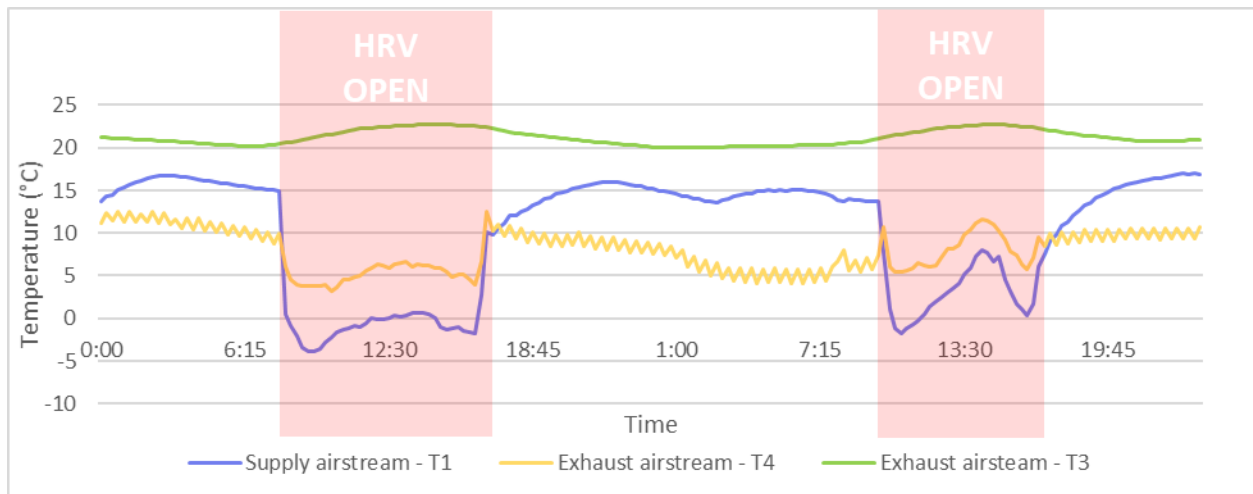


Figure 4-2 Supply and exhaust airstream temperatures passing through the ERV for two consecutive days.

For two analysed days an average sensible efficiency of 73.4% was recorded (Figure 4-3) which is very close to the efficiency given by the manufacturer.

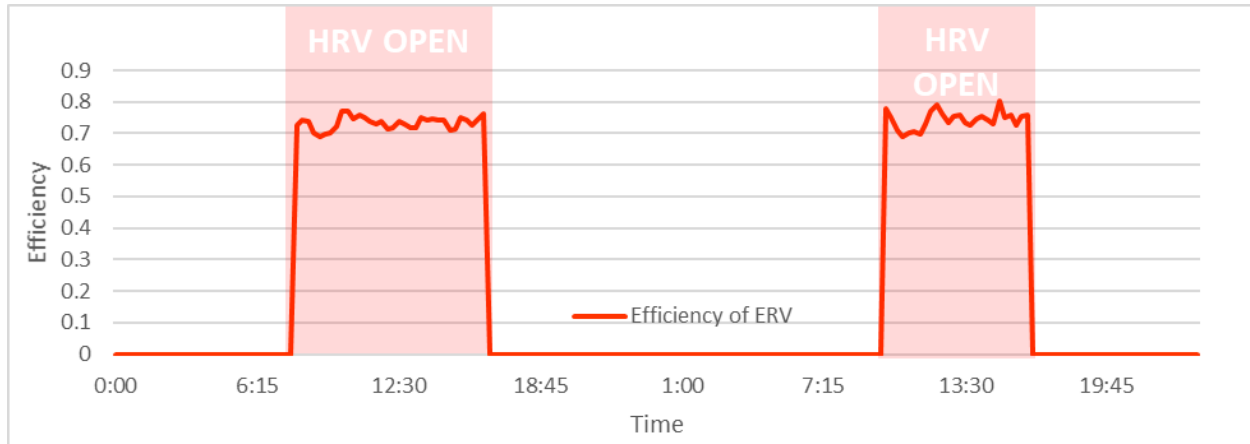


Figure 4-3 Calculated sensible efficiency of ERV for two consecutive days.

If the air flowing through the ERV is lower than the specified setpoint it is further heated or cooled by heating/cooling coils supplied by the ground source heat pump (GSHP), ensuring an adequate supply temperature of 18°C during the day. The COP of the GSHP is assumed equal to 3.1 according to energy performance standard for ground-source heat pumps provided by the Government of Canada. [50]

Hence, the additional electrical energy required to reach the given setpoint is:

$$Q_{ERV} = \frac{\dot{m} \cdot c_{air} \cdot \Delta T}{COP_{GSHP}} \quad (4-2)$$

where,

- \dot{m} : mass flow rate passing through the ERV (kg/s)
- c_{air} : specific heat of air (kJ/kg·K)
- ΔT : the temperature difference between setpoint and T_2
- COP_{GSHP} : coefficient of performance of the ground source heat pump

Air-to-Water Heat Pump (HP)

The next possible thermal application is enhancing the performance of an air-to-water heat pump. By increasing the inlet air temperature of an air-source heat pump by using the preheated air from the BIPV/T, the COP of the heat pump can significantly improve. As at this time this application is not applied in the actual system at the library, a theoretical system was simulated. A data-based model of an air-to-water heat pump using performance data available from the cold climate heat pump manufacturer Arctic Heat Pumps was developed. [31], [51] The source-side

air temperature range varied from -20°C to 35°C and for the supply-side water temperature between 15°C and 55°C. Reference data was selected arbitrarily since the coefficients used are relative to that reference. [31] For this work the HP requires an air flow rate of 1.66 kg/s, has a reference COP of 2.84 and heating capacity (HC) 29 kW for air and water temperature 0°C and 40°C respectively. As the air source temperature increases, we can achieve higher COPs (Figure 4-5). The heat pump is used solely for space heating in this case. A measured heating load profile during a cold sunny day at the library is used in the simulations and is shown in Figure 4-4. [48] The instantaneous COP at each sampling moment can be calculated as:

$$COP_{instantiateous} = COP_{reference} \cdot COP_{ratio} \quad (4-3)$$

In Figure 4-5 the distribution of the COP for different air and water temperatures is illustrated. From the graph it can be seen that, especially for lower water setpoints, the instantaneous COP of the HP can increase dramatically with an increase in the source-side air temperature. For example, for $T_{water} = 25^\circ\text{C}$ and an increase in air temperature from -20°C to 0°C, which is possible when using the BIPV/T, the COP can double (from 2 to 4). This essentially means we can consume half the electricity to run the heat pump compared to if outside air is used directly as a source. In our case, since the HP is used for space heating a water temperature setpoint of 50°C was chosen.

At each timestep, the power consumption of the HP is calculated as:

$$Q_{HP} = \frac{Q_{load}}{COP_{instantiateous}} \quad (4-4)$$

where,

- Q_{load} : the instantaneous electricity heating load at a sampling moment (kW)
- $COP_{instantiateous}$: the instantaneous COP of the heat pump at that moment.

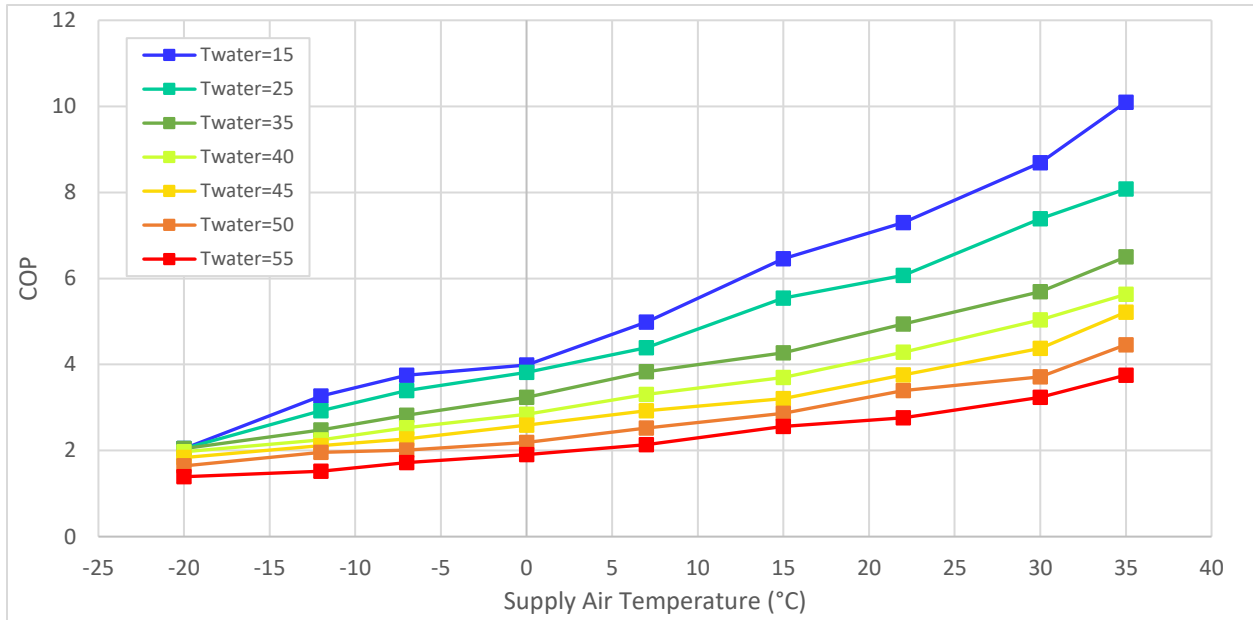


Figure 4-5 Heat Pump COP for different air and water temperatures.

A profile of the measured electricity heating load for a typical cold sunny day at the Varennes library was used for the simulations shown in Figure 4-4. Two peaks can be identified, during the morning hours (08:00 – 11:00) and evening (18:00 – 21:00). The BIPV/T is able to facilitate only in the morning peak reduction as it does not produce energy at the time of the evening peak.

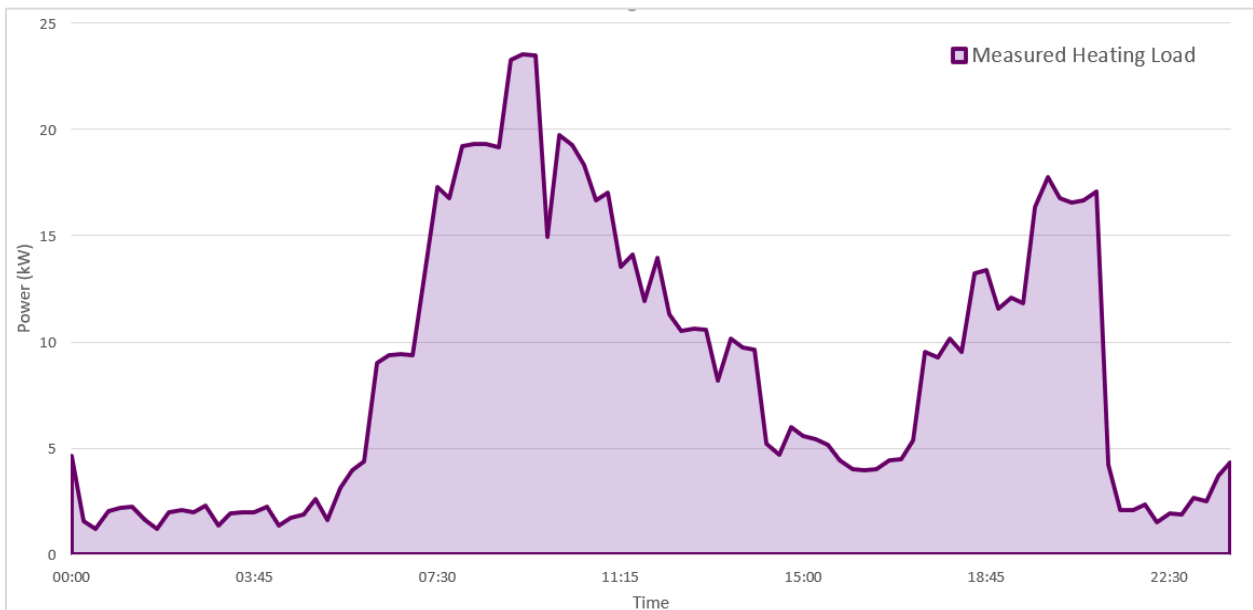


Figure 4-4 Electricity heating load for the Varennes library on a cold sunny day

Heat Delivery to Adjacent Buildings (HDAB)

Finally, in times where the library produces more heat than what is needed for its own needs, the possibility to send heat to nearby buildings is explored. Figure 4-6 illustrates the location of the Varennes library on the map along with some of the close-by building.



Figure 4-6 Display of Varennes library and adjacent daycare center (Ateliers De La Maison Bleu) on google maps with estimated distance between them.

Located at 80 & 88, rue Dalpé, right behind the Varennes library, are two preschool day care centres; The Ateliers De La Maison Bleu, Le Bateau & Le Phare. According to their website, the schools operate Monday to Friday 07:00am – 18:00pm. The schools welcome in total 116 children every day of the week and host a nursery for 10 infants aged between 0 and 18 months. A new municipal swimming pool is planned to be installed in the near future which will be used and water games and educational purposes for the children. [52]

It is important to note that since the peak heat production hours of the BIPV/T are between 11:00am-14:00pm, sending heat to adjacent residential buildings may not be as meaningful; people are often not home during these hours and the need for heat is relatively low. This highlights the significance of having the above-mentioned building so close to the library as the peak heating load for the day-care centre will generally align with the peak heat production of the BIPV/T thus reducing the requirement for thermal storage.

The excess heat produced by the BIPV/T collector is sent to the daycare to be used as preheated ventilation air. To calculate the minimum ventilation requirements for the daycare ASHRAE Standard 62.1 [53] was used. The breathing zone outdoor airflow is determined according to the equation:

$$V_{bz} = R_p \cdot P_z + R_a \cdot A_z \quad (4-5)$$

where,

- R_p : outdoor airflow rate required per person
- P_z : the largest number of people expected to occupy the zone during typical usage
- R_a : outdoor airflow rate required per unit area
- A_z : the net occupiable floor area of the *zone* m²

For a daycare with children up to 4 years old according to table 6.2.2.1, [53] $R_p = 5\text{L/s}\cdot\text{person}$, $P_z = 25\text{ people}/100\text{m}^2$, $R_a = 0.9\text{L/s}\cdot\text{m}^2$ and the estimated floor area of the daycare is $A_z = 1000\text{m}^2$ (Figure 4-7). The minimum ventilation rate for the daycare is calculated to be equal to 2150 L/s (2.58 kg/s) and the supply ventilation air setpoint is approximated to be 18°C. The losses occurring during the transport of the heated air from the library to the daycare are assumed to be equal to 10%.



Figure 4-7 Adjacent daycare center, area estimation on Google maps [58]

4.2 Methodology

In order to minimize the net energy consumption by controlling the mass flow rate within the BIPV/T collector, 3 control variables are identified. Namely, the mass flow rate of the air passing through of the BIPV/T (m_{bipvt}), and the portions of m_{bipvt} sent to each thermal application concerning the library needs (m_{erv} , m_{hp}). Each thermal application has the possibility to be either fully supplied by the BIPV/T collector or use a mix of BIPV/T and outside air. This is determined through the optimization algorithm with the objective to minimize the MPC cost function. In the case the heat production from the BIPV/T collector exceeds the needs of the library the heat is sent to fulfill the needs of adjacent buildings.

Two important parameters for the MPC formulation are the prediction and control horizon. The optimization algorithm forms a control profile over a specified prediction horizon. Once the algorithm determines the optimal control settings over the prediction horizon these settings are applied to the BIPV/T model over a shorter specified time (control horizon). The process is repeated at intervals equivalent to the determined control horizon. The methodology assumes all future predictions are precise.

The objective function of the MPC strategy was set to minimize the net electrical energy consumption of the library for the given prediction horizon P:

$$J_{tot} = \sum_{t=1}^P [Q_{ERV}(t) + Q_{HP}(t) - Q_{PV}(t) + Q_{fan}(t)] \quad (4-6)$$

where,

- Q_{ERV} : the additional electricity required by the EF to reach the ventilation setpoint³ (kW)
- Q_{HP} : the electricity consumption of the HP⁴ (kW)
- Q_{PV} : the electricity generation of the BIPV/T system (kW)
- Q_{fan} : the electricity consumption of the BIPV/T fan (kW)

The electricity generation from the BIPV/T is given by the equation:

³ See equation (4-2)

⁴ See equation (4-4)

$$Q_{PV} = \eta_{PV} \cdot A_{BIPV/T} \cdot PF \cdot G_{incident} \quad (4-7)$$

where,

- η_{PV} : electrical efficiency of PV modules⁵
- $A_{BIPV/T}$: area covered by BIPV/T (m²)
- PF: packing Factor of PV modules
- $G_{incident}$: incident solar radiation on BIPV/T

An important aspect of a BIPV/T system is the system's pressure drop. The total pressure drop of a BIPV/T collector is directly linked to the pumping power required by the fan to circulate the air. [12] Since the studied BIPV/T collector is a single inlet system, thus there is a single continuous channel, the flow is essentially known and regulated by the fan. The pressure drop along the BIPV/T channel due to the frictional losses can be calculated according to the Darcy-Weisbach equation [12]:

$$\Delta P_f = f \cdot \frac{L}{D_h} \cdot \rho \cdot \frac{V_{avg}^2}{2} \quad (4-8)$$

where,

- f: the Darcy friction factor (dimensionless)
- L: the length of the air collector (m)
- D_h : the hydraulic diameter of the air channel (m)
- ρ : the air density (kg/m³)
- V: the average air velocity inside the air channel (m/s)

In the case of laminar flow ($Re < 2300$) the empirical formula used is [12]:

$$f = \frac{64}{Re} \quad (4-9)$$

For the turbulent regime ($3000 < Re < 5 \cdot 10^4$) the equation by Petukhov is used [12]:

$$f = (0.79 \cdot \ln(Re) - 1.64)^{-2} \quad (4-10)$$

⁵ See equations (3-9) & (3-20)

The above pressure drop is then used to calculate the fan power consumption (kW) as:

$$Q_{fan} = \frac{\dot{m}_{BIPV/T} \cdot \Delta P}{\rho} \quad (4-11)$$

where,

- $\dot{m}_{bipv/t}$: the mass flow rate of the BIPV/T collector (kg/s)
- ΔP : the pressure drop along the collector (kPa)
- ρ : the density of the fluid (kg/m³)

A simplified flow chart of the basic steps followed for the MPC formulation shown in Figure 4-8.

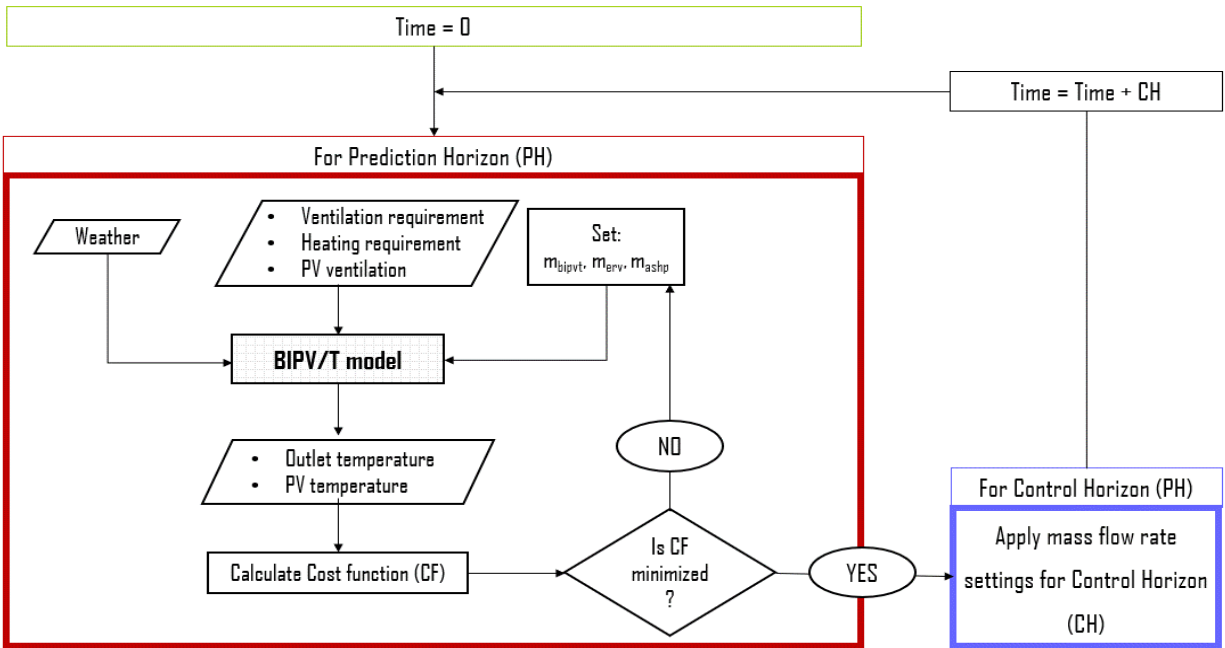


Figure 4-8 Flow chart of MPC algorithm

To minimize the cost function of the MPC the *minimize* function with method 'SLSQP' available in the Python library *SciPy.Optimize* was used. Considering the estimated time constant of the BIPV/T system calculated in the previous chapter the control horizon was decided to be set at 5 minutes. Below this duration would not be practical as the variable speed fan within the BIPV/T would constantly change settings leading to lower efficiency and reduced life expectancy of the equipment. A prediction horizon of 1 hour ahead was chosen as it was deemed as a good compromise between having an adequate amount of information for future conditions and

disturbances while keeping low the uncertainty of future weather predictions. Table 4-2 provides further information for the settings used for the simulations.

Table 4-2 Model Predictive Control simulation settings

Parameters	Values
Ventilation	$T_{\text{supply}}: 18^{\circ}\text{C}$, $T_{\text{exhaust}}: 22^{\circ}\text{C}$
ERV	airflow = 1.36 kg/s, sensible efficiency = 74.4%
Air-to-Water Heat Pump (HP)	airflow = 1.66 kg/s, COP = 2.84, HC = 29 kW
BIPV/T airflow bounds (m_{bipvt})	0.1 kg/s – 2.5 kg/s
Airflow sent to ERV from BIPV/T (m_{erv})	0 kg/s – 1.36 kg/s
Airflow sent to HP from BIPV/T (m_{hp})	0 kg/s – 1.66 kg/s
BIPV/T operation conditions	When $G_{\text{incident}} > 20\text{W}/\text{m}^2$
Constraints	$m_{\text{bipvt}} \geq m_{\text{erv}} + m_{\text{hp}}$
Control & Prediction horizons	5 minutes, 60 minutes

4.3 Scenarios explored

This section describes the different scenarios considered and compared in this study with the aim to evaluate the benefits of MPC for the air flow within the BIPV/T channel and explore the opportunities by covering a larger part of the library’s roof with BIPV/T. Figure 4-9 illustrates the actual systems covering the south-facing roof at the Varennes library.

Three different BIPV/T areas are examined (Figure 4-10).

- i) The actual BIPV/T area at the Varennes library (110m²).
- ii) The possibility to collect heat from the entire mechanically ventilated BIPV part, which results in a 278m² BIPV/T system. To avoid a very long air channel which can lead to PV overheat the system is considered to have two inlets and two outlets. Specifically, the actual BIPV/T system is left as is, adding the left BIPV corner resulting in a wider air-

channel of the same length (23.4m x 5.55m x 0.07m). The rest mechanically ventilated BIPV is considered as a second BIPV/T with air-channel dimensions 23.4m x 6.50m x 0.07m.

iii) The scenario of covering the whole south-facing roof with BIPV/T is tested. Four individual BIPV/T air channels are considered. Specifically, the two channels described in (ii) and two additional channels with dimensions 36m x 6.02m x 0.07m each.

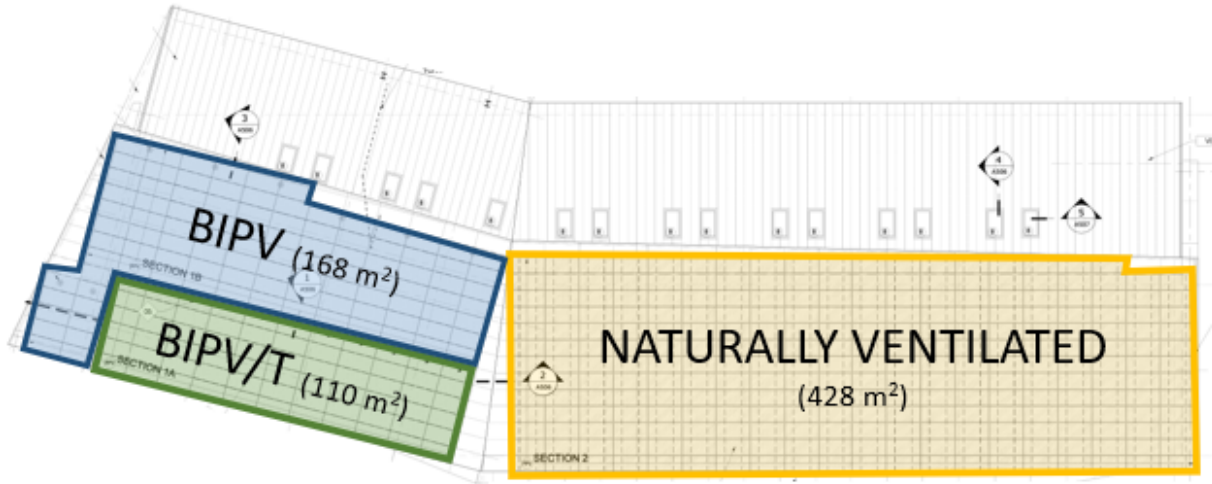


Figure 4-9 Discretization of PV systems covering the south-facing roof at the Varennes library. (actual system)

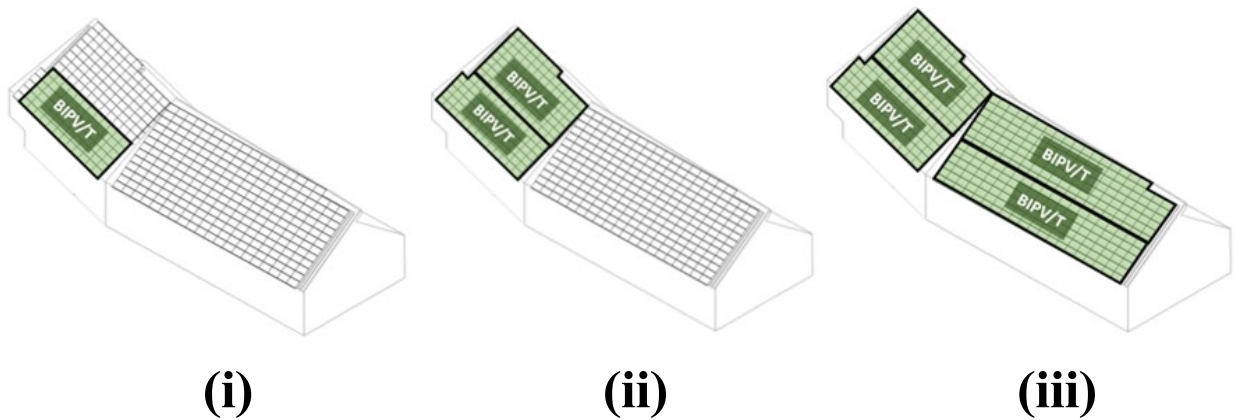


Figure 4-10 Different theoretical scenarios of BIPV/T area examined

As a means to evaluate the performance of the MPC strategy a comparison between applying MPC to the BIPV/T air flow and keeping the air flowing at a constant velocity of 1m/s was conducted. To avoid overheating the air sent to the ERV during days with higher ambient temperature a simple rule-based strategy determining the amount of BIPV/T air sent to the ERV

was applied shown in Figure 4-11. The rest of the BIPV/T air is sent to cover the ASHP needs and if there is excess air it is sent to adjacent buildings.

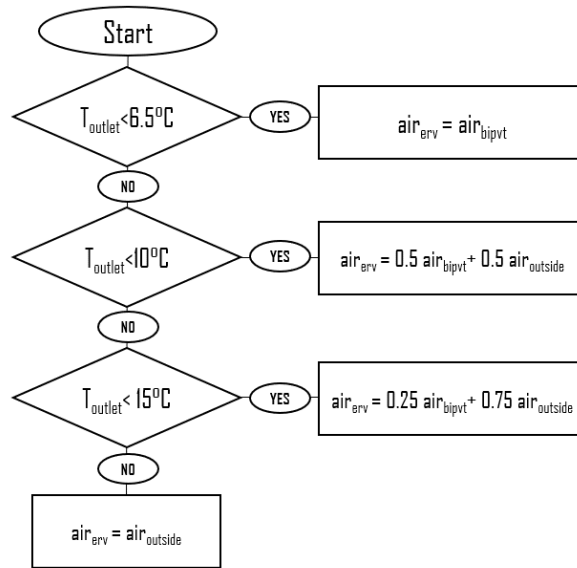


Figure 4-11 Rule-based strategy to avoid overheating the ventilation air under the steady flow control strategy.

Finally, the business-as-usual case was considered where the actual mass flow rate derived from the data was used for the BIPV/T model and the BIPV/T air is used solely for preheated ventilation air. Figure 4-12 summarizes all the examined cases in this thesis.

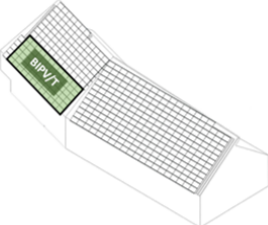
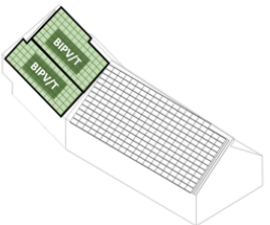
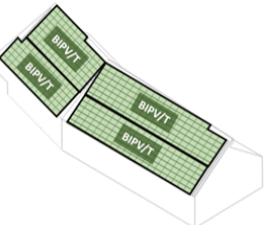
		
<p>base: Base case scenario The actual mass flow rate is applied to the BIPV/T model and all the BIPV/T air is sent to the ERV.</p>		
<p>i-s: Steady air velocity scenario with BIPV/T area (i) The air velocity is kept at 1m/s, BIPV/T covers 16% of the roof and the BIPV/T air is sent to the thermal applications with the following hierarchy: 1) ERV, 2) HP, 3)HDAB.</p>	<p>ii-s: Steady air velocity scenario with BIPV/T area (ii) The air velocity is kept at 1m/s, BIPV/T covers 40% of the roof and the BIPV/T air is sent to the thermal applications with the following hierarchy: 1) ERV, 2) HP, 3)HDAB.</p>	<p>iii-s: Steady air velocity scenario with BIPV/T area (iii) The air velocity is kept at 1m/s, BIPV/T covers 100% of the roof and the BIPV/T air is sent to the thermal applications with the following hierarchy: 1) ERV, 2) HP, 3)HDAB.</p>
<p>i-mpc: MPC scenario with BIPV/T area (i) The air velocity and the portions of BIPV/T air sent to each thermal application are determined by the MPC optimization algorithm, BIPV/T covers 16% of the roof.</p>	<p>ii-mpc: MPC scenario with BIPV/T area (ii) The air velocity and the portions of BIPV/T air sent to each thermal application are determined by the MPC optimization algorithm, BIPV/T covers 40% of the roof.</p>	<p>iii-mpc: MPC scenario with BIPV/T area (iii) The air velocity and the portions of BIPV/T air sent to each thermal application are determined by the MPC optimization algorithm, BIPV/T covers 100% of the roof.</p>

Figure 4-12 Description of all the different scenarios examined.

4.4 Results & Discussion

4.4.1 Transient vs Steady-State

From the results between the SS and TR models it was observed that the SS model was prone to more acute fluctuations of the outlet temperature prediction compared to the TR model where the addition of the thermal capacitance created a damping effect resulting in a more stable outlet temperature. One of the main external sources causing fluctuations in BIPV/T outlet temperature is the wind speed. Fluctuations of the wind speed result in fluctuations of the wind-driven convective heat transfer coefficient which in turn leads to fluctuations of the BIPV/T outlet temperature. Passing clouds which instantaneously block sunlight could also cause this type of behaviour however the wind was observed to have a stronger correlation. As high fluctuations can result in cycling of the fan which compromises its durability, it is important to investigate if this would affect the performance of the MPC controller. An analysis was conducted using both models to optimize the air flow for a windy and then for a still day.

Windy Day (March 13, 2020)

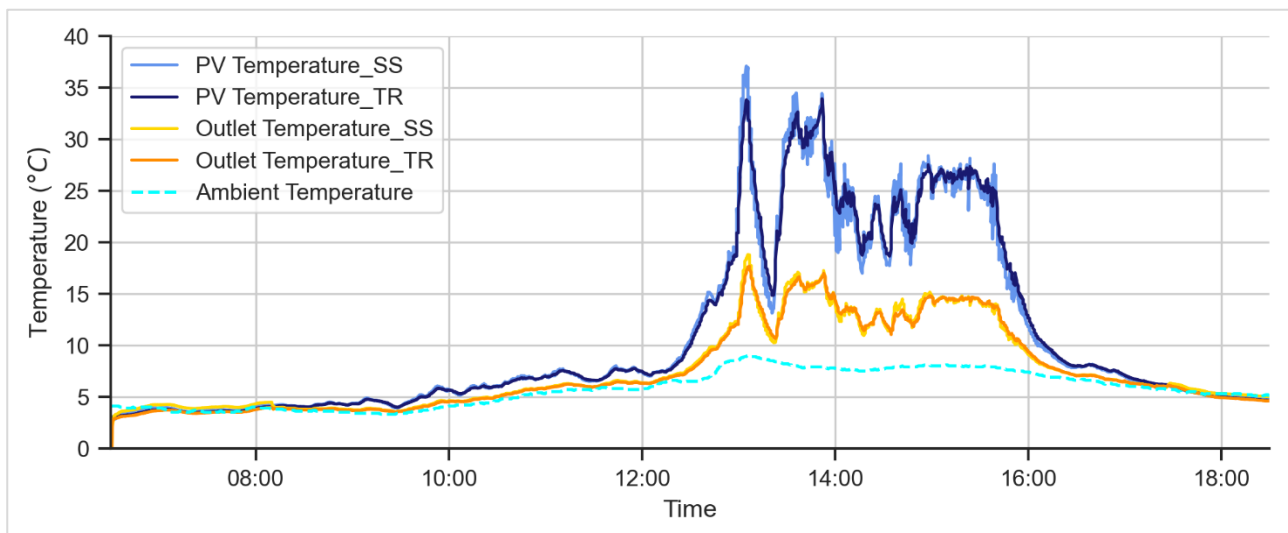


Figure 4-13 PV and Outlet temperature predictions on a windy day (March 13, 2020)

Figure 4-13 presents the PV and outlet temperatures for a day with high wind velocity and fluctuation of the irradiance levels. The SS model prediction has slightly higher fluctuations

however the difference is fairly small. When looking at the flow rate profiles in Figure 4-14, the overall profile is similar with very small differences.

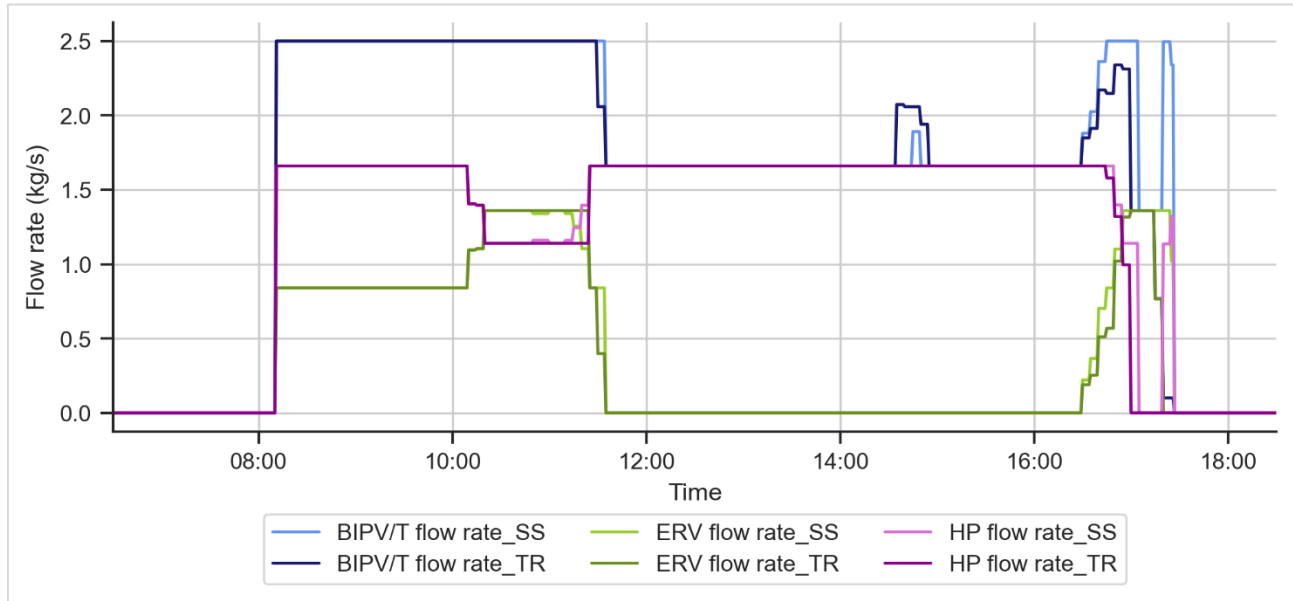


Figure 4-14 Mass flow rate profiles on a windy day (March 13, 2020)

Still Day (February 02, 2020)

When observing the respective graphs for a day with low wind, the difference between the two models is even smaller with the determined optimal flow rate profiles being almost identical.

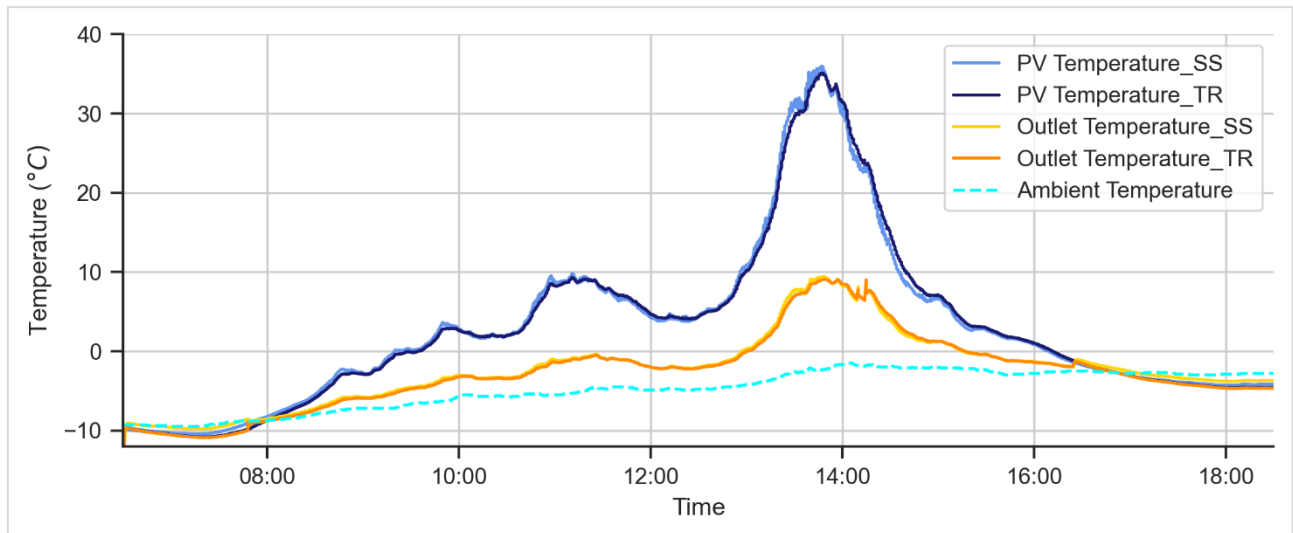


Figure 4-15 PV and Outlet temperature predictions on a still day (February 02, 2020)

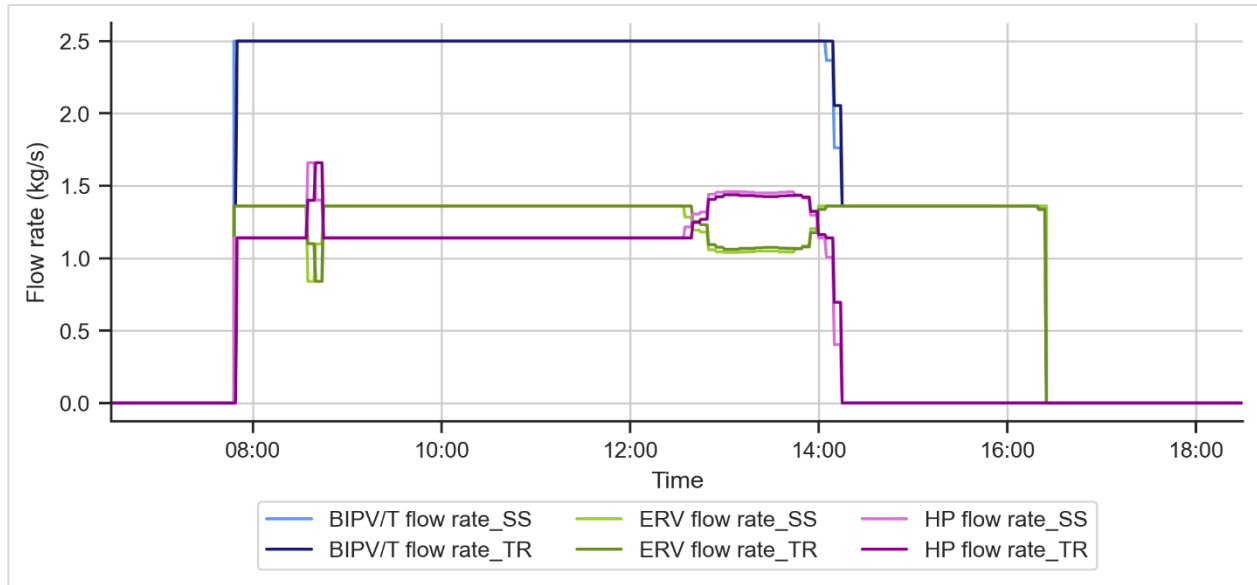


Figure 4-16 Mass flow rate profiles on a still day (February 02, 2020)

The difference in the overall energy consumption between the SS and TR model cases was marginal (Table 4-3).

Table 4-3 Net energy consumption for SS model and TR model case.

<i>Net Energy Consumption</i>	TR Model	SS Model
Windy Day (March 13, 2020)	19.9 kWh	19.86 kWh
Still Day (February 02, 2020)	42.28 kWh	42.15 kWh

One of the main motivations behind using a transient model was to minimize acute outlet temperature fluctuations so as to reduce cycling of the fan. However, when applying MPC, the controller does not allow the fan to change settings in less time than the specified control horizon eliminating this risk. These observations lead to the conclusion that the TR model did not give as many benefits as anticipated for this specific BIPV/T system while at the same time significantly increased the computation times.

Transient BIPV/T models may provide more advantages in systems with higher thermal capacity, for example, BIPV/T systems with incorporated Phase Change Materials (PCM) for which further investigation needs to be conducted.

4.4.2 MPC vs Base Case

In this section the benefits of applying MPC compared to the business-as-usual case are presented. Figure 4-17 presents the net energy for all four investigated days. In all days mpc outperforms the base case, with a more significant reduction on February 28, a mild sunny day.

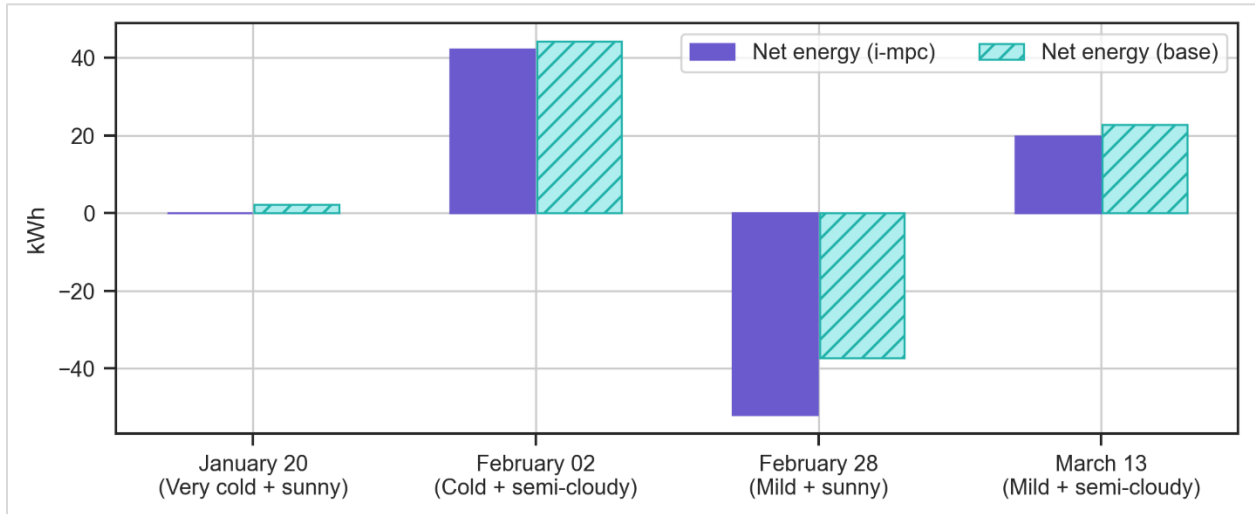


Figure 4-17 Net energy for the four investigated days (base and i-mpc case).

Very Cold Sunny Day (January 20, 2020)

Figure 4-18 and Figure 4-19 illustrate the flow rate profiles and power consumption for January 20 respectively. The most significant reduction in power consumption comes from reducing the

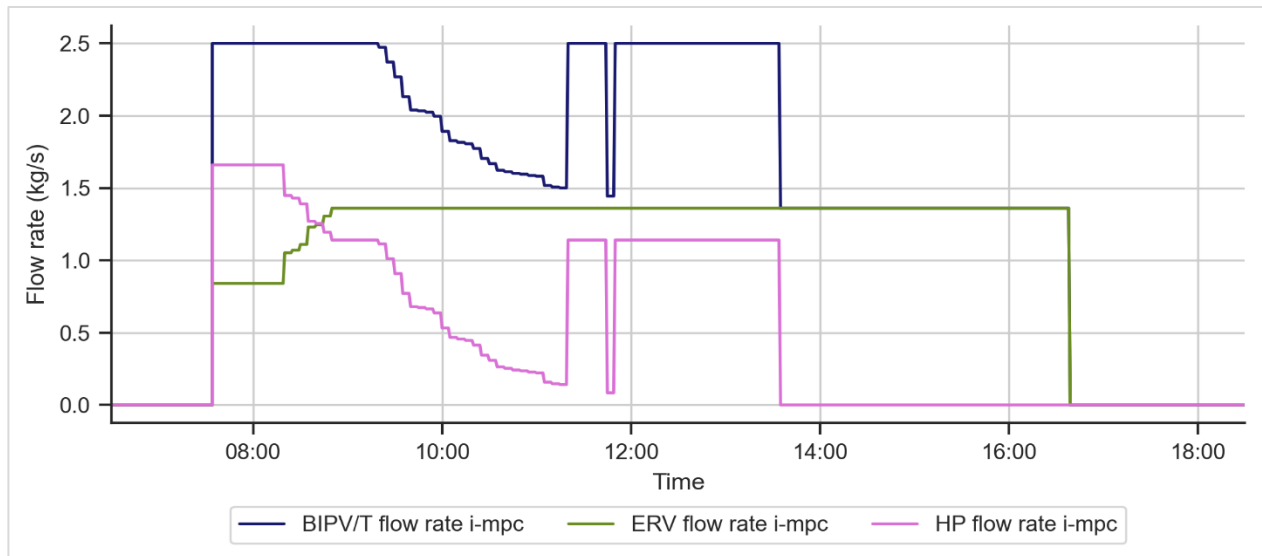


Figure 4-18 Mass flow rate profiles for January 20, 2020, a very cold sunny day (base and i-mpc case).

HP consumption, between 08:00 – 10:00 which is the time the heating demand is at the highest levels. As the heating load decreases less BIPV/T air is sent to the HP. By lowering the BIPV/T flowrate, the system is able to achieve a higher outlet temperature. During high irradiance hours (11:00 – 13:30) the controller increases the BIV/T flow to ventilate the PV panels.

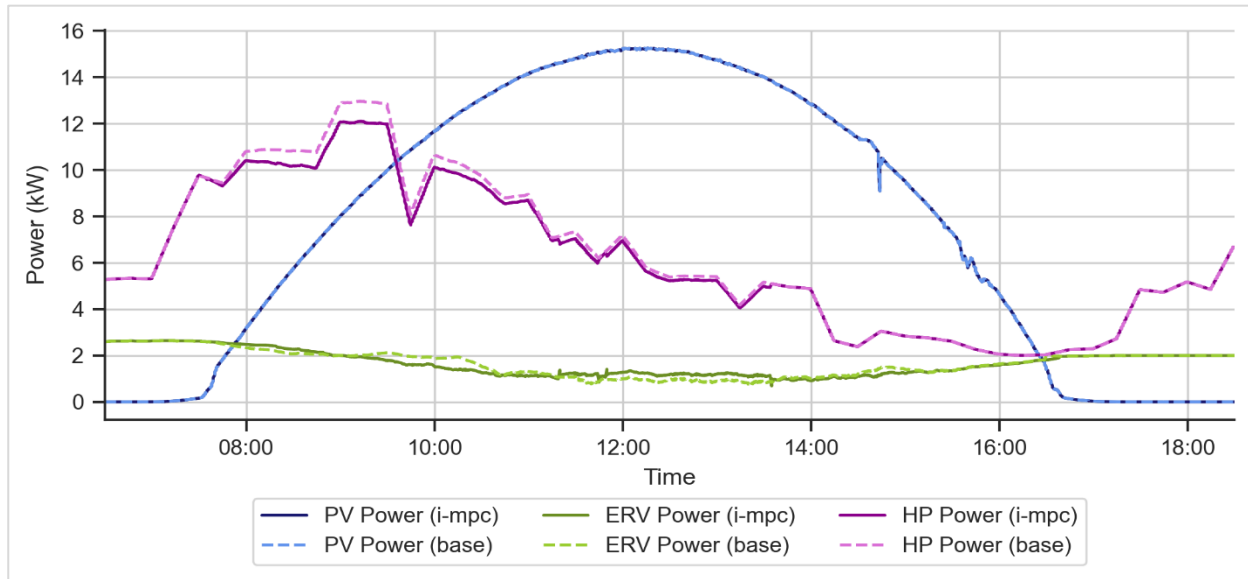


Figure 4-19 Power profiles for January 20, 2020, a very cold sunny day (base and i-mpc case).

Mild Sunny Day (February 28, 2020)

Figure 4-21 and Figure 4-20 show the flow rate profiles and power consumption during a mild sunny day. The ERV consumption has an important decrease throughout the day. The reason behind this comes from overheating the ventilation air during the base case. With mpc the algorithm predicts the ERV will sufficiently heat the ambient air without the assistance of the BIPV/T thus sends the entirety of the BIPV/T air to the HP for the majority of the day. During mid-day (13:00-15:00) the BIPV/T flow rate increases with the aim to lower the PV temperature. The mpc scenario increases the PV production by 2% for this day.

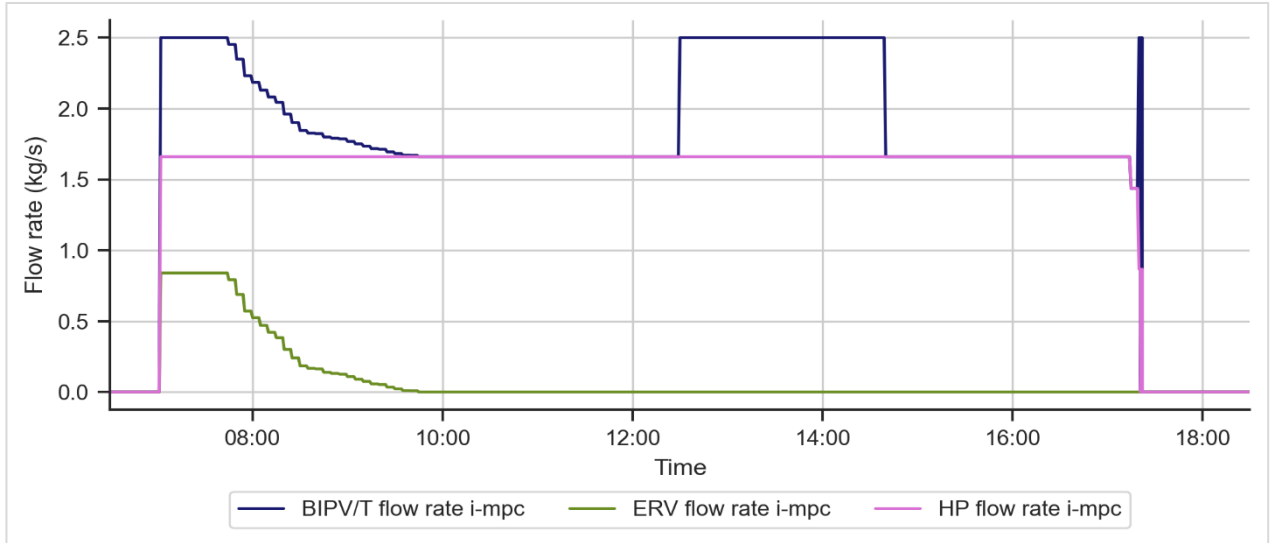


Figure 4-21 Mass flow rate profiles for February 28, 2020, a mild sunny day (base and i-mpc case).

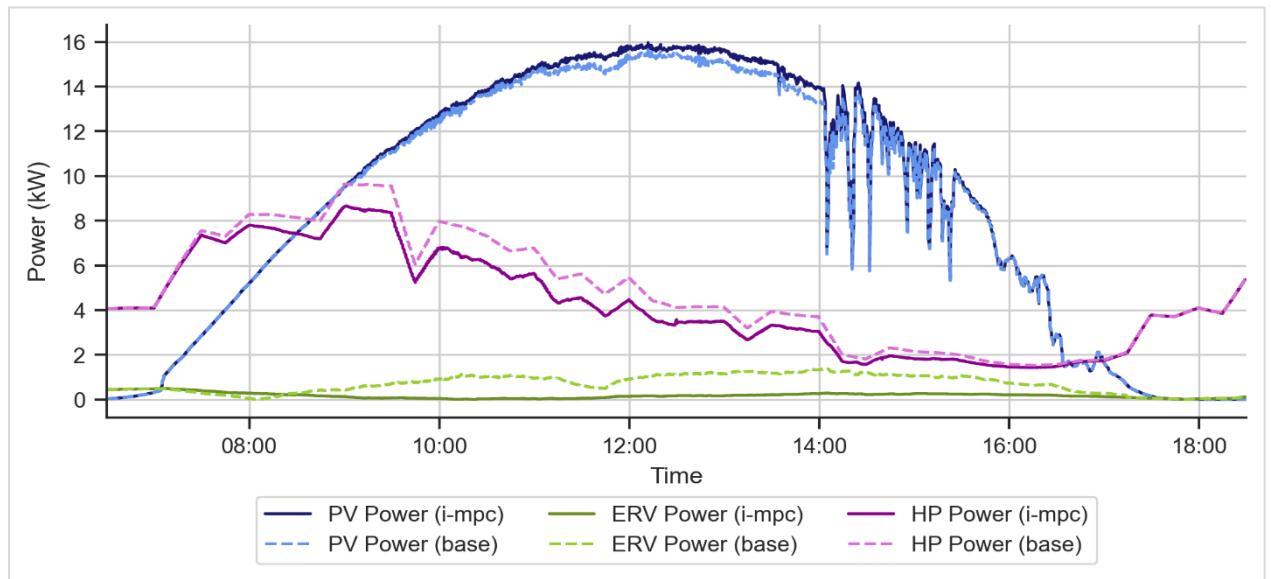


Figure 4-20 Power profiles for February 28, 2020, a mild sunny day (base and i-mpc case).

Table 4-4 presents the results for the base and i-mpc scenarios for the four investigated days. As mentioned above the mpc outperforms the base case for all four days with a more significant difference in days with higher temperatures (February 28 & March 13) as the base scenario consistently overheats the ventilation air resulting in the need for cooling.

Table 4-4 Energy consumption for base and i-mpc cases.

January 20, 2020 (very cold + sunny)	base	i-mpc	Increase/Decrease
--------------------------------------	------	-------	-------------------

PV Produced Energy (kWh)	93.46	93.46	0.00%
HP Consumed Energy (kWh)	75.68	73.41	- 2.98%
ERV Consumed Energy (kWh)	20.01	20.01	0.00%
Net Consumed Energy (kWh)	2.22	- 0.02	- 101.09%
<i>February 02, 2020 (cold + semi-cloudy)</i>			
PV Produced Energy (kWh)	37.41	37.80	+ 1.05%
HP Consumed Energy (kWh)	69.21	67.78	- 2.07%
ERV Consumed Energy (kWh)	12.39	12.16	- 1.87%
Net Consumed Energy (kWh)	44.19	42.15	- 4.62%
<i>February 28, 2020 (mild + sunny)</i>			
PV Produced Energy (kWh)	103.27	105.43	+ 2.09%
HP Consumed Energy (kWh)	57.56	51.29	- 10.88%
ERV Consumed Energy (kWh)	8.32	2.10	- 74.74%
Net Consumed Energy (kWh)	-37.39	-52.02	- 39.13%
<i>March 13, 2020 (mild + semi-cloudy)</i>			
PV Produced Energy (kWh)	39.29	39.41	+ 0.32%
HP Consumed Energy (kWh)	58.31	57.23	- 1.86%
ERV Consumed Energy (kWh)	3.81	2.06	- 46.79%
Net Consumed Energy (kWh)	22.83	19.86	- 13.04%

4.4.3 MPC vs Steady flow

Comparing the mpc strategy with the steady flow rate strategy showed that the mpc reduces the overall energy consumption. Figure 4-22 shows the net energy for all days for the i-mpc and i-s scenarios.

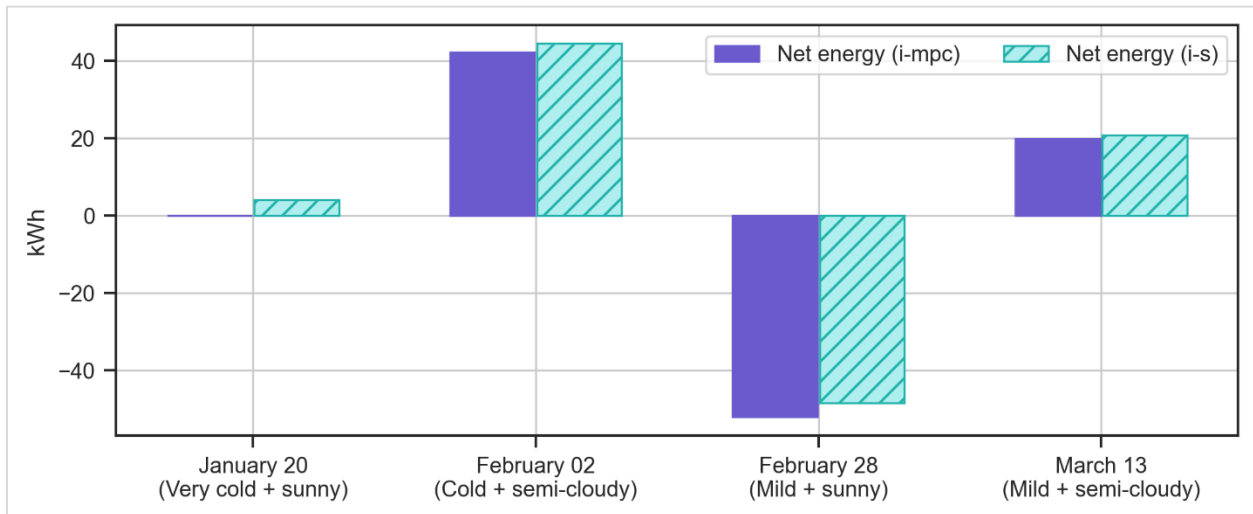


Figure 4-22 Net energy for the four investigated days (i-s and i-mpc case).

Mild Semi-cloudy Day (March 13, 2020)

March 13 is a mild semi-cloudy day with acute fluctuations in wind speed and irradiance levels throughout the day. The BIPV/T outlet temperature reflects these conditions resulting in a varying outlet temperature. Although the energy consumption does not have a big difference between the two scenarios (Figure 4-24) it is interesting to see the flow rate profiles during the day (Figure 4-23). The rule-based strategy applied to the steady flow rate scenarios to avoid overheating the ventilation air, causes the ERV and HP flow rates to go up and down multiple times throughout the day. In contrast the mpc strategy keeps a more steady profile and increases the flow rates more gradually. This is an important finding as frequent changes can significantly impact the life expectancy of the equipment.

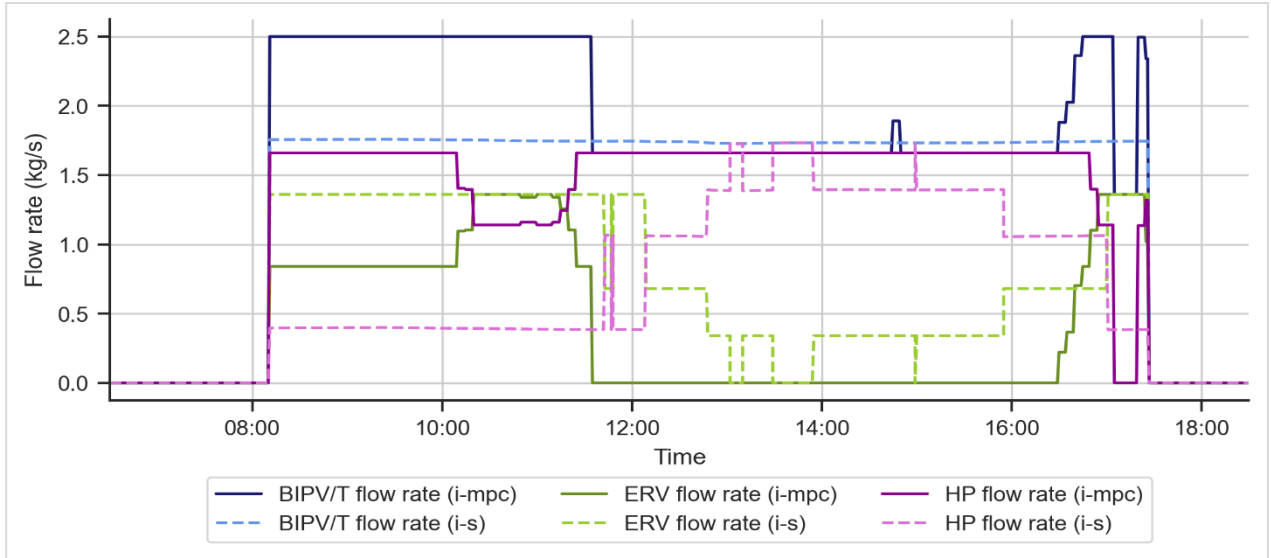


Figure 4-23 Mass flow rate profiles for March 13, 2020, a mild semi-cloudy day (i-s and i-mpc case).

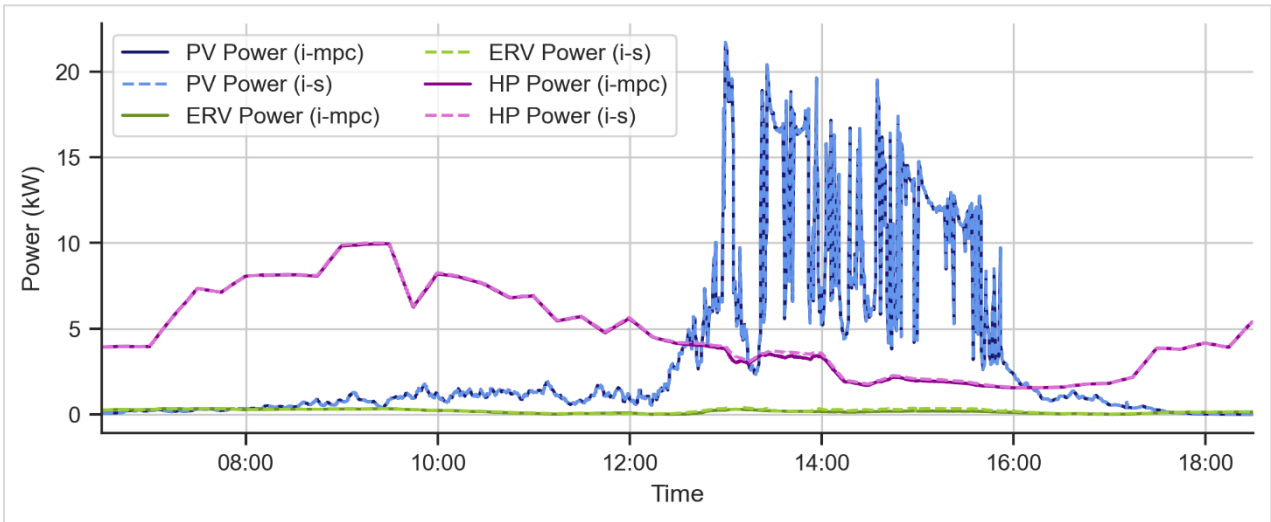


Figure 4-24 Power profiles for March 13, 2020, a mild semi-cloudy day (i-s and i-mpc case).

Table 4-5 lists the energy consumption for i-s and i-mpc cases for all four incistigated days.

Table 4-5 Energy consumption for i-s and i-mpc cases.

January 20, 2020 (very cold + sunny)	i-s	i-mpc	Increase/Decrease
PV Produced Energy (kWh)	93.46	93.46	0.00%
HP Consumed Energy (kWh)	74.4	73.41	- 1.32%
HRV Consumed Energy (kWh)	23.13	20.01	- 13.51%

Net Consumed Energy (kWh)	4.08	-0.02	- 100.60%
<i>February 02, 2020 (cold + semi-cloudy)</i>			
PV Produced Energy (kWh)	37.67	37.80	+ 0.35%
HP Consumed Energy (kWh)	68.51	67.78	- 1.07%
HRV Consumed Energy (kWh)	13.57	12.16	- 10.40%
Net Consumed Energy (kWh)	44.42	42.15	- 5.10%
<i>February 28, 2020 (mild + sunny)</i>			
PV Produced Energy (kWh)	105.16	105.43	+ 0.26%
HP Consumed Energy (kWh)	54.52	51.29	- 5.93%
HRV Consumed Energy (kWh)	2.17	2.10	- 3.26%
Net Consumed Energy (kWh)	-48.45	-52.02	- 7.37%
<i>March 13, 2020 (mild + semi-cloudy)</i>			
PV Produced Energy (kWh)	39.42	39.41	+ 0.02%
HP Consumed Energy (kWh)	57.85	57.23	- 1.08%
HRV Consumed Energy (kWh)	2.38	2.03	- 14.79%
Net Consumed Energy (kWh)	20.82	19.86	- 4.61%

4.4.4 Heat Pump COP improvement

By providing a higher air source temperature the COP of the HP can significantly improve. The following graphs present the results of coupling the BIPV/T with the ASHP during a very cold sunny day with a mean ambient temperature of -16°C (January 20, 2020) and for a mild sunny day with mean ambient temperature of 7°C (February 28, 2020). The different BIPV/T area scenarios are presented (i-mpc, ii-mpc and iii-mpc) as well as the achieved COP in the case ambient air is used as a source for the HP.

Very Cold Sunny Day (January 20, 2020)

During a very cold sunny day the outlet temperature was able to reach up to 20°C increase from the ambient temperature. Figure 4-26 presents the PV and outlet temperatures for the i-mpc, ii-

mpc and iii-mpc cases. As the BIPV/T area increases, thus more solar heated air is available, the mpc controller sends more BIPV/T air to the HP (Figure 4-25). As the heating load decreases after the morning peak the HP flow rate decreases as well. Figure 4-27 shows the achieved COP for the i-mpc, ii-mpc and iii-mpc cases as well as the regular cop if ambient air is used as a source. In the iii-mpc case where the HP is fully supplied by BIPV/T air the instantaneous COP is increased by up to 28%.

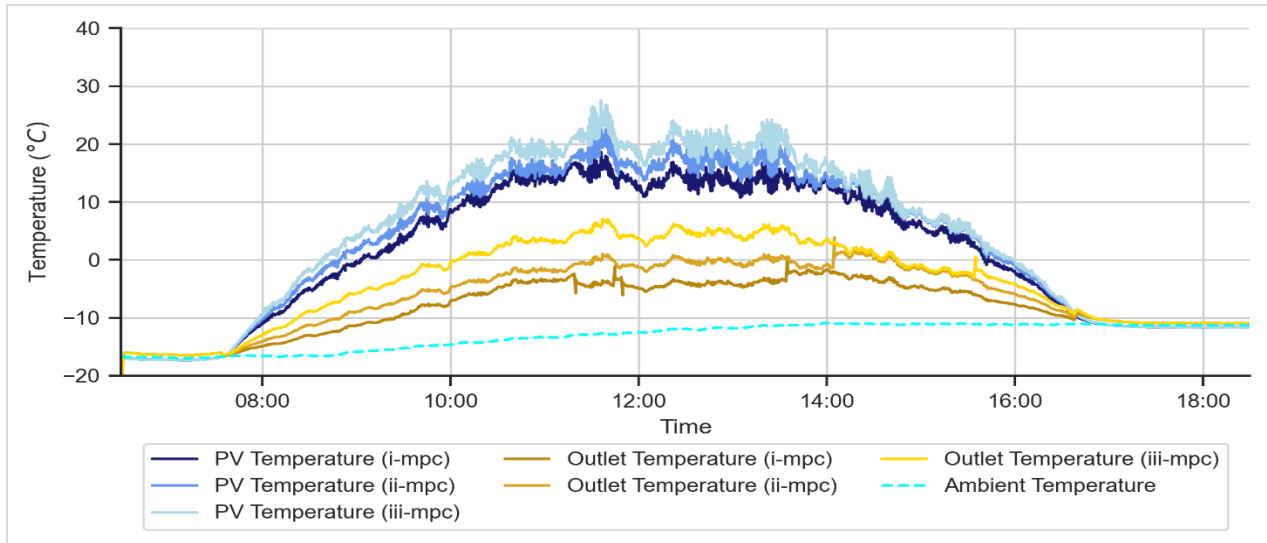


Figure 4-26 PV and outlet temperature predictions for January 20, 2020, a very cold sunny day (i-mpc, ii-mpc and iii-mpc cases).

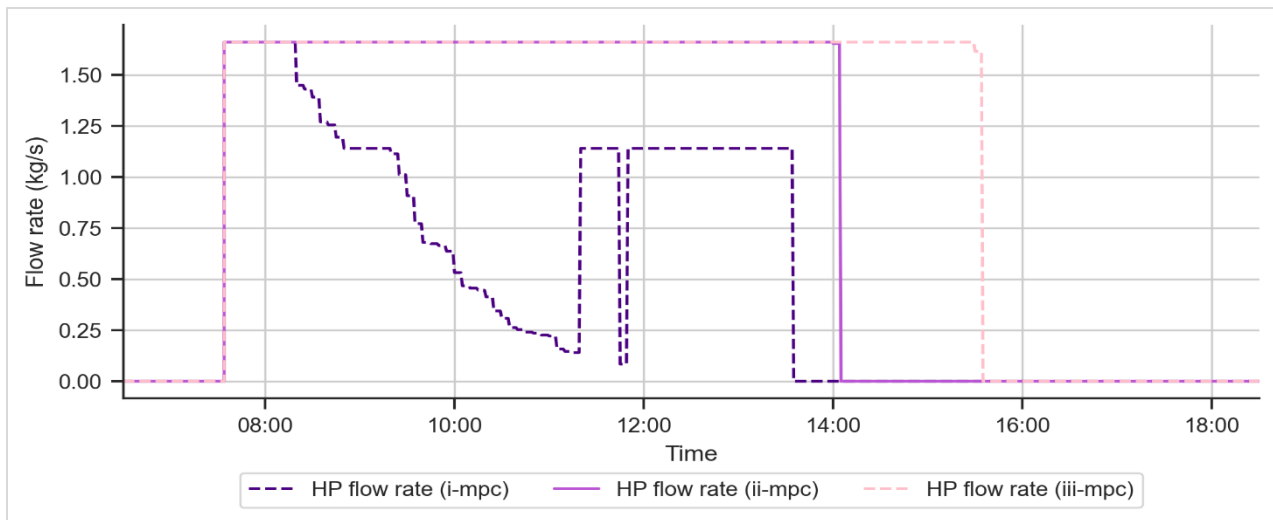


Figure 4-25 Mass flow rate sent to the ASHP for January 20, 2020, a very cold sunny day (regular, i-mpc, ii-mpc and iii-mpc cases).

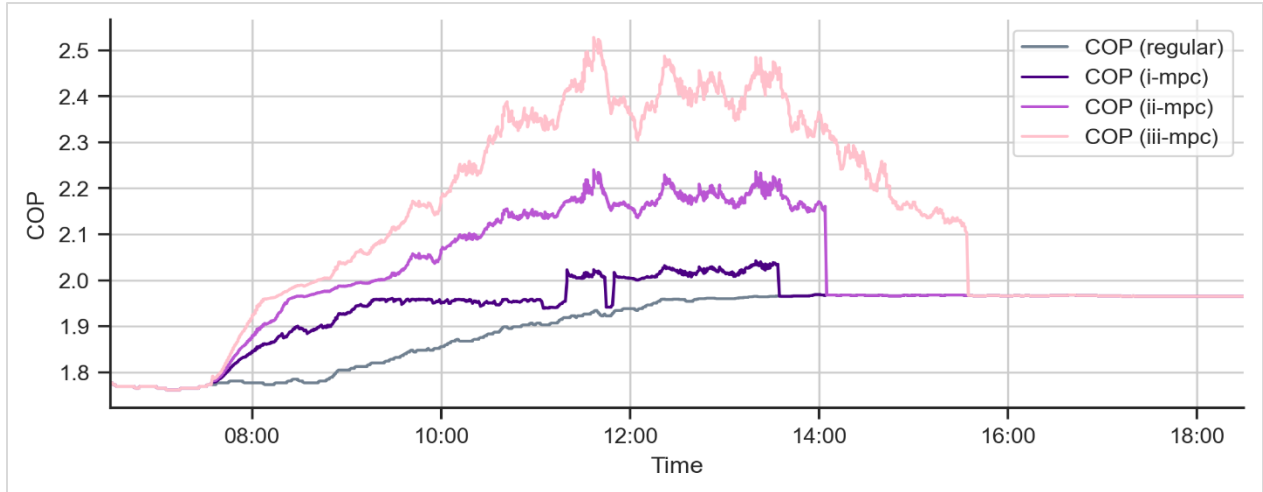


Figure 4-27 COP profile for January 20, 2020, a very cold sunny day (regular, i-mpc, ii-mpc and iii-mpc cases).

Mild Sunny Day (February 28, 2020)

Figure 4-28 illustrates the predicted PV and outlet temperatures showing a maximum of 12°C increase from the ambient air. The achieved ΔT in this case is smaller since the PVs are subject to overheating, leading the mpc controller to increase the BIPV/T flow rate to achieve a better cooling effect. With a higher flow rate the BIPV/T is able to fully supply the HP in all three cases (Figure 4-29).

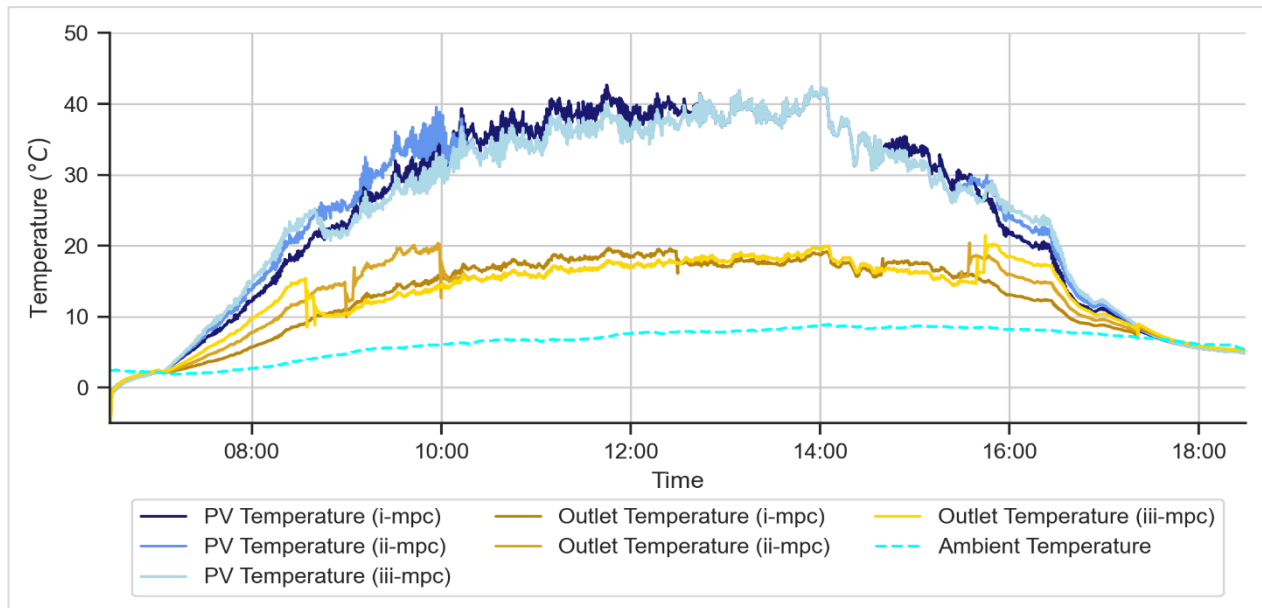


Figure 4-28 PV and outlet temperature predictions for February 28, 2020, a mild sunny day (i-mpc, ii-mpc and iii-mpc cases).

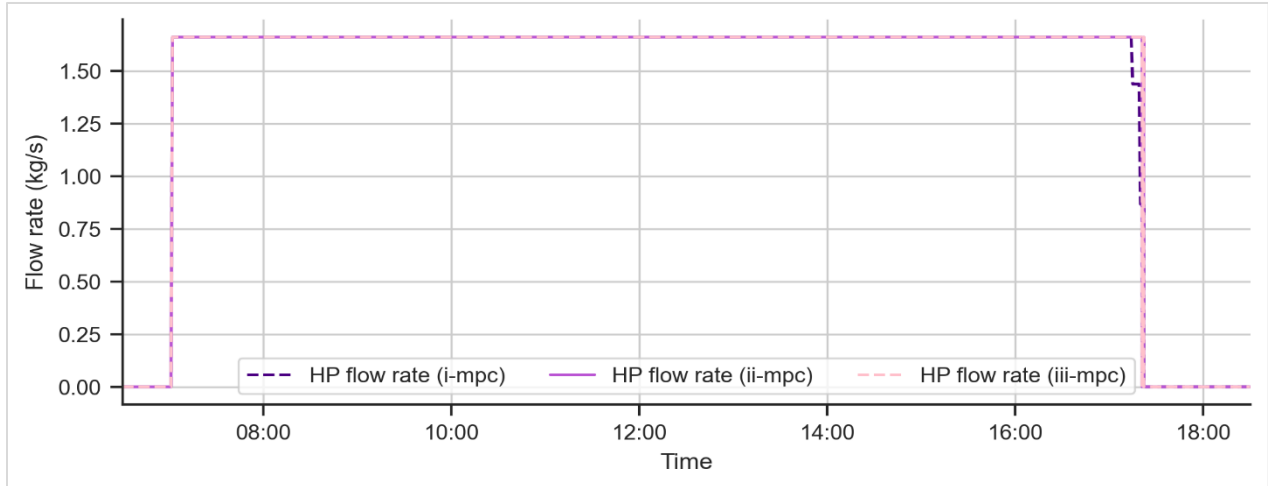


Figure 4-29 Mass flow rate sent to the ASHP for February 28, 2020, a mild sunny day (regular, i-mpc, ii-mpc and iii-mpc cases).

Figure 4-30 shows the COP profiles for all the cases. Since the BIPV/T is able to fully supply the HP regardless of the BIPV/T area for this day the results are fairly similar between the three cases.

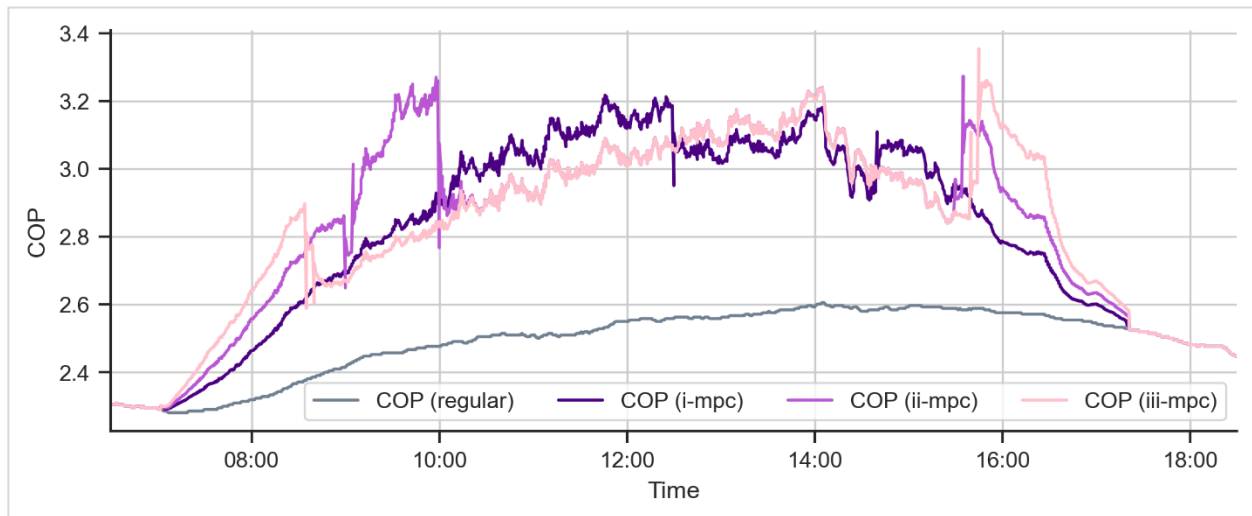


Figure 4-30 COP profile for February 28, 2020, a mild sunny day (regular, i-mpc, ii-mpc and iii-mpc cases).

Finally, in Table 4-6 the average COP for all days is listed. The increase in the solar-assisted HP COP compared to the conventional HP reaches up to 13.46%.

Table 4-6 Average COP for the four investigated days (regular, i-mpc, ii-mpc and iii-mpc cases).

Day	Average COP				Increase
	Regular	i-mpc	ii-mpc	iii-mpc	

<i>January 20, 2020</i> <i>(very cold +sunny)</i>	1.9	1.94	2.01	2.12	Up to + 11.78%
<i>February 02, 2020</i> <i>(cold + semi-cloudy)</i>	2.07	2.12	2.18	2.22	Up to + 7.34%
<i>February 28, 2020</i> <i>(mild + sunny)</i>	2.49	2.80	2.84	2.83	Up to + 13.46%
<i>March 13, 2020</i> <i>(mild + semi-cloudy)</i>	2.46	2.54	2.56	2.56	Up to + 3.87%

4.4.5 Larger BIPV/T area

As mentioned in the description of the archetype system the BIPV/T covers only 16% of the south-facing roof of the Varennes library. This section presents the possible energy savings for the library if a higher area was covered with BIPV/T.

Figure 4-31 demonstrates the total produced heat for the three considered BIPV/T areas for different environmental conditions. As the BIPV/T area increases more heat is produced. On February 28, 2020, a mild sunny day, the most heat is produced as the BIPV/T achieves the highest outlet temperatures and the fan runs generally in higher speeds to prevent PV overheat.

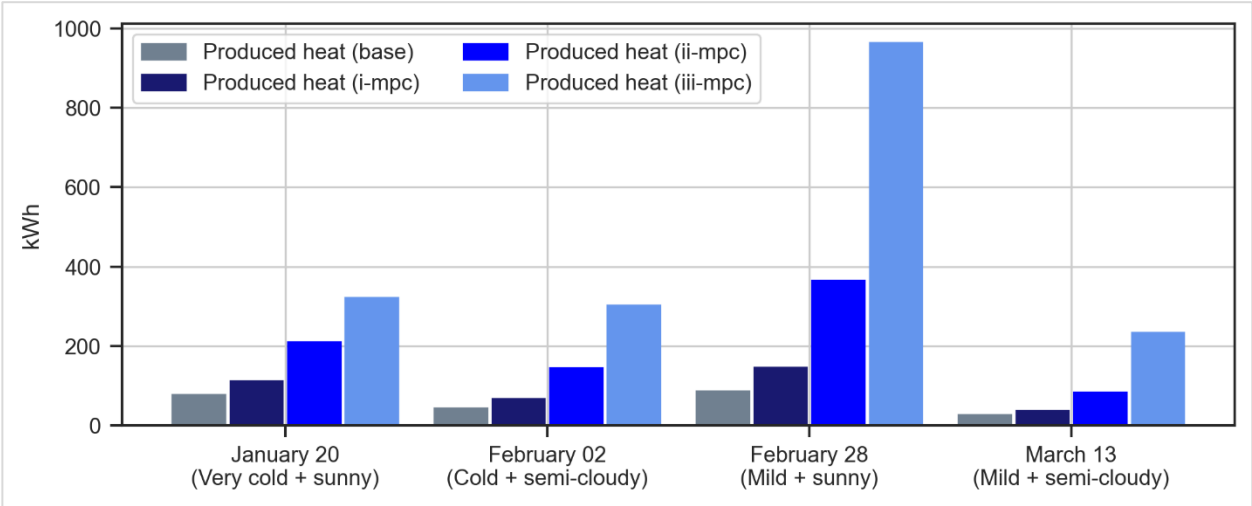


Figure 4-31 Produced heat for different BIPV/T areas for the four investigated days (i-mpc, ii-mpc and iii-mpc cases).

Table 4-7 lists the total energy produced by the BIPV/T for different roof coverage as well as the excess amount of heat which is not needed to cover the library’s needs produced each day. This heat can be sent to adjacent buildings and is further discussed in 4.4.6.

Table 4-7 Total and excess heat produced by the BIPV/T for the four investigated days (i-mpc, ii-mpc and iii-mpc cases).

<i>January 20, 2020 (very cold + sunny)</i>	i-mpc	ii-mpc	iii-mpc
Total Produced Heat (kWh)	111.5	210.5	321.3
Total Produced Heat (kWh/m²)	1.01	0.75	0.46
Excess Heat (kWh)	0	0	0
Excess Heat (kWh/m²)	0	0	0
<i>February 02, 2020 (cold + semi-cloudy)</i>			
Total Produced Heat (kWh)	67.7	144.5	302.3
Total Produced Heat (kWh/m²)	0.62	0.52	0.43
Excess Heat (kWh)	0	29.0	145.5
Excess Heat (kWh/m²)	0	0.17	0.2
<i>February 28, 2020 (mild + sunny)</i>			
Total Produced Heat (kWh)	145.5	365.5	964.6
Total Produced Heat (kWh/m²)	1.32	1.31	1.37
Excess Heat (kWh)	17.0	222.2	824.8
Excess Heat (kWh/m²)	0.15	0.8	1.17
<i>March 13, 2020 (mild + semi-cloudy)</i>			
Total Produced Heat (kWh)	36.7	83.9	234.0
Total Produced Heat (kWh/m²)	0.33	0.3	0.33
Excess Heat (kWh)	0.1	40.6	189.1
Excess Heat (kWh/m²)	0	0.15	0.27

Figure 4-32 shows the energy consumption of the HP and the ERV for 3 different BIPV/T areas (i-mpc, ii-mpc and iii-mpc) for all four days. Increasing the BIPV/T area has a bigger impact on

the energy consumption during cold days (January 20 & February 02). The heating needs of the building are already covered with a smaller BIPV/T during days with higher ambient temperature, thus increasing the BIPV/T area does not have a big effect.

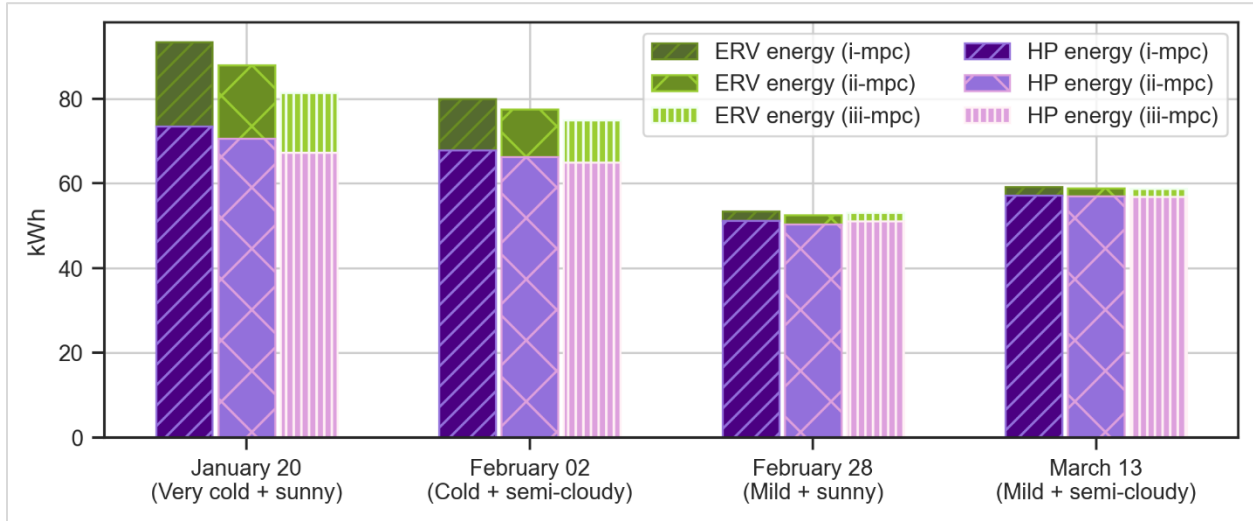


Figure 4-32 HP and ERV consumed energy for the four investigated days (i-mpc, ii-mpc and iii-mpc cases).

Very Cold Sunny Day (January 20, 2020)

Figure 4-33 shows the BIPV/T flow rate for the three cases. Although the BIPV/T area is increased by 84% between cases i-mpc and iii-mpc the BIPV/T flow rate never surpasses 3.0 kg/s. As the ambient temperature is very low during this day the mpc controller sets the flow rate

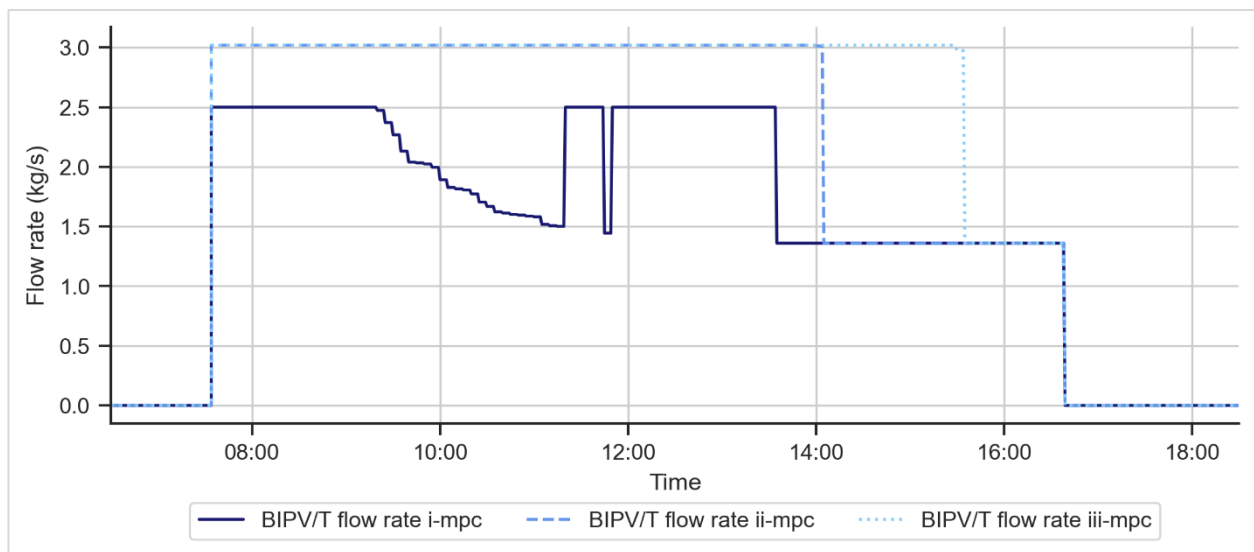


Figure 4-33 BIPV/T flow rate profiles for January 20, a very cold sunny day (i-mpc, ii-mpc and iii-mpc cases).

at low levels to achieve higher outlet temperatures. As in the first half of the day the heating load is high the controller aims to provide solar heated air to both the HP and ERV (Figure 4-34). In the ii-mpc and iii-mpc scenarios, the HP is fully supplied by the BIPV/T up to 14:00 and 15:30 respectively. For case i-mpc the BIPV/T is able to partly supply the HP in the early morning hours.

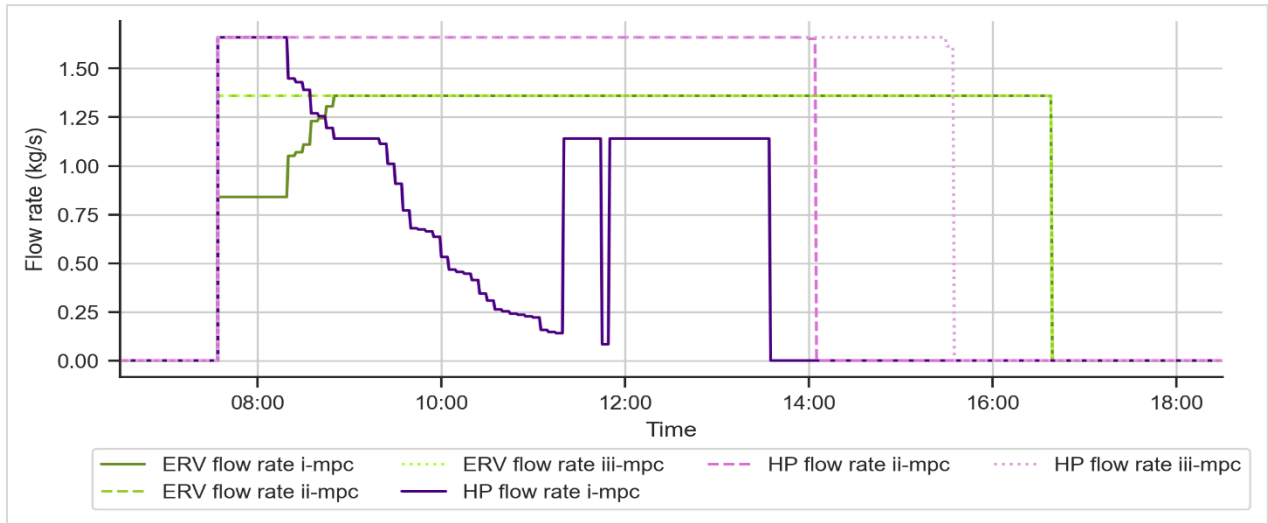


Figure 4-34 HP and ERV flow rate profiles for January 20, 2020, a very cold sunny day (i-mpc, ii-mpc and iii-mpc cases).

Figure 4-35 presents the power consumption of the HP and ERV for January 20, 2020. As expected, iii-mpc decreases the HP consumption as it provides adequate air to fully supply the HP. The ERV consumption is reduced as the BIPV/T area increases.

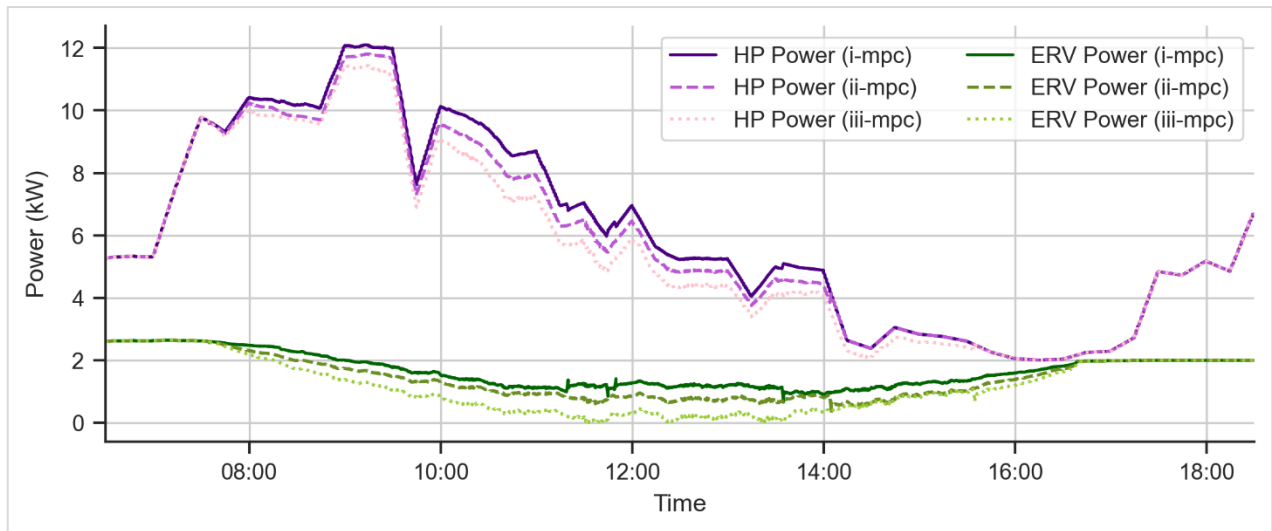


Figure 4-35 Power consumption profiles for January 20, 2020, a very cold sunny day (i-mpc, ii-mpc and iii-mpc cases).

Sunny Mild Day (February 28, 2020)

Figure 4-36 and Figure 4-37 present the BIPV/T, HP and ERV flow rate profiles for February 28, 2020. In the case of i-mpc the BIPV/T flow rate is kept almost constant at around 2 kg/s throughout the day. However, as the BIPV/T area increases the total BIPV/T flow rate is increased during hours with high irradiance levels. The BIPV/T fully supplies the ERV during morning hours and slowly decreases reaching zero around 10:00.

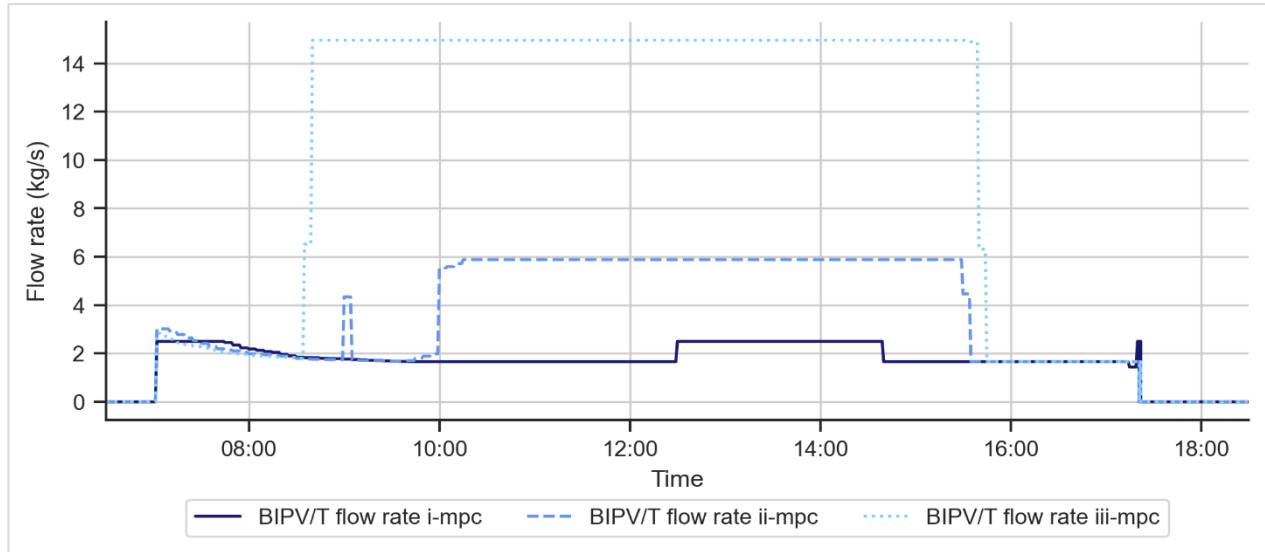


Figure 4-36 BIPV/T flow rate profiles for February 28, 2020, a mild sunny day (i-mpc, ii-mpc and iii-mpc cases).

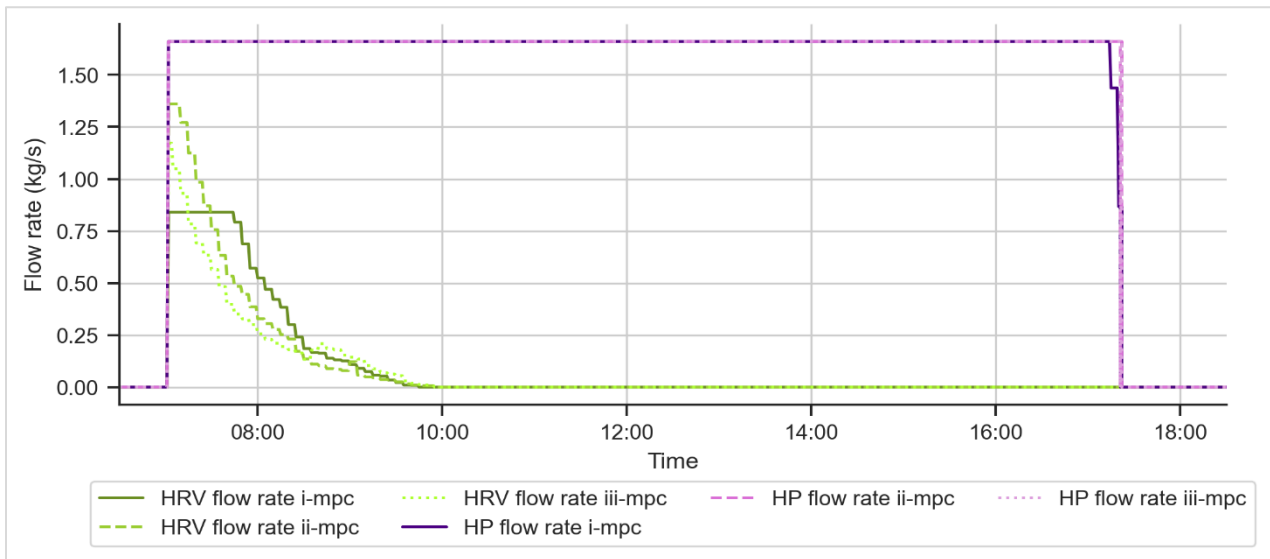


Figure 4-37 HP and ERV flow rate profiles for February 28, 2020, a mild sunny day (i-mpc, ii-mpc and iii-mpc cases).

Figure 4-38 shows the power consumption of the HP and ERV for the three scenarios. No significant change is noticed, leading to the conclusion that the i-mpc scenario is adequate to fulfill the energy needs of the library during this day.

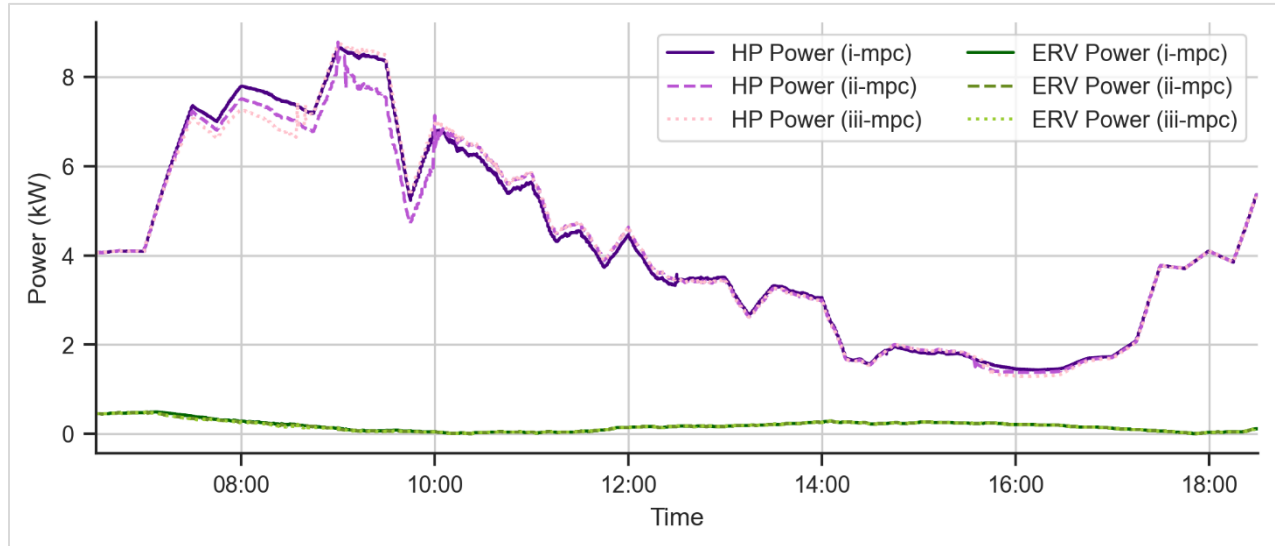


Figure 4-38 Power consumption profiles for March 13, 2020, a mild semi-cloudy day (i-mpc, ii-mpc and iii-mpc cases).

Table 4-8 lists the HP and ERV consumptions for the three scenarios for all days. A maximum decrease in HP consumption and ERV consumption (8.28% and 29.49% respectively) was noted on January 20, 2020 a very cold sunny day.

Table 4-8 HP and ERV consumed energy for the four investigated days (i-mpc, ii-mpc and iii-mpc cases).

<i>January 20, 2020 (very cold + sunny)</i>	i-mpc	ii-mpc	Decrease	iii-mpc	Decrease
HP Consumed Energy (kWh)	73.41	70.57	- 3.87%	67.33	- 8.28%
HP Consumed Energy (kWh/m²)	0.67	0.25		0.10	
ERV Consumed Energy (kWh)	20.01	17.36	- 13.24%	14.11	- 29.49%
ERV Consumed Energy (kWh/m²)	0.18	0.06		0.02	
<i>February 02, 2020 (cold + semi-cloudy)</i>					
HP Consumed Energy (kWh)	67.78	66.26	- 2.24%	64.91	- 4.23%
HP Consumed Energy (kWh/m²)	0.62	0.24		0.09	
ERV Consumed Energy (kWh)	12.16	11.21	- 7.81%	10.02	- 17.60%

ERV Consumed Energy (kWh/m²)	0.11	0.04		0.01	
<i>February 28, 2020 (mild + sunny)</i>					
HP Consumed Energy (kWh)	51.29	50.44	- 1.66%	51.04	- 0.49%
HP Consumed Energy (kWh/m²)	0.47	0.18		0.07	
ERV Consumed Energy (kWh)	2.10	2.06	- 1.90%	2.03	- 3.33%
ERV Consumed Energy (kWh/m²)	0.02	0.01		0.00	
<i>March 13, 2020 (mild + semi-cloudy)</i>					
HP Consumed Energy (kWh)	57.23	56.96	- 0.47%	56.91	- 0.56%
HP Consumed Energy (kWh/m²)	0.52	0.20		0.08	
ERV Consumed Energy (kWh)	2.03	1.93	- 4.93%	1.86	- 8.37%
ERV Consumed Energy (kWh/m²)	0.02	0.01		0.00	

4.4.6 Energy savings for adjacent buildings

As described in section 4.1, in times where the heated air from the BIPV/T is not entirely used for the needs of the library it is sent to an adjacent day-care to be used as pre-heated ventilation air. Figure 4-39 displays the percentage of excess produced heat available to cover needs of adjacent buildings. This percentage is higher for mild days where higher outlet temperatures and air velocities are reached by the BIPV/T.

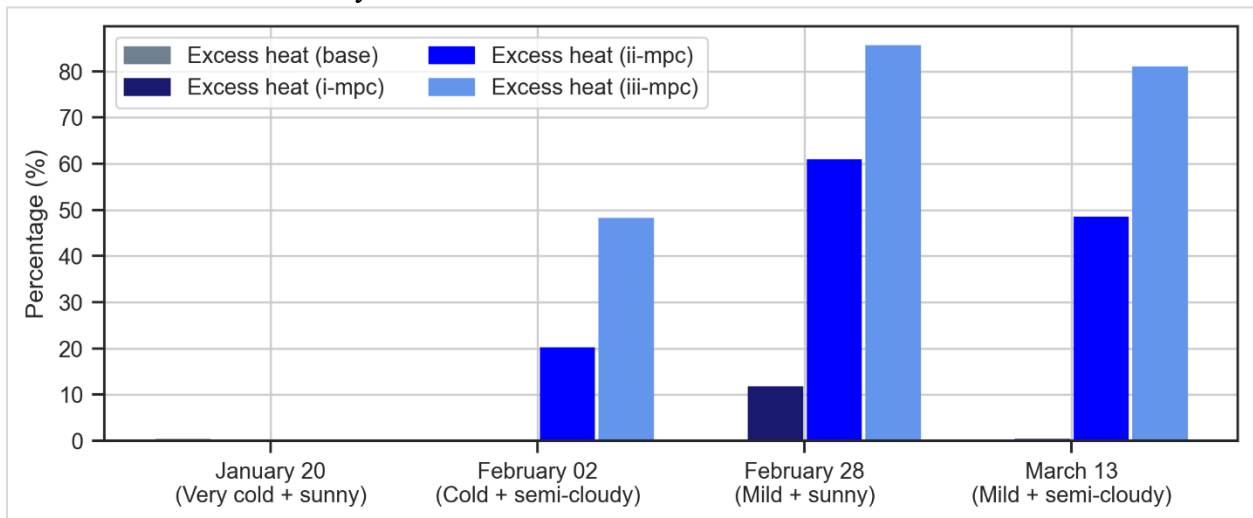


Figure 4-39 Percentage of produced heat sent to adjacent buildings (i-mpc, ii-mpc and iii-mpc cases).

Figure 4-40 shows the saved energy for all four investigated days for the cases i-mpc, ii-mpc and iii-mpc. For February 28, 2020 the most energy is saved reaching a decrease of up to 36.76% in energy usage. As this day has the highest irradiation levels combined with a higher ambient temperature, the mpc controller runs the fan at higher speeds to cool down the PVs resulting in excess heated air. As the area of the BIPV/T increases, so does the amount of excess heated air creating a greater opportunity for energy savings by adjacent buildings.

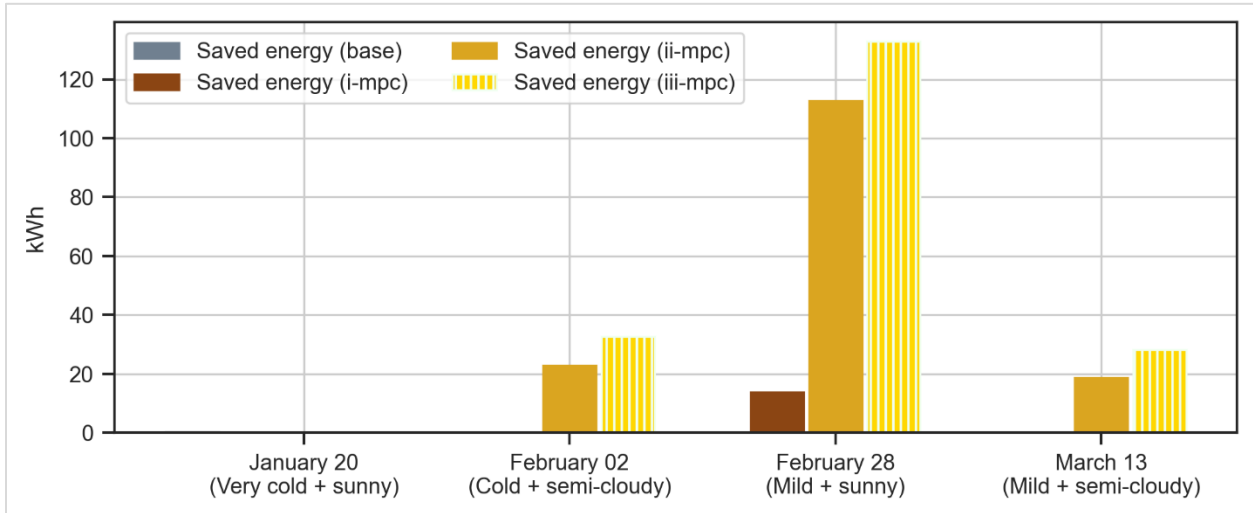


Figure 4-40 Energy savings for adjacent building (i-mpc, ii-mpc and iii-mpc cases).

Table 4-9 lists the energy consumption for heating the ventilation air of the day-care, without any assistance from the library and for cases i-mpc, ii-mpc and iii-mpc, for all days.

Table 4-9 Energy consumption for ventilation air in adjacent building (no assistance, i-mpc, ii-mpc and iii-mpc cases).

Day	Energy consumption for ventilation of the day-care				Decrease
	No assistance (kWh)	i-mpc (kWh)	ii-mpc (kWh)	iii-mpc (kWh)	
January 20, 2020 (very cold + sunny)	969.73	969.73	969.73	969.73	0
February 02, 2020 (cold + semi-cloudy)	711.6	711.6	688.72	678.94	Up to - 4.59%

<i>February 28, 2020 (mild + sunny)</i>	361.44	347.67	248.82	228.58	Up to - 36.76%
<i>March 13, 2020 (mild + semi- cloudy)</i>	382.20	382.14	363.6	354.18	Up to - 7.33%

The solar heated air can be sent to other applications as well, such as assisting air source heat pumps of adjacent buildings or extracting the heat through a heat exchanger. This is only a small demonstration of the numerous possibilities created by connecting nearby buildings and fulfilling each other's energy demands when possible, facilitating in the development of net-zero energy communities.

Chapter 5 Summary & Conclusions

This thesis presents a methodology for developing grey-box control-oriented models for air-based open loop BIPV/T systems and the application of MPC in the scope of achieving optimal BIPV/T-HVAC integration and maximizing the amount of useful heat.

The first part of this thesis focuses on the development of the grey-box BIPV/T model. By using experimental data obtained from an experimental procedure carried out in the SSEC laboratory in Concordia University, the BIPV/T model was validated. However, in the process of calibrating the model, it was found that the steady conditions in the laboratory were not ideal in order to evaluate the addition of the thermal capacitance in the BIPV/T model.

A full-scale BIPV/T system located at the Varennes library, the first institutional net-zero energy building in Canada was used as a case study in order to further develop the BIPV/T model and apply MPC of the BIPV/T flow rate. The commissioned BIPV/T system is closely monitored by numerous sensors throughout the BIPV/T and AHU of the library. However, there was no sensor for measuring the mass flow rate within the BIPV/T channel. To overcome this barrier a virtual sensor was developed calculating the estimated flow rate. This process resulted in the identification of the most important parameters to apply MPC in a commissioned BIPV/T

system. The most important ones include reliable measurements of the flow rate within the BIPV/T channel, outlet temperature and PV temperature at the end of the channel. Furthermore, it was found that, adding the thermal capacitance of the materials in the BIPV/T model played a role only during semi-cloudy, high-wind days. However, for conventional BIPV/T systems the difference is marginal, leading to the conclusion that steady-state models are a better fit for control purposes as they significantly reduce computation times. Additionally, through applying MPC and setting a restriction that does not allow the fan to change settings in a time duration less than the given control horizon, cycling is prevented, further reducing the need of including the thermal capacitance in the BIPV/T model. However, it is still worth investigating transient models for BIPV/T systems with higher thermal capacitance, such as BIPV/T with Phase Change Materials (PCM).

Finally, the MPC strategy development for controlling the flow rate within the BIPV/T air channel is presented in chapter 4. This is the first time MPC is applied to air-based open-loop BIPV/T systems and was found to have many benefits. The possibility to have multiple thermal applications with simultaneous heat delivery was considered, with the MPC controller defining the optimal use of the produced heat at each sampling moment. The overall energy consumption was reduced compared to the base (business-as-usual) case or the steady flow rate strategy. The considered thermal applications included assistance of an ERV, providing solar heated air as a source for an ASHP and sending excess heat to fulfil the needs of adjacent buildings, facilitating in the development of net-zero energy communities.

5.1 Contributions

- A complete grey-box control-oriented modelling approach for BIPV/T systems was introduced and developed for the first time. An evaluation of including the thermal capacitance in the model for control purposes was conducted leading to the conclusion that steady-state BIPV/T models can perform adequately for conventional BIPV/T systems.
- This study contributed to the identification of the most important parameters when applying MPC to a commissioned BIPV/T system. The most important ones include

reliable measurements of i) the mass flow rate, ii) outlet temperature and iii) PV temperature at the end of the channel.

- Finally, a model predictive control strategy for control of the air flow in air based BIPV/T systems was developed. Optimal connection with the building HVAC can enable broader realization of BIPV/T systems. MPC facilitates this effort by optimizing the BIPV/T fan flow rate and achieving simultaneous heat delivery to different thermal applications while preventing PV overheating.

5.2 Future Work

Further research that builds on this work can include:

- The addition of thermal storage charging as a possible thermal application for the produced heat from the BIPV/T. More specifically the heated air could be used:
 - i) to charge a water tank and use the heat for hydronic heating or DHW during the summer months,
 - ii) to increase the temperature of a ventilated concrete slab or rock bed. This way the heat can be utilized during the evening peak (18:00pm – 21:00pm) when the BIPV/T does not produce heat.
- This study was limited to the control of a specific sub-system of the building considering a specific measured heating load and a constant ventilation requirement throughout the day. Further work is needed to optimally connect the BIPV/T control with the supervisory control of the building and consider possible real-time interactions between the two.
- An optimization routine that will identify the control and prediction horizon combination which can facilitate in better MPC performance. It is possible different control/prediction horizons could be used for different environmental conditions. For example, during a windy, semi-cloudy day a shorter control horizon may be necessary compared to a day with relatively steady environmental conditions (clear, low-wind).
- A significant assumption made for this work is that all future predictions are 100% accurate which would not be the case under a real implementation of MPC. Thus, an

analysis considering the uncertainty, especially of the wind forecast, should be conducted to evaluate how this would reflect the performance of the MPC controller.

- Different thermal enhancements (addition of fins, PCM addition) to the BIPV/T system can be investigated which by increasing the thermal capacity of the system can possibly lead to better performance of the MPC controller.

Bibliography

- [1] Natural Resources Canada, "Zero Emission Vehicle Infrastructure Program," 2022. [Online]. Available: <https://www.nrcan.gc.ca/energy-efficiency/transportation-alternative-fuels/zero-emission-vehicle-infrastructure-program/21876>.
- [2] . International Renewable Energy Agency, "Smart Electrification with Renewables: Driving the transformation of energy services," Abu Dhabi, 2022.
- [3] L. Xia, Z. Ma, G. Kokogiannakis, S. Wang and X. Gong, "A model-based optimal control strategy for ground source heat pump systems with integrated solar photovoltaic thermal collectors," 10 2018. [Online].
- [4] Y. Luo, L. Zhang, M. Bozlar, Z. Liu, H. Guo and F. Meggers, "Active building envelope systems toward renewable and sustainable energy," 4 2019. [Online].
- [5] S. Attia, S. Bilir, T. Safy, C. Struck, R. Loonen and F. Goia, "Current trends and future challenges in the performance assessment of adaptive façade systems," 11 2018. [Online].
- [6] H. Alkhatib, P. Lemarchand, B. Norton and D. T. O'Sullivan, "Deployment and control of adaptive building facades for energy generation, thermal insulation, ventilation and daylighting: A review," 2 2021. [Online].
- [7] Z. Ioannidis, A. Buonomano, A. Athienitis and T. Stathopoulos, "Modeling of double skin façades integrating photovoltaic panels and automated roller shades: Analysis of the thermal and electrical performance," 11 2017. [Online].
- [8] Q. Zhu, X. Xu, J. Wang and F. Xiao, "Development of dynamic simplified thermal models of active pipe-embedded building envelopes using genetic algorithm," 2 2014. [Online].
- [9] . International Renewable Energy Agency, "Trading into a bright energy future: The case for open, high-quality solar photovoltaic markets," 2021.

- [10] A. Athienitis, S. Kalogirou, L. Candanedo and E. Rounis, "Modeling and Simulation of Passive and Active Solar Thermal Systems," 1 2021. [Online].
- [11] R. S. Kamel and A. S. Fung, "Modeling, simulation and feasibility analysis of residential BIPV/T+ASHP system in cold climate—Canada," 10 2014. [Online].
- [12] E. D. Rounis, A. Athienitis and T. Stathopoulos, "Review of air-based PV/T and BIPV/T systems - Performance and modelling," 1 2021. [Online].
- [13] E. D. Rounis, A. Athienitis and T. Stathopoulos, "BIPV/T curtain wall systems: Design, development and testing," 10 2021. [Online].
- [14] T. Yang and A. Athienitis, "A review of research and developments of building-integrated photovoltaic/thermal (BIPV/T) systems," 12 2016. [Online].
- [15] L. Candanedo Ibarra, A. Athienitis, J. Candanedo, W. O'Brien and Y. Chen, "Transient and steady state models for open-loop air-based BIPV/T systems," 2010. [Online].
- [16] T. Yang and A. Athienitis, "Experimental investigation of a two-inlet air-based building integrated photovoltaic/thermal (BIPV/T) system," *Applied Energy*, vol. 159, pp. 70-79, 12 2015.
- [17] J. I. Bilbao and A. B. Sproul, "Detailed PVT-water model for transient analysis using RC networks," 5 2015. [Online].
- [18] L. W. Florschuetz, "Extension of the Hottel-Whillier model to the analysis of combined photovoltaic/thermal flat plate collectors," 1976. [Online].
- [19] A. Athienitis, J. Bambara, B. O'Neill and J. Faille, "A prototype photovoltaic/thermal system integrated with transpired collector," 1 2011. [Online].
- [20] K. Sopian, K. Yigit, H. Liu, S. Kakaç and T. Veziroglu, "Performance analysis of photovoltaic thermal air heaters," 11 1996. [Online].

- [21] B. Agrawal and G. N. Tiwari, "Optimizing the energy and exergy of building integrated photovoltaic thermal (BIPVT) systems under cold climatic conditions," 2 2010. [Online].
- [22] J. K. Tonui and Y. Tripanagnostopoulos, "Performance improvement of PV/T solar collectors with natural air flow operation," 1 2008. [Online].
- [23] J. Assadeg, A. H. Al-Waeli, A. Fudholi and K. Sopian, "Energetic and exergetic analysis of a new double pass solar air collector with fins and phase change material," 9 2021. [Online].
- [24] J. Čurpek and M. Čekon, "Climate response of a BiPV façade system enhanced with latent PCM-based thermal energy storage," 6 2020. [Online].
- [25] . ASHRAE Epidemic Task Force, "Building Readiness," 2020.
- [26] ASHRAE, "Air-to-Air Energy Recovery Equipment," 2020. [Online].
- [27] J. G. Ahn, J. H. Kim and J. T. Kim, "A Study on Experimental Performance of Air-Type PV/T Collector with HRV," 11 2015. [Online].
- [28] A. Shahsavari and S. Khanmohammadi, "Feasibility of a hybrid BIPV/T and thermal wheel system for exhaust air heat recovery: Energy and exergy assessment and multi-objective optimization," 1 2019. [Online].
- [29] M. Ahmed-Dahmane, A. Malek and T. Zitoun, "Design and analysis of a BIPV/T system with two applications controlled by an air handling unit," 11 2018. [Online].
- [30] J. M. Tardif, J. Tamasauskas, V. Delisle and M. Kegel, "Performance of Air Based BIPV/T Heat Management Strategies in a Canadian Home," 1 2017. [Online].
- [31] R. Dumoulin, E. D. Rounis and A. Athienitis, "Operation and grid interaction modeling of a house with a building integrated photovoltaic thermal (BIPV/T) system coupled to an air-source heat pump," 10 2021. [Online].

- [32] Y. Chen, K. Galal and A. Athienitis, "Modeling, design and thermal performance of a BIPV/T system thermally coupled with a ventilated concrete slab in a low energy solar house: Part 2, ventilated concrete slab," 11 2010. [Online].
- [33] S. Pintaldi, J. Li, S. Sethuvenkatraman, S. White and G. Rosengarten, "Model predictive control of a high efficiency solar thermal cooling system with thermal storage," 8 2019. [Online].
- [34] J. Candanedo, V. Raissi Dehkordi and P. Lopez, "A control-oriented simplified building modelling strategy," 2013. [Online].
- [35] S. Li, J. Joe, J. Hu and P. Karava, "System identification and model-predictive control of office buildings with integrated photovoltaic-thermal collectors, radiant floor heating and active thermal storage," 3 2015. [Online].
- [36] Q. Chen and N. Li, "Model predictive control for energy-efficient optimization of radiant ceiling cooling systems," 11 2021. [Online].
- [37] J. Ma, A. S. Fung, M. Brands, O. M. Abul Moyeed, A. Mhanna and N. Juan, "Effects of photovoltaic/thermal (PV/T) control strategies on the performance of liquid-based PV/T assisted heat pump for space heating," 7 2021. [Online].
- [38] D. Christ and M. Kaltschmitt, "Modelling of photovoltaic-thermal collectors for the provision of electricity and low temperature heat—Comparison of different flow rate control approaches to optimize the electrical yield," 6 2021. [Online].
- [39] F. Dittus and L. Boelter, "Heat transfer in automobile radiators of the tubular type," *International Communications in Heat and Mass Transfer*, vol. 12, no. 1, pp. 3-22, 1 1985.
- [40] L. M. Candanedo, A. Athienitis and K. W. Park, "Convective heat transfer coefficients in a building-integrated photovoltaic/thermal system," 2011. [Online].

- [41] J. A. Palyvos, "A survey of wind convection coefficient correlations for building envelope energy systems' modeling," *Applied Thermal Engineering*, vol. 28, no. 8-9, pp. 801-808, 6 2008.
- [42] A. D. Jones and C. P. Underwood, A thermal model for photovoltaic systems, vol. 70, Pergamon, 2001, pp. 349-359.
- [43] M. Usama Siddiqui, A. F. Arif, L. Kelley and S. Dubowsky, Three-dimensional thermal modeling of a photovoltaic module under varying conditions, vol. 86, Pergamon, 2012, pp. 2620-2631.
- [44] E. D. Rounis, Z. Ioannidis, O. Kruglov, A. Athienitis and K. Kapsis, "Experimental investigation and characterization of Building Intergrated Photovoltaic/thermal envelope system with thermal enhancements for roof and curtain wall applications," in *International Solar Energy Society*, 2017.
- [45] E. Dimitrios Rounis, Z. Ioannidis, A. M. Sigounis, A. Athienitis and T. Stathopoulos, "A novel approach for the modelling of convective phenomena for building integrated photovoltaic thermal (BIPV/T) systems", vol. 232, Pergamon, 2022, pp. 328-343.
- [46] ASHRAE, ASHRAE Handbook—Fundamentals, 2017.
- [47] V. Dermardiros, "Data-Driven Optimized Operation of Buildings with Intermittent Renewables and Application to a Net-Zero Energy Library," 12 2020. [Online].
- [48] Emil Jalilov, "Development of heuristic model-based predictive control strategies for an institutional net-zero energy building," 11 2021. [Online].
- [49] Wikipedia, "Cross-validation (statistics)," [Online]. Available: [https://en.wikipedia.org/wiki/Cross-validation_\(statistics\)](https://en.wikipedia.org/wiki/Cross-validation_(statistics)).
- [50] G. o. C. nrcan, "Ground-soucre heat pumps," 2022. [Online]. Available: <https://www.nrcan.gc.ca/energy-efficiency/energy-efficiency-regulations/guide-canadas-energy-efficiency-regulations/ground-source-heat-pumps/6919>.

- [51] Arctic Heat Pumps, "Arctic Heat Pumps," [Online]. Available:
https://www.arcticheatpumps.com/?gclid=CjwKCAjwi6WSBhA-EiwA6Nioky0tc__RRbin-TCx3AHQ4x8U1DR_JpdM5qtl_MG_XgZTIfdHslCmlxoC92oQAvD_BwE.
- [52] "La Maison Bleue, centre de la petite enfance," 2022. [Online]. Available:
<https://cpelamaisonbleue.com/>.
- [53] ASHRAE, "ASHRAE Standard 62.1," [Online].
- [54] . Paolo Corti, . Pierluigi Bonomo, . Francesco Frontini, . Philippe Macé and . Elina Bosch, "Building Integrated Photovoltaics: A practical handbook for solar buildings' stakeholders," 2020.
- [55] Cold Climate Housing Research Center, "Energy Recovery Ventilators in Cold Climates," [Online].
- [56] A. Guiavarch and B. Peuportier, "Photovoltaic collectors' efficiency according to their integration in buildings.," *Solar Energy* , vol. 80, no. 1, pp. 65-77, 2006.
- [57] "Varenes Net-Zero Library – Award of Excellence," 2022. [Online]. Available:
<https://www.canadianconsultingengineer.com/features/varenes-net-zero-library-award-excellence/>.
- [58] Google, "Google maps," 2022. [Online].
- [59] Y. Chen, A. Athienitis and K. Galal, "Modeling, design and thermal performance of a BIPV/T system thermally coupled with a ventilated concrete slab in a low energy solar house: Part 1, BIPV/T system and house energy concept," 11 2010. [Online].

APPENDIX A

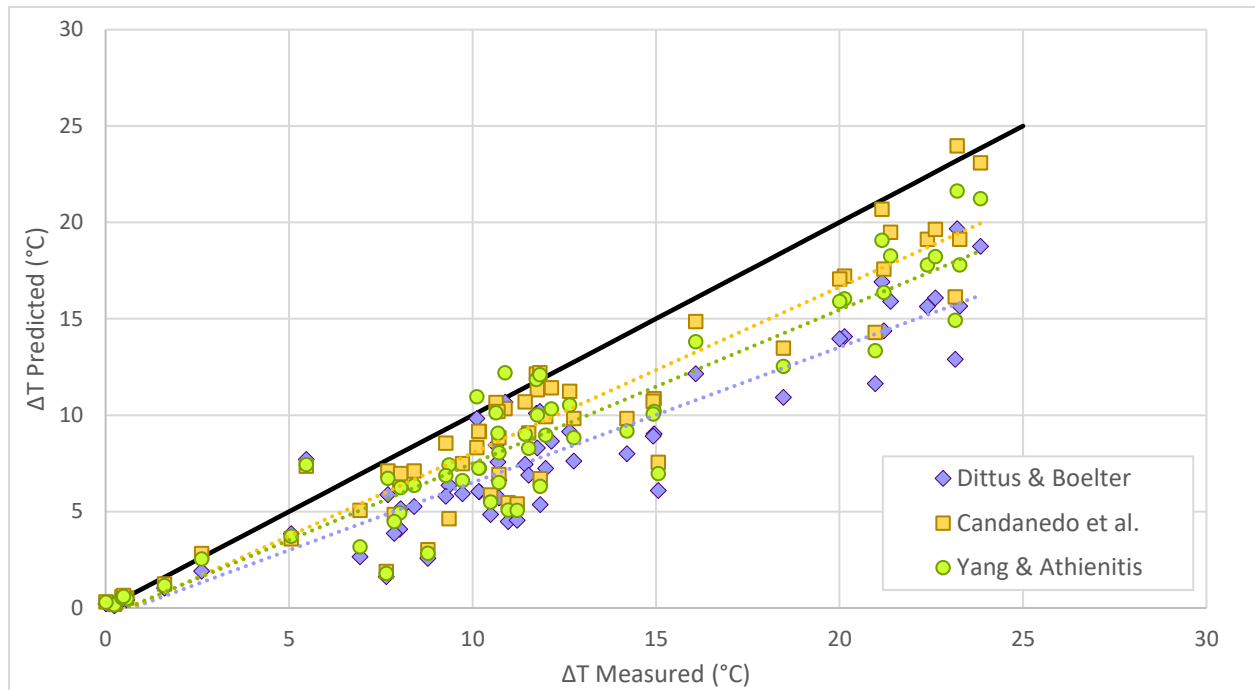


Figure 0-1 Scatter plot of predicted and measured ΔT for the Varennes BIPV/T data

Table 0-1 Energy consumption for all scenarios and all four examined days (TR model)

<i>Jan-20 (TR Model)</i>	base	i-mpc	i-s	ii-mpc	ii-s	iii-mpc	iii-s
PV Produced Energy (kWh)	93.46	93.46	93.46	239.81	239.81	608.43	608.43
HP Consumed Energy (kWh)	75.67	73.82	74.44	70.73	73.37	67.53	73.37
HRV Consumed Energy (kWh)	20.10	19.96	23.19	17.49	22.96	14.25	22.96
Net Consumed Energy (kWh)	2.32	0.34	4.18	-151.58	-143.46	-526.65	-512.04
<i>Feb-02 (TR Model)</i>	base	i-mpc	i-s	ii-mpc	ii-s	iii-mpc	iii-s
PV Produced Energy (kWh)	37.46	37.83	37.70	96.86	96.71	245.96	245.38

HP Consumed Energy (kWh)	69.21	67.85	68.54	66.40	67.93	65.15	67.93
HRV Consumed Energy (kWh)	12.41	12.24	13.63	11.35	13.55	10.23	13.55
Net Consumed Energy (kWh)	44.16	42.28	44.48	-19.10	-15.22	-170.55	-163.85
<i>Feb-28 (TR Model)</i>	base	i-mpc	i-s	ii-mpc	ii-s	iii-mpc	iii-s
PV Produced Energy (kWh)	103.11	105.14	105.03	270.67	269.33	688.72	683.36
HP Consumed Energy (kWh)	57.56	51.19	54.55	50.43	54.21	51.12	54.21
HRV Consumed Energy (kWh)	8.42	2.12	2.19	2.08	2.16	2.05	2.16
Net Consumed Energy (kWh)	-37.13	-51.82	-48.28	-218.12	-212.93	-635.42	-626.92
<i>Mar-13 (TR Model)</i>	base	i-mpc	i-s	ii-mpc	ii-s	iii-mpc	iii-s
PV Produced Energy (kWh)	39.33	39.45	39.46	101.13	101.23	257.17	256.85
HP Consumed Energy (kWh)	58.31	57.29	57.87	56.94	57.73	56.99	57.73
HRV Consumed Energy (kWh)	3.86	2.05	2.40	1.96	2.39	1.91	2.39
Net Consumed Energy (kWh)	22.84	19.90	20.82	-42.20	-41.09	-198.21	-196.66

Table 0-2 Energy consumption for all scenarios and all four examined days (SS model)

<i>Jan-20 (SS-Model)</i>	base	i-mpc	i-s	ii-mpc	ii-s	iii-mpc	iii-s
PV Produced Energy (kWh)	93.46	93.46	93.46	239.81	239.81	608.40	608.43
HP Consumed Energy (kWh)	75.67	73.41	74.40	70.57	73.29	67.33	73.29
HRV Consumed Energy (kWh)	20.01	20.01	23.13	17.36	22.90	14.11	22.90
Net Consumed Energy (kWh)	2.22	-0.02	4.08	-151.87	-143.59	-526.96	-512.18
<i>Feb-02 (SS-Model)</i>	base	i-mpc	i-s	ii-mpc	ii-s	iii-mpc	iii-s
PV Produced Energy (kWh)	37.41	37.80	37.67	96.79	96.63	245.82	245.17
HP Consumed Energy (kWh)	69.21	67.78	68.51	66.26	67.86	64.91	67.86

HRV Consumed Energy (kWh)	12.39	12.16	13.57	11.21	13.49	10.02	13.49
Net Consumed Energy (kWh)	44.19	42.15	44.42	-19.31	-15.25	-170.86	-163.75
<i>Feb-28 (SS-Model)</i>	base	i-mpc	i-s	ii-mpc	ii-s	iii-mpc	iii-s
PV Produced Energy (kWh)	103.27	105.43	105.16	271.08	269.66	689.55	684.20
HP Consumed Energy (kWh)	57.56	51.29	54.52	50.44	54.17	51.04	54.17
HRV Consumed Energy (kWh)	8.32	2.10	2.17	2.06	2.14	2.03	2.14
Net Consumed Energy (kWh)	-37.39	-52.02	-48.45	-218.55	-213.32	-636.35	-627.81
<i>Mar-13 (SS-Model)</i>	base	i-mpc	i-s	ii-mpc	ii-s	iii-mpc	iii-s
PV Produced Energy (kWh)	39.29	39.41	39.42	101.06	101.14	257.00	256.61
HP Consumed Energy (kWh)	58.31	57.23	57.85	56.96	57.70	56.91	57.70
HRV Consumed Energy (kWh)	3.81	2.03	2.38	1.93	2.36	1.86	2.36
Net Consumed Energy (kWh)	22.83	19.86	20.82	-42.14	-41.05	-198.17	-196.48

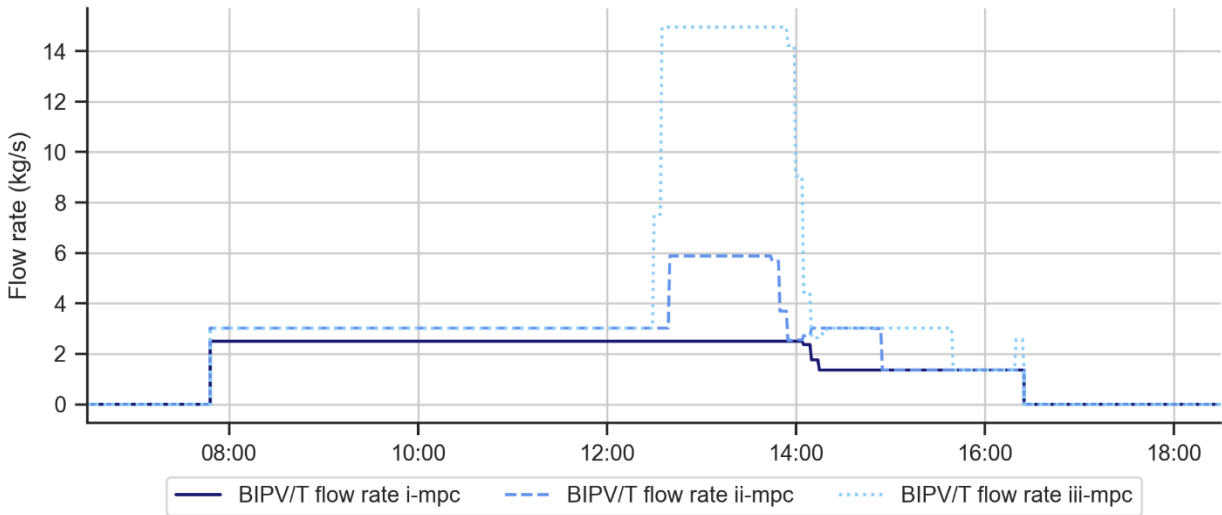


Figure 0-2 BIPV/T flow rate profiles for February 02, a mild semi-cloudy day (i-mpc, ii-mpc and iii-mpc cases).

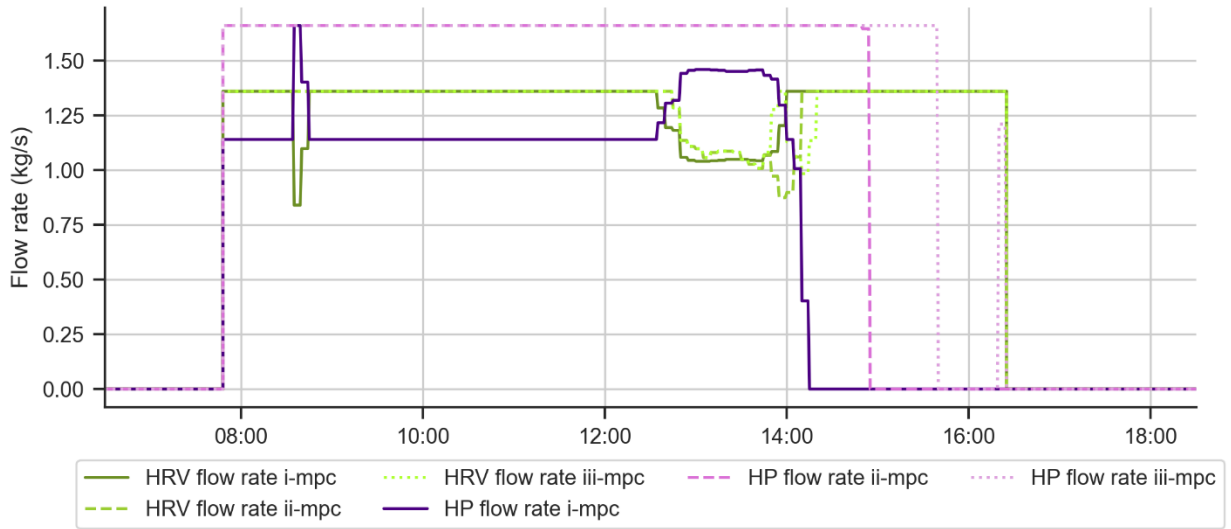


Figure 0-4 HP and ERV flow rate profiles for February 02, a mild semi-cloudy day (i-mpc, ii-mpc and iii-mpc cases).

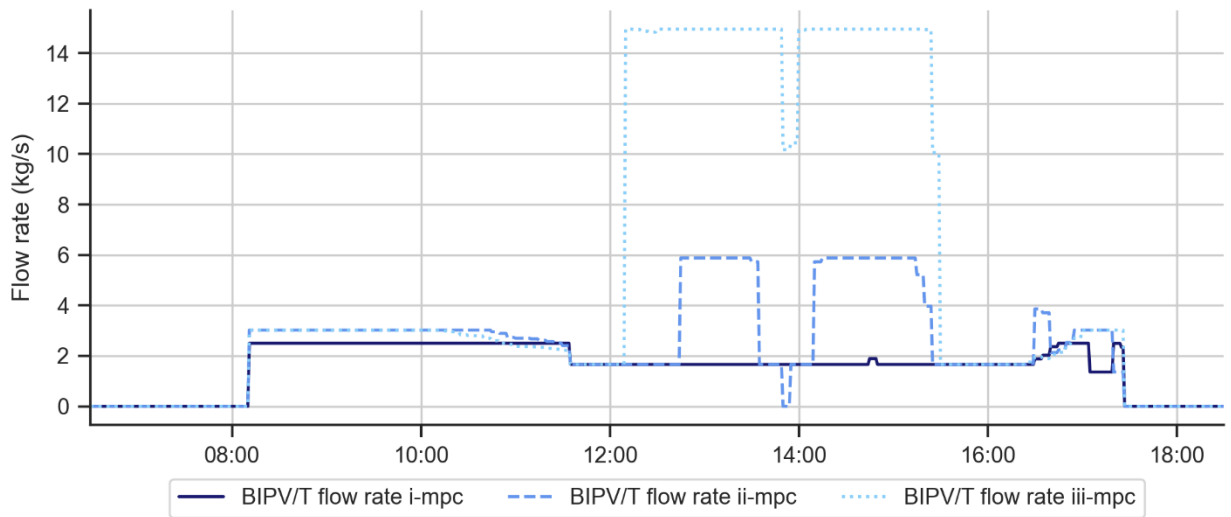


Figure 0-3 BIPV/T flow rate profiles for March 13, a mild semi-cloudy day (i-mpc, ii-mpc and iii-mpc cases).

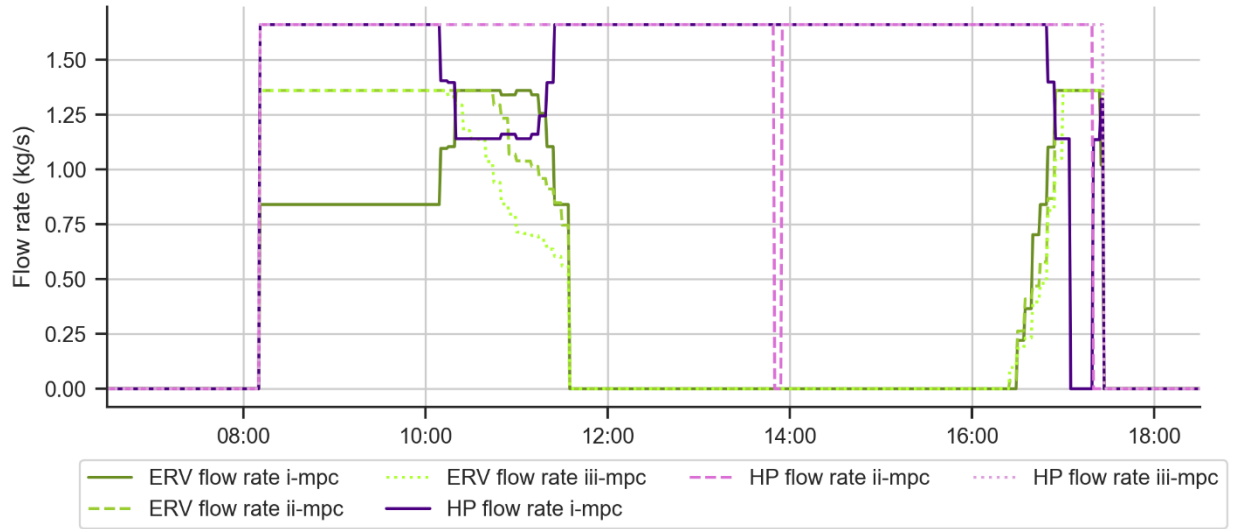


Figure 0-5 HP and ERV flow rate profiles for March 13, a mild semi-cloudy day (i-mpc, ii-mpc and iii-mpc cases).

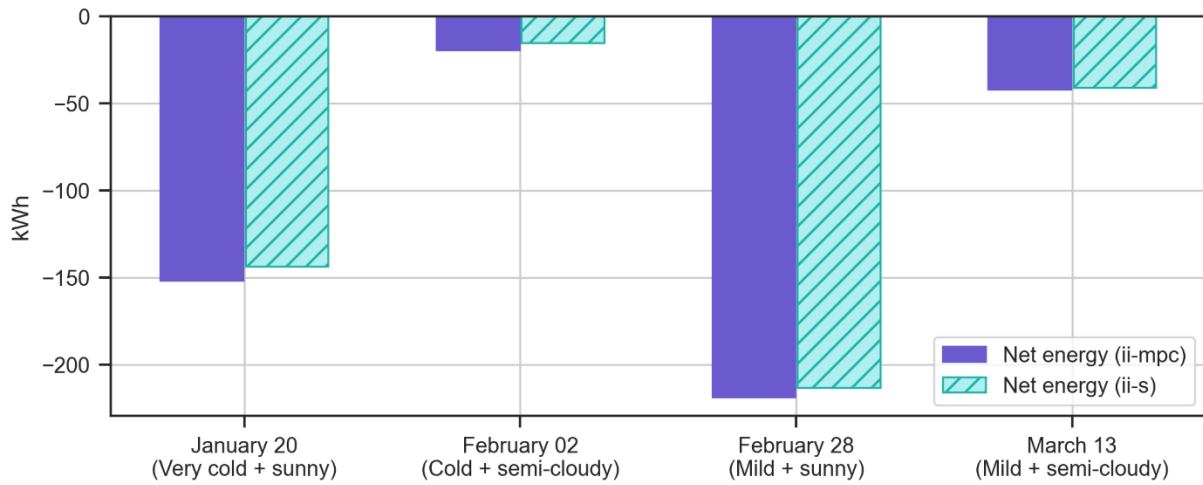


Figure 0-6 Net energy for the four investigated days (ii-s and ii-mpc case).

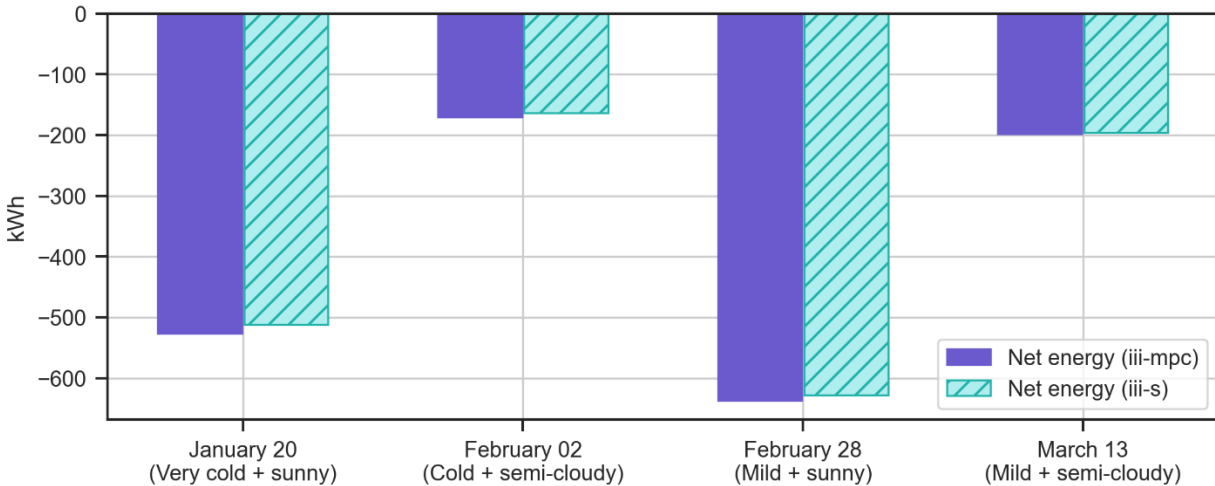


Figure 0-7 Net energy for the four investigated days (iii-s and iii-mpc case).

APPENDIX B

Calibration code sample (Python)

```
import numpy as np
import pandas as pd
from matplotlib import pyplot as plt
from CoolProp.CoolProp import PropsSI
import scipy.optimize as spo
from scipy.optimize import least_squares

sigma = 5.67 * 10**(-8)
# Stephan Boltzman constant (W/m2/K4)
cp_air = 1006
# Specific heat of air (J/kg*K)

# FUNCTIONS FOR HEAT TRANSFER COEFFICIENTS NAD AIR PROPERTIES -----

def h_radiation(sigma, VF, T1, T2, e_1, e_2):
    # Temperatures in C
    "Calculates radiative heat transfer coefficient"
    T1_K = T1 + 274.15
    T2_K = T2 + 274.15
    return (sigma*VF*(T1_K+T2_K)*(T1_K**2+T2_K**2))/(1/e_1+1/e_2-1)

def hc_channel_Candanedo(v_air,k_air,rho_air,vel_fan,HD):
    "Calculates convective heat transfer coefficients within BIPV/T channel
with Candanedos equations"
    Pr = 1006*v_air/k_air
    Re = rho_air*vel_fan*HD/v_air
```

```

    if Re<0:
        print('re<0')
        print(ρ_air, vel_fan, HD, v_air)
        Nu_t = 0.052*(Re**0.78)*(Pr**0.4)
# Top part of channel for Re<7500
        Nu_b = 1.017*(Re**0.471)*(Pr**0.4)
# Bottom part of channel for Re<7100
        hc_PV = Nu_t*k_air/HD
# CHTC for top part of channel [W/(m2*K)]
        hc_ins = Nu_b*k_air/HD
        return hc_PV, hc_ins

def hc_channel_Yang(v_air,k_air,ρ_air,vel_fan,HD):
    "Calculates convective heat transfer coefficients within BIPV/T channel
with Candanedos equations"
    Pr = 1006*v_air/k_air
    Re = ρ_air*vel_fan*HD/v_air
    if Re<0:
        print('re<0')
        print(ρ_air, vel_fan, HD, v_air)
        Nu_t = 0.014*(Re**0.9)*(Pr**0.4)
# Top part of channel for Re<7500
        Nu_b = 0.014*(Re**0.9)*(Pr**0.4)
# Bottom part of channel for Re<7100
        hc_PV = Nu_t*k_air/HD
# CHTC for top part of channel [W/(m2*K)]
        hc_ins = Nu_b*k_air/HD
        return hc_PV, hc_ins

def hc_channel_Dittus(v_air,k_air,ρ_air,vel_fan,HD):
    "Calculates convective heat transfer coefficients within BIPV/T channel
with Dittus-Boelter equations"
    Pr = 1006*v_air/k_air
    Re = ρ_air*vel_fan*HD/v_air
    if Re<0:
        print('re<0')
        print(ρ_air, vel_fan, HD, v_air)
    Nu = 0.023*(Re**0.8)*(Pr**0.4)
    hc_PV = Nu*k_air/HD
    hc_ins = Nu*k_air/HD
    return hc_PV, hc_ins

def hc_channel_Chen(vel_fan):
    "Calculates convective heat transfer coefficients within BIPV/T channel
with Chens equations"
    if vel_fan<0.6:
        hc_PV = 10.2
        hc_ins = 10.2
    else:
        hc_PV = 12*vel_fan + 3
        hc_ins = 12*vel_fan + 3
    return hc_PV, hc_ins

def air_properties(Tma):
    ρ_air = -0.0041*Tma+1.2826

```

```

    v_air = 0.0000000477*Tma+0.000017246
# viscosity of air (Pa*s)
    k_air = 0.00007*Tma+0.0241
# density of air (kg/m3)
    if Tma<-344 :
        ρ_air = -0.0041*-344+1.2826
        v_air = 0.0000000477*-344+0.000017246
# viscosity of air (Pa*s)
    k_air = 0.00007*-344+0.0241
# thermal conductivity of air (W/m*K)
    if Tma>312 :
        ρ_air = -0.0041*312+1.2826
        v_air = 0.0000000477*312+0.000017246
# viscosity of air (Pa*s)
    k_air = 0.00007*312+0.0241
# thermal conductivity of air (W/m*K)
    return ρ_air, v_air, k_air

# FUNCTION FOR STEADY STATE BIPVT MODEL -----

def
BIPVT_SS(weather_before, hc_PV, hc_ins, hc_wind, u_bot, BIPVT_characteristics, m_kg
_s_before, T_PV_before, T_ins_before, T_inlet_before, \

T_room_before, hr_sky_before, u_PV_top, u_PV_bot, hr_channel_before, hi):
    """Calculates the temperatures on surfaces on a BIPV/T, the outlet
temperature, convective and radiative htc and the radiation turned in to
heat.

    The calculation considers only one timestep and one Control Volume.

    BIPVT_characteristics = np.array([L_channel, W_channel, Hydraulic_D,
η_theo, PF, a_BIPVT, VF_sky, VF_PV_ins, e_PV_top, e_PV_bot, e_ins,
D_channel, t_STPV, a_ins])

    T_PV = np.array([T_PV_top, T_PV_mid, T_PV_bot])

    T_ins = np.array([T_ins_top, T_ins_mid, T_ins_bot])

    weather_before = np.array([T_amb, T_sky, Incident_R])
    """
    no_x = 11
    x_CV = np.zeros([no_x])
    for i in range (0, no_x):
        x_CV[i] = (BIPVT_characteristics[0]/(no_x-1))*i
# Points for vertical temperature calculation
    T = np.zeros([len(x_CV)])
    CSA = BIPVT_characteristics[1] * BIPVT_characteristics[11]
    for j in range(0, len(x_CV)):
        T[j] =
((hc_PV*T_PV_before[2]+hc_ins*T_ins_before[0])/(hc_PV+hc_ins))+
(T_inlet_before -
(hc_PV*T_PV_before[2]+hc_ins*T_ins_before[0])/(hc_PV+hc_ins)) * np.exp(-
BIPVT_characteristics[1] * x_CV[j] * ((hc_PV+hc_ins) / (m_kg_s_before *
1006)))
        Tma = np.mean(T[:])
        T_PV_after = np.zeros([3])

```

```

T_ins_after = np.zeros([3])
if T_PV_before[1]>25:
    h_bipvt_before = BIPVT_characteristics[3]*(1-0.0045*(T_PV_before[1]-
25))
else:
    h_bipvt_before = BIPVT_characteristics[3]
    H_P_before = (weather_before[2]*BIPVT_characteristics[5] -
h_bipvt_before*BIPVT_characteristics[4]*weather_before[2])
    T_PV_after[0] = (weather_before[0]*hc_wind +
weather_before[1]*hr_sky_before +
T_PV_before[1]*u_PV_top)/(hc_wind+hr_sky_before+u_PV_top)
    T_PV_after[1] = T_PV_after[1] =
(T_PV_before[2]*u_PV_bot+T_PV_before[0]*u_PV_top +
H_P_before)/(u_PV_bot+u_PV_top)
    T_PV_after[2] =
(T_PV_before[1]*u_PV_bot+Tma*hc_PV+T_ins_before[0]*hr_channel_before)/(u_PV_b
ot+hc_PV+hr_channel_before)
    T_ins_after[0] = (Tma*hc_ins + T_ins_before[1]*2*u_bot +
T_PV_before[2]*hr_channel_before +
weather_before[2]*BIPVT_characteristics[12]*BIPVT_characteristics[13])/(hc_in
s+2*u_bot+hr_channel_before)
    T_ins_after[1] = (T_ins_before[0]*2*u_bot + T_ins_before[2]*2*u_bot
)/(2*u_bot+2*u_bot)
    T_ins_after[2] = (T_ins_before[1]*2*u_bot + T_room_before*hi)/(2*u_bot +
hi)
    q_air_before = hc_PV*(T_PV_before[2]-Tma)+hc_ins*(T_ins_before[0]-Tma)
    q_air_before = m_kg_s_before*cp_air*(T[len(x_CV)-1]-T_inlet_before)
    hr_sky_after = h_radiation(5.67 * 10**(-8), BIPVT_characteristics[6],
weather_before[1], T_PV_after[0], 1, BIPVT_characteristics[8])
    hr_channel_after = h_radiation(5.67 * 10**(-8), BIPVT_characteristics[7],
T_PV_after[2], T_ins_after[0], BIPVT_characteristics[9],
BIPVT_characteristics[10])
    rho_air_after, v_air_after, k_air_after = air_properties(Tma)
    vel_fan_before = m_kg_s_before/(CSA*rho_air_after)
    hc_PV_after, hc_ins_after =
hc_channel_Candanedo(v_air_after,k_air_after,rho_air_after,vel_fan_before,BIPVT
_characteristics[2])
    # hc_PV_after, hc_ins_after =
hc_channel_Dittus(v_air_after,k_air_after,rho_air_after,vel_fan_before,BIPVT_ch
aracteristics[2])
    # hc_PV_after, hc_ins_after = hc_channel_Chen(vel_fan_before)
    # hc_PV_after, hc_ins_after =
hc_channel_Yang(v_air_after,k_air_after,rho_air_after,vel_fan_before,BIPVT_char
acteristics[2])
    Toutlet = T[len(x_CV)-1]
    return
Tma,T_PV_after,T_ins_after,q_air_before,hr_sky_after,hr_channel_after,hc_PV_a
fter,hc_ins_after,Toutlet

def nrmse(actual: np.ndarray, predicted: np.ndarray):
    """ Normalized Root Mean Squared Error """
    return np.sqrt(np.mean(np.square(actual - predicted))) / (actual.max() -
actual.min())

# BIPV/T GEOMETRY & CHARACTERISTICS -----

```

```

L_channel = 5.55
# Channel Length (m)
W_channel = 19.800
# Channel Width (m)
D_channel = 0.07
# Channel Depth (m)
Cross_S_Area = W_channel * D_channel
# Cross Sction Area (m2)
Hydraulic_D = 4*Cross_S_Area/(2*D_channel+2*W_channel)
# Hydraylic Diameter for rectangle shape (m)

PackFac = 0.85
# Packing Factor
η_theo = 0.159
beta_pv = 0.0045
# for crystalline Si cells
# Theoretical efficiency
a_PV = 0.88
# PV absorptance
t_PV = 0
# PV transmittance
a_ins = 0.86
# Insulation absorptance
e_PV = 0.89
# PV emissivity
e_ins = 0.8
# Insulation emissivity
VF_sky = 0.3
# View Factor PV to sky
VF_PV_ins = 0.86
# View Factor PV to insulation

CV = 5
# No of control volumes
L_CV = L_channel/CV
# Length of Control Volume (m)

BIPVT_characteristics = np.array([L_CV, W_channel, Hydraulic_D, η_theo,
PackFac, a_PV, VF_sky, VF_PV_ins, e_PV, e_PV, e_ins, D_channel, t_PV, a_ins])

# THERMAL CONDUCTANCES -----
u_PV_top = 486.9479
# Thermal conductance for top half of PV (W/m2K)
u_PV_bot = 486.9479
# Thermal conductance for bottom half of PV (W/m2K)
# u_PV_top = 2.40004085e+02
# Thermal conductance for top half of PV (W/m2K) - From calibration
# u_PV_bot = 2.40004085e+02
# Thermal conductance for bottom half of PV (W/m2K) - From calibration

```

```

u_bot = 0.119
# Thermal conductance for back surface (W/m2K) - From Varennes paper roof R-
value
# u_bot = 0.119
# Thermal conductance for back surface (W/m2K) - From calibration

Ri = 0.11
# Film coefficient [ASHRAE fundamentals Table 10, Chapter 26] (m2K/W)
hi = 1/Ri
# (W/m2K)

Dt = 30

# WEATHER DATA -----
df_data_weather = pd.read_csv (r"C:\Users\Ansi\OneDrive - Concordia
University - Canada\Documents\Concordia\Research\Python files\Spyder\BIPVT
model\mpc\mpc after cobee\Dataset 5 - weather.csv", parse_dates =
["Timestamp"], index_col = "Timestamp")
df_data_weather.replace('', np.nan, inplace=True)
df_data_weather = df_data_weather.dropna()
df_data_weather =
df_data_weather.resample("30S").interpolate(method='linear')
df_data_numpy_weather = df_data_weather.to_numpy()

weather = np.zeros([len(df_data_numpy_weather),3])
weather[:,0] = df_data_numpy_weather[:,0]
# Ambient Temperature
weather[:,1] = df_data_numpy_weather[:,0].copy() - 20
# Jones & Underwood, 2001; Siddiqui et al, 2012 (Sky Temperature)
# weather[:,1] = 0.0552*(df_data_numpy_weather[:,0].copy())**1.5
# Swinbank 1962 (Sky Temperature)
weather[:,2] = df_data_numpy_weather[:,2]
# Incident Irradiation w/m2

V_wind = df_data_numpy_weather[:,1]
# Wind speed on top of the collector (m/s)
wind_dir = df_data_numpy_weather[:,3]
# Wind direction (0-north, 90-east, 180-south, 270-west)

# INITIAL CONDITIONS -----
df_data_initialconditions = pd.read_csv (r"C:\Users\Ansi\OneDrive - Concordia
University - Canada\Documents\Concordia\Research\Python files\Spyder\BIPVT
model\mpc\mpc after cobee\Dataset 5 - initial conditions.csv", parse_dates =
["Timestamp"], index_col = "Timestamp")
df_data_initialconditions.replace('', np.nan, inplace=True)
df_data_initialconditions = df_data_initialconditions.dropna()
df_data_initialconditions =
df_data_initialconditions.resample("30S").interpolate(method='linear')
df_data_numpy_initialconditions = df_data_initialconditions.to_numpy()

T_pv = np.zeros([len(df_data_numpy_weather),3])
T_pv[:,0] = df_data_numpy_initialconditions[:,1].copy()
# PV Temperature at the top
T_pv[:,1] = df_data_numpy_initialconditions[:,1].copy()
# PV Temperature at the middle

```

```

T_pv[:,2] = df_data_numpy_initialconditions[:,1].copy()
# PV Temperature at the bottom

T_ins = np.zeros((len(df_data_numpy_weather),3))
T_ins[:,0] = df_data_numpy_initialconditions[:,1].copy() - 15
# Insulation Temperature at the top
T_ins[:,1] = df_data_numpy_initialconditions[:,1].copy() - 15
# Insulation Temperature at the middle
T_ins[:,2] = df_data_numpy_initialconditions[:,1].copy() - 15
# Insulation Temperature at the bottom

T_inlet = df_data_numpy_initialconditions[:,3].copy()
# Inlet Temperature
Toutlet = df_data_numpy_initialconditions[:,2].copy()

# T_room = np.full(len(df_data_numpy_weather), 20)
# Room Temperature (constant at 20 C)
# Air speed within the channel (m/s)
T_room = df_data_numpy_weather[:,0].copy()
q_air = np.zeros((len(df_data_numpy_weather)))
# For lab conditions
Tma = np.zeros((len(df_data_numpy_weather)))

# MEASURED DATA FOR MODEL VALIDATION -----
PV_T = df_data_numpy_initialconditions[:,1]
T_OUTLET_MEASURED = df_data_numpy_initialconditions[:,2]

# Massflow calculations & convective heat transfer initial - - - - -
rho_air = np.zeros(len(df_data_numpy_weather))
v_air = np.zeros(len(df_data_numpy_weather))
k_air = np.zeros(len(df_data_numpy_weather))

for i in range (0, len(df_data_numpy_weather)):
    rho_air[i], v_air[i], k_air[i] = air_properties(weather[i,0])

m_kg_s = df_data_numpy_initialconditions[:,4]*0.001*rho_air
# Mass flow rate (kg/s)
for i in range (0, len(df_data_numpy_weather)):
    if m_kg_s[i]==0:
        m_kg_s[i] = 0.00001
Vol_Massflow = m_kg_s/rho_air
# Volumetric Massflow rate (m3/s)
vel_air = Vol_Massflow/Cross_S_Area

hc_PV = np.zeros(len(df_data_numpy_weather)) + 0.001
hc_ins = np.zeros(len(df_data_numpy_weather)) + 0.001

for i in range (0, len(df_data_numpy_weather)):
    # hc_PV[i], hc_ins[i] =
hc_channel_Dittus(v_air[i],k_air[i],rho_air[i],vel_air[i],Hydraulic_D)      #
CHTC for top and bottom part of channel [W/(m2*K)]
    hc_PV[i], hc_ins[i] =
hc_channel_Candanedo(v_air[i],k_air[i],rho_air[i],vel_air[i],Hydraulic_D)

# Wind driven losses - - - - -

```

```

hc_wind = np.zeros(len(df_data_numpy_weather))

for i in range (0, len(df_data_numpy_weather)):
    if wind_dir[i]>=90 and wind_dir[i]<=270:
        hc_wind[i] = 7.4 + 4*V_wind[i]
# Palyvos 2008 (windward)
    else:
        hc_wind[i] = 4.2 + 3.5*V_wind[i]
# Palyvos 2008 (leeward)

# Radiative heat transfer initial - - - - -
hr_sky = np.zeros(len(df_data_numpy_weather))
hr_channel = np.zeros(len(df_data_numpy_weather))

for i in range (0, len(df_data_numpy_weather)):
    hr_sky[i] = h_radiation(sigma, VF_sky, weather[i,1], T_pv[i,0], 1, e_PV)
    hr_channel[i] = h_radiation(sigma, VF_PV_ins, T_ins[i,0], T_pv[i,0],
e_ins, e_PV)

# CALIBRATION -----
Tma = np.zeros([len(df_data_numpy_weather)])
error = np.zeros(len(df_data_numpy_weather))
RMSE = np.zeros(len(df_data_numpy_weather))

a = 0.6

def BIPVT_SS_Opt_Toutlet(x):
    """x = np.array([u_PV, u_bot])"""
    for i in range (0,len(df_data_numpy_weather)-1):

Tma[i],T_pv[i+1,:],T_ins[i+1,:],q_air[i+1],hr_sky[i+1],hr_channel[i+1],hc_PV[
i+1],hc_ins[i+1],Toutlet[i+1] =\
    BIPVT_SS
(weather[i],hc_PV[i],hc_ins[i],hc_wind[i],x[1]*0.1,BIPVT_characteristics,m_kg
_s[i+1],T_pv[i,:],T_ins[i,:],T_inlet[i],\
    T_room[i],hr_sky[i],2*x[0]*100,2*x[0]*100,hr_channel[i],hi)
    # NRMSE = nrmse(T_OUTLET_MEASURED,Toutlet) + nrmse(PV_T,T_pv[:,2])
    Toutlet_NRMSE = Toutlet.copy()
    T_pv_NRMSE = T_pv.copy()
    for j in range (0,len(df_data_numpy_weather)-1):
        if weather[j,2]<100 :
            Toutlet_NRMSE[j] = T_OUTLET_MEASURED[j]
            T_pv_NRMSE[j,1] = PV_T[j]
    NRMSE = a*nrmse(T_OUTLET_MEASURED,Toutlet_NRMSE) + (1-
a)*nrmse(PV_T[:,2],T_pv_NRMSE[:,2])
    return NRMSE

# Starting guess
#x0 = (7.57849378e+03, 1.75020040e+04, 5.68618161e-01, 5.68618161e-01)
x0 = (2.413, 1.19) # Initial guesses estimated by material properties
(upv=241.43W/m2K (SSEC module), uins=0.119w/m2K (Varenes paper R-value of
roof))

# Bounds
b0 = (0.2413, 24.13)

```



```

b1 = (0.119, 11.9)
bnds = (b0,b1)

sol = spo.minimize(BIPVT_SS_Opt_Toutlet, x0,
method='SLSQP',options={'disp':True}, bounds = bnds)

if sol.success:
    print("for a",a)
    print("VALUES",sol.x)
    print("NRMSE - CAL",sol.fun)
else:
    print("not possible")
NRMSE_TOTAL = nrmse(T_OUTLET_MEASURED,Toutlet) + nrmse(PV_T,T_pv[:,2])
NRMSE_PV = nrmse(PV_T,T_pv[:,2]) # Normalized Root mean square error
NRMSE_OUTLET = nrmse(T_OUTLET_MEASURED,Toutlet) # Normalized Root mean
square error
print("NRMSE TOTAL:", NRMSE_TOTAL)
print("NRMSE PV:", NRMSE_PV)
print("NRMSE OUTLET:", NRMSE_OUTLET)

print("done")

```

MPC code sample (Python)

```

import numpy as np
import pandas as pd
from matplotlib import pyplot as plt
import scipy.optimize as spo

sigma = 5.67 * 10**(-8)
# Stephan Boltzman constant (W/m2/K4)
cp_air = 1006
# Specific heat of air (J/kg*K)

# FUNCTIONS FOR HEAT TRANSFER COEFFICIENTS NAD AIR PROPERTIES -----

def h_radiation(sigma, VF, T1, T2, e_1, e_2):
# Temperatures in C
    "Calculates radiative heat transfer coefficient"
    T1_K = T1 + 274.15
    T2_K = T2 + 274.15
    return (sigma*VF*(T1_K+T2_K)*(T1_K**2+T2_K**2))/(1/e_1+1/e_2-1)

def hc_channel_Candanedo(v_air,k_air,ρ_air,vel_fan,HD):
    "Calculates convective heat transfer coefficients within BIPV/T channel
with Candanedos equations"
    Pr = 1006*v_air/k_air
    Re = ρ_air*vel_fan*HD/v_air
    if Re<0:
        print('re<0')
        print(ρ_air, vel_fan, HD, v_air)
    Nu_t = 0.052*(Re**0.78)*(Pr**0.4)
# Top part of channel for Re<7500
    Nu_b = 1.017*(Re**0.471)*(Pr**0.4)
# Bottom part of channel for Re<7100

```

```

    hc_PV = Nu_t*k_air/HD
# CHTC for top part of channel [W/(m2*K)]
    hc_ins = Nu_b*k_air/HD
    return hc_PV, hc_ins

def hc_channel_Dittus(v_air,k_air,ρ_air,vel_fan,HD):
    "Calculates convective heat transfer coefficients within BIPV/T channel
with Dittus-Boelter equations"
    Pr = 1006*v_air/k_air
    Re = ρ_air*vel_fan*HD/v_air
    if Re<0:
        print('re<0')
        print(ρ_air, vel_fan, HD, v_air)
    Nu = 0.023*(Re**0.8)*(Pr**0.4)
    hc_PV = Nu*k_air/HD
    hc_ins = Nu*k_air/HD
    return hc_PV, hc_ins

def hc_channel_Chen(vel_fan):
    "Calculates convective heat transfer coefficients within BIPV/T channel
with Chens equations"
    if vel_fan<0.6:
        hc_PV = 10.2
        hc_ins = 10.2
    else:
        hc_PV = 12*vel_fan + 3
        hc_ins = 12*vel_fan + 3
    return hc_PV, hc_ins

def air_properties(Tma):
    ρ_air = -0.0041*Tma+1.2826
    v_air = 0.0000000477*Tma+0.000017246
# viscosity of air (Pa*s)
    k_air = 0.00007*Tma+0.0241
# density of air (kg/m3)
    if Tma<-344 :
        ρ_air = -0.0041*-344+1.2826
        v_air = 0.0000000477*-344+0.000017246
# viscosity of air (Pa*s)
    k_air = 0.00007*-344+0.0241
# thermal conductivity of air (W/m*K)
    if Tma>312 :
        ρ_air = -0.0041*312+1.2826
        v_air = 0.0000000477*312+0.000017246
# viscosity of air (Pa*s)
    k_air = 0.00007*312+0.0241
# thermal conductivity of air (W/m*K)
    return ρ_air, v_air, k_air

def hc_channel_natural_convection(k_air,HD):
    "Calculates convective heat transfer coefficients when the fan isn't
working"
    Nu = 4
    hc_PV = Nu*k_air/HD
    hc_ins = Nu*k_air/HD
    return hc_PV, hc_ins

```

```

# FUNCTION FOR STEADY-STATE BIPVT MODEL -----
-----

def
BIPVT_SS(weather_before, hc_PV, hc_ins, hc_wind, u_bot, BIPVT_characteristics, m_kg
_s_before, T_PV_before, T_ins_before, T_inlet_before, \

T_room_before, hr_sky_before, u_PV_top, u_PV_bot, hr_channel_before, hi):
    """Calculates the temperatures on surfaces on a BIPV/T, the outlet
    temperature, convective and radiative htc and the radiation turned in to
    heat.
        The calculation considers only one timestep and one Control Volume.

        BIPVT_characteristics = np.array([L_channel, W_channel, Hydraulic_D,
    η_theo, PF, a_BIPVT, VF_sky, VF_PV_ins, e_PV_top, e_PV_bot, e_ins,
    D_channel, t_STPV, a_ins])

        T_PV = np.array([T_PV_top, T_PV_mid, T_PV_bot])

        T_ins = np.array([T_ins_top, T_ins_mid, T_ins_bot])

        weather_before = np.array([T_amb, T_sky, Incident_R])
    """
    no_x = 11
    x_CV = np.zeros([no_x])
    for i in range(0, no_x):
        x_CV[i] = (BIPVT_characteristics[0]/(no_x-1))*i
# Points for vertical temperature calculation
    T = np.zeros([len(x_CV)])
    CSA = BIPVT_characteristics[1] * BIPVT_characteristics[11]
    for j in range(0, len(x_CV)):
        T[j] =
((hc_PV*T_PV_before[2]+hc_ins*T_ins_before[0])/(hc_PV+hc_ins))+
(T_inlet_before -
(hc_PV*T_PV_before[2]+hc_ins*T_ins_before[0])/(hc_PV+hc_ins)) * np.exp(-
BIPVT_characteristics[1] * x_CV[j] * ((hc_PV+hc_ins) / (m_kg_s_before *
1006)))
        Tma = np.mean(T[:])
        T_PV_after = np.zeros([3])
        T_ins_after = np.zeros([3])
        if T_PV_before[1]>25:
            h_bipvt_before = BIPVT_characteristics[3]*(1-0.0045*(T_PV_before[1]-
25))
        else:
            h_bipvt_before = BIPVT_characteristics[3]
            H_P_before = (weather_before[2]*BIPVT_characteristics[5] -
h_bipvt_before*BIPVT_characteristics[4]*weather_before[2])
            T_PV_after[0] = (weather_before[0]*hc_wind +
weather_before[1]*hr_sky_before +
T_PV_before[1]*u_PV_top)/(hc_wind+hr_sky_before+u_PV_top)
            T_PV_after[1] = T_PV_after[1] =
(T_PV_before[2]*u_PV_bot+T_PV_before[0]*u_PV_top +
H_P_before)/(u_PV_bot+u_PV_top)
            T_PV_after[2] =
(T_PV_before[1]*u_PV_bot+Tma*hc_PV+T_ins_before[0]*hr_channel_before)/(u_PV_b
ot+hc_PV+hr_channel_before)

```

```

T_ins_after[0] = (Tma*hc_ins + T_ins_before[1]*2*u_bot +
T_PV_before[2]*hr_channel_before +
weather_before[2]*BIPVT_characteristics[12]*BIPVT_characteristics[13])/(hc_in
s+2*u_bot+hr_channel_before)
T_ins_after[1] = (T_ins_before[0]*2*u_bot + T_ins_before[2]*2*u_bot
)/(2*u_bot+2*u_bot)
T_ins_after[2] = (T_ins_before[1]*2*u_bot + T_room_before*hi)/(2*u_bot +
hi)
# q_air_before = hc_PV*(T_PV_before[2]-Tma)+hc_ins*(T_ins_before[0]-Tma)
q_air_before = m_kg_s_before*cp_air*(T[len(x_CV)-1]-T_inlet_before)
hr_sky_after = h_radiation(5.67 * 10**(-8), BIPVT_characteristics[6],
weather_before[1], T_PV_after[0], 1, BIPVT_characteristics[8])
hr_channel_after = h_radiation(5.67 * 10**(-8), BIPVT_characteristics[7],
T_PV_after[2], T_ins_after[0], BIPVT_characteristics[9],
BIPVT_characteristics[10])
rho_air_after, v_air_after, k_air_after = air_properties(Tma)
vel_fan_before = m_kg_s_before/(CSA*rho_air_after)
# hc_PV_after, hc_ins_after =
hc_channel_Candanedo(v_air_after,k_air_after,rho_air_after,vel_fan_before,BIPVT
_characteristics[2])
hc_PV_after, hc_ins_after =
hc_channel_Dittus(v_air_after,k_air_after,rho_air_after,vel_fan_before,BIPVT_ch
aracteristics[2])
# hc_PV_after, hc_ins_after = hc_channel_Chen(vel_fan_before)
Toutlet = T[len(x_CV)-1]
return
Tma,T_PV_after,T_ins_after,q_air_before,hr_sky_after,hr_channel_after,hc_PV_a
fter,hc_ins_after,Toutlet

```

```

def enthalpy(Temperature, Rel_Hum):

```

```

    Temp_AP = pd.read_csv (r"C:\Users\Anna-Maria\OneDrive - Concordia
University - Canada\Documents\Concordia\Research\Python
files\Spyder\Experimental Model\Temperature - absolute pressure.csv")
    Temp_AP.replace('', np.nan, inplace=True)
    Temp_AP = Temp_AP.dropna()
    Temp_AP_table = Temp_AP.to_numpy()
    for j in range (0,len(Temp_AP_table)-1):
        if Temp_AP_table[j,0]<Temperature and
Temp_AP_table[j+1,0]>Temperature:
            abs_pr = Temp_AP_table[j+1,1] - ((Temp_AP_table[j+1,0] -
Temperature)*(Temp_AP_table[j+1,1] -
Temp_AP_table[j,1])/(Temp_AP_table[j+1,0] - Temp_AP_table[j,0]))
            elif Temp_AP_table[j,0]==Temperature:
                abs_pr = Temp_AP_table[j,1]
    W = 0.621945*abs_pr*Rel_Hum/(101.325 - abs_pr*Rel_Hum)
    h = 1.006*Temperature + W*(2500.77 + 1.86*Temperature)
    return h, W

```

```

def fan_consumption(L_ch, Dh, CSA, fluid_density, fluid_viscosity, m_kg_s):

```

```

    "Gives fan consumption in kW"
    m_m3_s = m_kg_s/fluid_density
# Volumetric mass flow rate (m3/s)
    fluid_velocity = m_m3_s/CSA
# air speed within the channel
    Re = fluid_density*fluid_velocity*Dh/fluid_viscosity
    if Re<2300:

```

```

        f = 64/Re
# Darcy friction factor for laminar flow (Stratos thesis)
    else:
        f=(0.79*np.log(Re)-1.64)**-2
# Darcy friction factor for turbulent flow (Stratos thesis)

    Dp = f*L_ch*fluid_density*fluid_velocity**2/(Dh*2)
# Pressure drop
    Pfan = m_m3_s*Dp*0.001
# Fan consumption (kW)
    return Pfan

# BIPV/T GEOMETRY & CHARACTERISTICS -----

L_channel = 5.55
# Channel Length (m)
W_channel = 19.800
# Channel Width (m)
D_channel = 0.07
# Channel Depth (m)
Cross_S_Area = W_channel * D_channel
# Cross Sction Area (m2)
Hydraulic_D = 4*Cross_S_Area/(2*D_channel+2*W_channel)
# Hydraylic Diameter for rectangle shape (m)
A_bipvt = L_channel*W_channel

PackFac = 0.85
# Packing Factor
eta_theo = 0.159
beta_pv = 0.0045
# for crystalline Si cells
# Theoretical efficiency
a_PV = 0.88
# PV absorptance
t_PV = 0
# PV transmittance
a_ins = 0.86
# Insulation absorptance
e_PV = 0.89
# PV emissivity
e_ins = 0.8
# Insulation emissivity
VF_sky = 0.3
# View Factor PV to sky
VF_PV_ins = 0.86
# View Factor PV to insulation

CV = 1
# No of control volumes
L_CV = L_channel/CV
# Length of Control Volume (m)

BIPVT_characteristics = np.array([L_CV, W_channel, Hydraulic_D, eta_theo,
PackFac, a_PV, VF_sky, VF_PV_ins, e_PV, e_PV, e_ins, D_channel, t_PV, a_ins])

```

```

# THERMAL CONDUCTANCES -----

# u_PV = 486.9479*2
# Thermal conductance half of PV white box (W/m2K)

u_PV_top = 0.28751258*2*100
# Thermal conductance for top half of PV (W/m2K) - From calibration
u_PV_bot = 0.28751258*2*100
# Thermal conductance for bottom half of PV (W/m2K) - From calibration

u_bot = 1.119*0.1
# Thermal conductance for back surface (W/m2K) - From Varennes paper roof R-
value

Ri = 0.11
# Film coefficient [ASHRAE fundamentals Table 10, Chapter 26] (m2K/W)
hi = 1/Ri
# (W/m2K)

Dt = 30

# WEATHER DATA -----
df_data_weather = pd.read_csv (r"C:\Users\Ansi\OneDrive - Concordia
University - Canada\Documents\Concordia\Research\Python files\Spyder\BIPVT
model\mpc\mpc after cobee\Dataset 4 - weather.csv", parse_dates =
["Timestamp"], index_col = "Timestamp")
df_data_weather.replace(' ', np.nan, inplace=True)
df_data_weather = df_data_weather.dropna()
df_data_weather =
df_data_weather.resample("30S").interpolate(method='linear')
df_data_numpy_weather = df_data_weather.to_numpy()

weather = np.zeros((len(df_data_numpy_weather),3))
weather[:,0] = df_data_numpy_weather[:,0]
# Ambient Temperature
weather[:,1] = df_data_numpy_weather[:,0].copy() - 12
# Jones & Underwood, 2001; Siddiqui et al, 2012 (Sky Temperature)
# weather[:,1] = 0.0552*(df_data_numpy_weather[:,0].copy())**1.5
# Swinbank 1962 (Sky Temperature)
weather[:,2] = df_data_numpy_weather[:,2]
# Incident Irradiation w/m2

V_wind = df_data_numpy_weather[:,1]
# Wind speed on top of the collector (m/s)
wind_dir = df_data_numpy_weather[:,3]
# Wind direction (0-north, 90-east, 180-south, 270-west)
Rel_Hum = df_data_numpy_weather[:,4]
# Relative Humidity (%)

# INITIAL CONDITIONS -----

```

```

df_data_initialconditions = pd.read_csv (r"C:\Users\Ansi\OneDrive - Concordia
University - Canada\Documents\Concordia\Research\Python files\Spyder\BIPVT
model\mpc\mpc after cobee\Dataset 4 - initial conditions.csv", parse_dates =
["Timestamp"], index_col = "Timestamp")
df_data_initialconditions.replace('', np.nan, inplace=True)
df_data_initialconditions = df_data_initialconditions.dropna()
df_data_initialconditions =
df_data_initialconditions.resample("30S").interpolate(method='linear')
df_data_numpy_initialconditions = df_data_initialconditions.to_numpy()

T_pv = np.zeros([len(df_data_numpy_weather),3])
T_pv[:,0] = df_data_numpy_initialconditions[:,1].copy()
# PV Temperature at the top
T_pv[:,1] = df_data_numpy_initialconditions[:,1].copy()
# PV Temperature at the middle
T_pv[:,2] = df_data_numpy_initialconditions[:,1].copy()
# PV Temperature at the bottom

T_ins = np.zeros([len(df_data_numpy_weather),3])
T_ins[:,0] = df_data_numpy_initialconditions[:,1].copy() - 15
# Insulation Temperature at the top
T_ins[:,1] = df_data_numpy_initialconditions[:,1].copy() - 15
# Insulation Temperature at the middle
T_ins[:,2] = df_data_numpy_initialconditions[:,1].copy() - 15
# Insulation Temperature at the bottom

T_inlet = df_data_numpy_initialconditions[:,3].copy()
# Inlet Temperature
Toutlet = df_data_numpy_initialconditions[:,2].copy()

T_room = np.full(len(df_data_numpy_weather), 20)
# Room Temperature (constant at 20 C)
# T_room = df_data_numpy_weather[:,0].copy()
# For the lab
q_air = np.zeros([len(df_data_numpy_weather)])
Tma = np.zeros([len(df_data_numpy_weather)])
heating_load = df_data_numpy_initialconditions[:,5].copy()
# Electricity load for heating from Emils thesis for cold sunny day

# MEASURED DATA FOR MODEL VALIDATION -----
PV_T = df_data_numpy_initialconditions[:,1]
T_OUTLET_MEASURED = df_data_numpy_initialconditions[:,2]

# Massflow calculations & convective heat transfer initial - - - - -
rho_air = np.zeros(len(df_data_numpy_weather))
v_air = np.zeros(len(df_data_numpy_weather))
k_air = np.zeros(len(df_data_numpy_weather))

for i in range (0, len(df_data_numpy_weather)):
    rho_air[i], v_air[i], k_air[i] = air_properties(weather[i,0])

m_kg_s = df_data_numpy_initialconditions[:,4]/3600
# Mass flow rate (kg/s)
for i in range (0, len(df_data_numpy_weather)):
    if m_kg_s[i]==0:

```

```

        m_kg_s[i] = 0.00001
Vol_Massflow = m_kg_s/ρ_air
# Volumetric Massflow rate (m3/s)
vel_air = Vol_Massflow/Cross_S_Area

hc_PV = np.zeros(len(df_data_numpy_weather)) + 0.001
hc_ins = np.zeros(len(df_data_numpy_weather)) + 0.001

for i in range (0, len(df_data_numpy_weather)):
    hc_PV[i], hc_ins[i] =
hc_channel_Dittus(v_air[i],k_air[i],ρ_air[i],vel_air[i],Hydraulic_D)      #
# CHTC for top and bottom part of channel [W/(m2*K)]
    # if m_kg_s[i]<0.01:
    #     hc_PV[i], hc_ins[i] =
hc_channel_natural_convection(k_air[i],Hydraulic_D)

# Wind driven losses - - - - -
hc_wind = np.zeros(len(df_data_numpy_weather))

for i in range (0, len(df_data_numpy_weather)):
    if wind_dir[i]>=90 and wind_dir[i]<=270:
        hc_wind[i] = 7.4+4*V_wind[i]
# Palyvos 2008 (windward)
    else:
        hc_wind[i] = 4.2 + 3.5*V_wind[i]
# Palyvos 2008 (leeward)

# Radiative heat transfer initial - - - - -
hr_sky = np.zeros(len(df_data_numpy_weather))
hr_channel = np.zeros(len(df_data_numpy_weather))

for i in range (0, len(df_data_numpy_weather)):
    hr_sky[i] = h_radiation(sigma, VF_sky, weather[i,1], T_pv[i,0], 1, e_PV)
    hr_channel[i] = h_radiation(sigma, VF_PV_ins, T_ins[i,0], T_pv[i,0],
e_ins, e_PV)

# ___Heat Pump___

# Reference Heat Pump (3 Types)
HP_Qref = np.array([8.22, 11.5, 29])
# KW
HP_COPref = np.array([2.82, 2.75, 2.84])
HP_W_m = np.array([0.4, 0.7, 0.8])
# water mass flow kg/s
HP_A_m = np.array([0.42, 0.83, 1.66])

def HP_air_to_water(T_supply_air, T_water_setpoint):
    "Gives COP depending on supply air temperature and water setpoint"
    # INPUT DATA
    hp_data = pd.read_csv (r"C:\Users\Ansi\OneDrive - Concordia University -
Canada\Documents\Concordia\Research\Python files\Spyder\Experimental
Model\Heat Pump\SAASHP Performance File (Remi thesis).csv")
    hp_data.replace('', np.nan, inplace=True)
    hp_data = hp_data.dropna()
    hp_data_numpy = hp_data.to_numpy()
    Q_Ratio = hp_data_numpy[:,0]

```



```

Power_Ratio = hp_data_numpy[:,1]
COP_Ratio = hp_data_numpy[:,2]
T_air_hp = hp_data_numpy[:,3]
T_water = hp_data_numpy[:,4]
condition = True
while condition == True:
    for j in range (0,len(hp_data_numpy)-1):
        if T_water_setpoint == T_water[j]:
            if T_supply_air>T_air_hp[j] and T_supply_air<T_air_hp[j+1]:
                COP_insta = (COP_Ratio[j] - (T_air_hp[j] -
T_supply_air)*(COP_Ratio[j] - COP_Ratio[j+1])/(T_air_hp[j] -
T_air_hp[j+1]))*HP_COPref[2]
                Q_insta = (Q_Ratio[j] - (T_air_hp[j] -
T_supply_air)*(Q_Ratio[j] - Q_Ratio[j+1])/(T_air_hp[j] -
T_air_hp[j+1]))*HP_Qref[2]
                condition = False
            elif T_supply_air==T_air_hp[j]:
                COP_insta = COP_Ratio[j]*HP_COPref[2]
                Q_insta = Q_Ratio[j]*HP_Qref[2]
                condition = False
    return COP_insta, Q_insta

# ERV

T_exhaust = 22
# Temperature leaving the building
Vent_req = 1.36
# Ventilation requirements for Varennes kg/s
e_sensible = 0.744
# ERV sensible effectiveness
vent_setpoint = np.full(len(df_data_numpy_weather),18)

def ERV(e_sensible, m_supply, m_exhaust, T1, T3, cp_air):
    "Temperature of supply air after passing through the ERV"
    m_min = min(m_supply, m_exhaust)
    T2 = (m_supply*cp_air*T1 - e_sensible*m_min*(cp_air*T1 -
cp_air*T3))/(m_supply*cp_air)
    return T2

# MPC

pr_h = 120
# prediction horizon (steps ---> 60 minutes)
c_h = 10
# control horizon (steps ---> 5 minutes)

m_times = (len(df_data_numpy_weather)-1)//c_h
# how many massflow setpoints I will have
m_sp = np.zeros(len(df_data_numpy_weather))
# massflow setpoints
m_sp_hp = np.zeros(len(df_data_numpy_weather))
m_sp_hrv = np.zeros(len(df_data_numpy_weather))
hrv_signal = np.zeros(len(df_data_numpy_weather))

# MPC FUNCTION -----

```

```

def BIPVT_2C_Toutlet_Control(x, start):
    """x[0] = m_kg_s from bipvt, x[1] = m_kg_s for hp from bipvt, x[2] =
    m_kg_s for hrv from bipvt"""
    finish = start + pr_h
    if finish > len(df_data_numpy_weather)-1:
        finish = len(df_data_numpy_weather)-1
    for v in range (0,CV):
        for i in range (start,finish):

Tma[i],T_pv[i+1,:],T_ins[i+1,:],q_air[i+1],hr_sky[i+1],hr_channel[i+1],hc_PV[
i+1],hc_ins[i+1],Toutlet[i+1] =\
        BIPVT_SS
(weather[i],hc_PV[i],hc_ins[i],hc_wind[i],u_bot,BIPVT_characteristics,x[0]*0.
01,T_pv[i,:],T_ins[i,:],T_inlet[i],\
        T_room[i],hr_sky[i],u_PV_top,u_PV_bot,hr_channel[i],hi)
    m_out_hp = HP_A_m[2] - x[1]*0.01 # defining
massflow from outside for heat pump
    m_out_hrv = Vent_req - x[2]*0.01 # defining
massflow from outside for hrv
    T_mix_hp = np.zeros(len(df_data_numpy_weather))
    T_mix_hrv = np.zeros(len(df_data_numpy_weather))
    T2_hrv = np.zeros(len(df_data_numpy_weather))
    h_bipvt = np.zeros(len(df_data_numpy_weather))
    # add_energy_no_hrv = np.zeros(len(df_data_numpy_weather))
    # add_energy_yes_hrv = np.zeros(len(df_data_numpy_weather))
    add_energy_hrv = np.zeros(len(df_data_numpy_weather))
    add_energy_hp = np.zeros(len(df_data_numpy_weather))
    add_energy_fan = np.zeros(len(df_data_numpy_weather))
    cop_insta = np.zeros(len(df_data_numpy_weather))
    q_insta = np.zeros(len(df_data_numpy_weather))
    prod_energy_pv = np.zeros(len(df_data_numpy_weather))
    Dt_hrv = np.zeros(len(df_data_numpy_weather))
    for j in range (start,finish):
        rho_air, v_air, k_air = air_properties(Toutlet[j])
        T_mix_hp[j] = (0.01*x[1]*Toutlet[j] +
m_out_hp*weather[j,0])/(0.01*x[1] + m_out_hp) # Tmix for heat pump
        cop_insta[j], q_insta[j] = HP_air_to_water(T_mix_hp[j], 50)
        if heating_load[j]<=q_insta[j]:
            add_energy_hp[j] = heating_load[j]/cop_insta[j]
# Additional energy required operate heat pump (kW)
        else:
            add_energy_hp[j] = heating_load[j]/cop_insta[j]
            print ("!!Heating load to big for HP capacity!!")
        T_mix_hrv[j] = (0.01*x[2]*Toutlet[j] +
m_out_hrv*weather[j,0])/(0.01*x[2] + m_out_hrv) # Tmix for hrv
        Dt_hrv[j] = np.abs(vent_setpoint[j] - T_mix_hrv[j])
        T2_hrv[j] = ERV(e_sensible, Vent_req, Vent_req, T_mix_hrv[j],
T_exhaust, cp_air) # Air temperature after passing through the HRV
        add_energy_hrv[j] = (Vent_req*cp_air*np.abs(vent_setpoint[j] -
T2_hrv[j]))*0.001/3.1
        if T_pv[j,1]>25:
            h_bipvt[j] = BIPVT_characteristics[3]*(1-0.0045*(T_pv[j,1]-25))
        else:
            h_bipvt[j] = BIPVT_characteristics[3]
        prod_energy_pv[j] = h_bipvt[j]*A_bipvt*weather[j,2]*0.001
# Power produced from the PVs (kW)

```

```

        add_energy_fan[j] = fan_consumption(L_channel, Hydraulic_D,
Cross_S_Area, ρ_air, v_air, x[0]*0.01)
        net_energy = add_energy_hp + add_energy_hrv - prod_energy_pv
        print ("bipvt massflow",x[0]*0.01, "hp massflow",x[1]*0.01,"hrv
massflow",x[2]*0.01)
        print ("cop average",cop_insta[start:finish].mean())
        return np.sum(net_energy[start:finish])

x0 = 200
bnds = ((10,250),(0,166),(0,136)) # air velocity bounds 0.06m/s - 1.5m/s for
bipvt, hp massflow max 0.83kg/s, hrv massflow max 1.36kg/s
start = 0

# Constraints
def constraint1(x):
    return x[0] - x[1] - x[2] # x[0] >= x[1] + x[2]

cons = (({'type': 'ineq', 'fun':constraint1})
        # ,({'type': 'eq', 'fun':constraint2})

for v in range (0,m_times):
    sol = spo.minimize(BIPVT_2C_Toutlet_Control, x0,
method='SLSQP',args=(start), bounds=bnds, constraints=cons)
    if sol.success:
        print("success")
        print("optimal massflow is",sol.x[0]*0.01)
        print("optimal hp massflow is",sol.x[1]*0.01)
        print("optimal hrv massflow is",sol.x[2]*0.01)
        print("Power consumption",sol.fun)
        m_sp[start:start + c_h] = sol.x[0]*0.01
        m_sp_hp[start:start + c_h] = sol.x[1]*0.01
        m_sp_hrv[start:start + c_h] = sol.x[2]*0.01
    else:
        print("not possible")
    start = start + c_h

for i in range (0, len(df_data_numpy_weather)):
    if weather[i,2]<20:
        m_sp[i] = 0
        m_sp_hp[i] = 0
        m_sp_hrv[i] = 0

m_kg_s = m_sp[:,] + 0.000000001
# Mass flow rate (kg/s)
m_kg_s_hp = m_sp_hp[:,] + 0.000000001
# Mass flow rate for heat pump (kg/s)
m_kg_s_hrv = m_sp_hrv[:,] + 0.000000001
# Mass flow rate for hrv (kg/s)

m_out_hp = HP_A_m[2] - m_kg_s_hp
m_out_hrv = Vent_req - m_kg_s_hrv

Vol_Massflow = m_kg_s/ρ_air
# Volumetric Massflow rate (m3/s)
vel_air = Vol_Massflow/Cross_S_Area

```

```

# ENERGY BALANCE -----
T_inlet = df_data_numpy_initialconditions[:,3].copy()
Tma = np.zeros([len(df_data_numpy_weather)])
for v in range (0,CV):
    for i in range (0,len(df_data_numpy_weather)-1):

Tma[i],T_pv[i+1,:],T_ins[i+1,:],q_air[i+1],hr_sky[i+1],hr_channel[i+1],hc_PV[
i+1],hc_ins[i+1],Toutlet[i+1] = \
    BIPVT_SS
(weather[i],hc_PV[i],hc_wind[i],u_bot,BIPVT_characteristics,m_kg_s[
i+1],T_pv[i,:],T_ins[i,:],T_inlet[i],\
    T_room[i],hr_sky[i],u_PV_top,u_PV_bot,hr_channel[i],hi)
    T_inlet[:] = Toutlet[:]

# ENERGY CONSUMPTION -----

T_mix_hp = np.zeros(len(df_data_numpy_weather))
T_mix_hrv = np.zeros(len(df_data_numpy_weather))
T2_hrv = np.zeros(len(df_data_numpy_weather))
h_bipvt = np.zeros(len(df_data_numpy_weather))
cop_insta = np.zeros(len(df_data_numpy_weather))
q_insta = np.zeros(len(df_data_numpy_weather))
cop_insta_normal = np.zeros(len(df_data_numpy_weather))
q_insta_normal = np.zeros(len(df_data_numpy_weather))

add_energy_no_hrv = np.zeros(len(df_data_numpy_weather))
add_energy_yes_hrv = np.zeros(len(df_data_numpy_weather))
add_energy_hrv = np.zeros(len(df_data_numpy_weather))
add_energy_hp = np.zeros(len(df_data_numpy_weather))
add_energy_fan = np.zeros(len(df_data_numpy_weather))
prod_energy_pv = np.zeros(len(df_data_numpy_weather))

for j in range (0,len(df_data_numpy_weather)-1):
    T_mix_hp[j] = (m_kg_s_hp[j]*Toutlet[j] +
m_out_hp[j]*weather[j,0])/(m_kg_s_hp[j] + m_out_hp[j])          # Tmix for
heat pump
    cop_insta[j], q_insta[j] = HP_air_to_water(T_mix_hp[j], 50)
    cop_insta_normal[j], q_insta_normal[j] = HP_air_to_water(weather[j,0],
50)
    if heating_load[j]<=q_insta[j]:
        add_energy_hp[j] = heating_load[j]/cop_insta[j]
# Additional energy required operate heat pump (kW)
    else:
        print ("!!Heating load to big for HP capacity!!")
        add_energy_hp[j] = heating_load[j]/cop_insta[j]
# Additional energy required operate heat pump (kW)
    T_mix_hrv[j] = (m_kg_s_hrv[j]*Toutlet[j] +
m_out_hrv[j]*weather[j,0])/(m_kg_s_hrv[j] + m_out_hrv[j])          # Tmix for hrv
    T2_hrv[j] = ERV(e_sensible, Vent_req, Vent_req, T_mix_hrv[j], T_exhaust,
cp_air)
    add_energy_hrv[j] = (Vent_req*cp_air*np.abs(vent_setpoint[j] -
T2_hrv[j]))*0.001/3.1
    if T_pv[j,1]>25:
        h_bipvt[j] = BIPVT_characteristics[3]*(1-0.0045*(T_pv[j,1]-25))
    else:
        h_bipvt[j] = BIPVT_characteristics[3]

```

```

    prod_energy_pv[j] = h_bipvt[j]*A_bipvt*weather[j,2]*0.001
# Power produced from the PVs (kW)
    add_energy_fan[j] = fan_consumption(L_channel, Hydraulic_D, Cross_S_Area,
    rho_air[j], v_air[j], m_kg_s[j])

net_energy = add_energy_hp + add_energy_hrv + add_energy_fan - prod_energy_pv

sum_PV_pr_energy = sum(prod_energy_pv[:])*Dt/3600
# in kWh
sum_HP_con_energy = sum(add_energy_hp)*Dt/3600
# in kWh
sum_HRV_con_energy = sum(add_energy_hrv)*Dt/3600
# in kWh
sum_net_energy = sum(net_energy)*Dt/3600
# in kWh

excess_flowrate = m_kg_s - m_kg_s_hp - m_kg_s_hrv

# Heated air sent to adjacent buildings -----
vent_req_daycare = 2.58
# Ventilation setpoint for daycares according to ASHRAE 62.1
vent_set_daycare = 18
# 18C

initial_add_power_vent = vent_req_daycare*cp_air*(vent_set_daycare -
weather[:,0])*0.001
add_power_vent = np.zeros([len(df_data_numpy_weather)])
Tmix_daycare = np.zeros([len(df_data_numpy_weather)]-1)
Toutlet_daycare = Toutlet*0.9 # assuming 10% losses in the transition
for i in range (0,len(df_data_numpy_weather)):
    if excess_flowrate[i]>=vent_req_daycare:
        Tmix_daycare[i] = Toutlet_daycare[i]
    else:
        Tmix_daycare[i] = (excess_flowrate[i]*Toutlet_daycare[i] +
(vent_req_daycare - excess_flowrate[i])*weather[i,0]) / vent_req_daycare
    if Tmix_daycare[i]<weather[i,0]:
        Tmix_daycare[i] = weather[i,0]
    add_power_vent[i] = vent_req_daycare*cp_air*(vent_set_daycare -
Tmix_daycare[i]) * 0.001
    if add_power_vent[i]<0:
        add_power_vent[i] = 0

savings = initial_add_power_vent - add_power_vent
sum_savings_daycare = sum(savings)*Dt/3600
# kWh

```

